



City Research Online

City St George's, University of London

Citation: Witton-Dauris, Julia B. (2012). Centrifuge modelling of high shear capacity ribbed piles in stiff clay. (Unpublished Doctoral thesis, City University London)

This is the unspecified version of the paper.

This version of the publication may differ from the final published version. To cite this item please consult the publisher's version.

Permanent repository link: <https://openaccess.city.ac.uk/id/eprint/3673/>

Copyright and Reuse: Copyright and Moral Rights remain with the author(s) and/or copyright holders. Copies of full items can be used for personal research or study, educational, or not-for-profit purposes without prior permission or charge, unless otherwise indicated, provided that the authors, title and full bibliographic details are credited, a hyperlink and/or URL is given for the original metadata page and the content is not changed in any way. For full details of reuse please refer to [City Research Online policy](#).

CENTRIFUGE MODELLING OF HIGH SHEAR CAPACITY RIBBED PILES
IN STIFF CLAY

Julia Beatrice Witton-Dauris

Master of Philosophy

City University London

Geotechnical Engineering Research Group

September 2012

CONTENTS

ACKNOWLEDGEMENTS.....	5
DECLARATION.....	6
ABSTRACT	7
CHAPTER 1: INTRODUCTION.....	8
1.1 Background	8
1.1.1 Initial development of the rib-cutting tool.....	8
1.1.2 Further development of the rib-cutting tool.....	9
1.1.3 Further research into the behaviour of the ribbed pile.....	9
1.1.4 Implications of the research in the construction industry.....	10
1.2 Objectives.....	11
1.3 Summary of the thesis.....	11
CHAPTER 2: LITERATURE REVIEW.....	12
2.1 Introduction.....	12
2.2 Pile Design.....	12
2.2.1 Shaft Bearing Capacity.....	13
2.2.2 End Bearing Capacity.....	13
2.2.3 Pile Settlement.....	15
2.3 Pile-soil interface.....	16
2.4 Pile testing.....	17
2.4.1 Maintained Load Test.....	18
2.4.2 Constant Rate of Penetration Test.....	19
2.4.3 Interpretation of Pile Test Results.....	19
2.5 Conclusions.....	20
CHAPTER 3: THE CENTRIFUGE MODEL.....	22
3.1 Introduction.....	22
3.2 Principles of Centrifuge Modelling.....	23
3.2.1 Scaling Laws.....	24
3.2.2 Errors in Centrifuge Modelling.....	26
3.2.2.1 Vertical Acceleration Field.....	26
3.2.2.2 Radial Acceleration Error.....	28
3.2.2.3 Alignment of Model Piles.....	28
3.2.2.4 Boundary Effects.....	29
3.2.2.5 Soil Errors.....	29
3.2.2.6 Summary.....	30

CHAPTER 4: METHODOLOGY (APPARATUS DESIGN AND DEVELOPMENT)	31
4.1 The Geotechnical Centrifuge.....	31
4.2 Model Design	32
4.2.1 Model Container	32
4.2.2 Model Preparation.....	32
4.2.3 Model Geometry	33
4.3 Apparatus Design and Development.....	34
4.3.1 Pile Installation	34
4.3.1.1 The Pile Cutting Tool	35
4.3.1.2 The Rib Cutting Tool.....	36
4.3.1.3 The Guide	37
4.3.1.4 Casting The Piles	38
4.3.2 Carrying Out The Test	39
4.3.2.1 Loading Apparatus.....	39
4.3.2.2 Standpipe (or Controlling the Water Table).....	43
4.3.2.3 Instrumentation	44
 CHAPTER 5: TESTING PROCEDURE.....	 45
5.1 Preparation of instrumentation	45
5.1.1 PPTs	45
5.1.2 Load Cells	45
5.1.3 LVDTs	46
5.2 Preparation of the sample	46
5.2.1 Consolidation of the clay sample	46
5.2.2 PPT Installation.....	48
5.2.3 Preparation for model construction.....	49
5.3 Construction of the model	50
5.3.1 Construction of the model piles	50
5.3.2 Preparation of the model for testing.....	51
5.4 The Centrifuge Test.....	52
5.4.1 Further consolidation of the sample.....	52
5.4.2 Loading the model piles	53
5.4.3 Dismantling the model.....	53
 CHAPTER 6: EXPERIMENTAL WORK & RESULTS.....	 54
6.1 Test JW01	55
6.1.1 Sample Preparation	55
6.1.2 Model Construction.....	55
6.1.3 Centrifuge Test.....	56
6.2 Test JW02.....	57
6.2.1 Sample Preparation	Error! Bookmark not defined.
6.2.2 Model Construction.....	57
6.2.2 Centrifuge Test.....	58
6.3 Test JW03	59
6.3.1 Sample Preparation	Error! Bookmark not defined.
6.3.2 Model Construction.....	59
6.3.3 Centrifuge Test.....	60
6.4 Test JW04.....	61

6.4.1 Sample Preparation	Error! Bookmark not defined.
6.4.2 Model Construction.....	61
6.4.3 Centrifuge Test.....	62
6.5 Test JW05.....	63
6.5.1 Sample Preparation	Error! Bookmark not defined.
6.5.2 Model Construction.....	63
6.5.3 Centrifuge Test.....	63
6.6 Test JW06.....	65
6.6.1 Sample Preparation	Error! Bookmark not defined.
6.6.2 Model Construction.....	65
6.6.3 Centrifuge Test.....	65
CHAPTER 7: OBSERVATIONS & DISCUSSION.....	67
7.1 Observations.....	67
7.1.1 JW01_SP.....	68
7.1.2 JW01_RP.....	68
7.1.3 JW05_RPa.....	69
7.1.4 JW05_RPb.....	69
7.1.5 JW06_RPa.....	70
7.1.6 JW06_RPb.....	70
7.2 Geometry comparison.....	71
7.2.1 Rib outstand.....	71
7.2.2 Rib thickness.....	71
7.2.3 Rib spacing.....	72
7.3 Other observations and comments.....	73
CHAPTER 8: CONCLUSIONS AND RECOMMENDATIONS.....	74
LIST OF FIGURES.....	76
BIBLIOGRAPHY.....	Error! Bookmark not defined.

ACKNOWLEDGEMENTS

I was fortunate to receive an array of help and support from a number of different people during my time working towards this research project, and I would like to take this opportunity to show my appreciation.

I would like to thank to the entire department at the Geotechnical Engineering Research Centre in City University. First of all thanks should go to Andrew McNamara, my supervisor at City University, for his time and guidance during the project and write-up. The tests carried out for this project would not have been possible without the time and input of the researchers, technicians and my fellow postgraduate students. My gratitude extends to Richard, Neil, Sarah, Melvyn and Keith for their technical guidance and expertise. I am indebted to Leonora, Linda and Alexis for their considerable time and support.

Many thanks to Expanded Piling Co Ltd for proposing and part funding this project, and for the practical piling experience I was offered. Arup Geotechnics also aided in giving me practical experience and furthering my geotechnical understanding, and I very much enjoyed my time there. The project was also part funded by City University and I am extremely appreciative of their contribution.

I should also thank my employer, RWE Npower Plc, and manager, David VanderCruyssen, for offering to fund my write-up fee and giving me the study leave to complete this dissertation.

Finally, I am immensely grateful to my family and close friends who have supported me during my time on the project and cannot thank them enough.

DECLARATION

Powers of discretion are granted to the University Librarian to allow this thesis to be copied in whole or in part without further reference to the author. This permission covers only single copies made for study purposes, subject to normal conditions of acknowledgement.

ABSTRACT

Piling contractors are constantly on the lookout for innovative solutions that can put them a step ahead of their competitors. The idea of the High Shear Capacity Ribbed Pile, whereby the construction of ribs along the length of the pile shaft might significantly increase the shaft capacity, has been considered by contractors in the past. Various tools with which to construct these ribs, using different methods, have been explored in an effort to find an efficient method of construction. Through experimentation of these tools in the field, and subsequent pile tests, it has been confirmed that the construction of ribs does indeed increase the shaft capacity of piles. The extent to which the shaft capacity is increased compared with a similar straight shafted pile and what exactly the factors affecting this increase in shaft capacity might be are, as yet, uncertain. Thus it is not known whether the construction of this type of pile would be a more efficient alternative to a normal straight shafted pile.

This research project aims to identify the important factors in rib geometry of a ribbed pile in order to optimise its shaft capacity, and to compare with the shaft capacity of a similar straight shafted pile. This has primarily been investigated through physical modelling of the ribbed pile in a geotechnical centrifuge. Tools with which to install and load the piles have been developed so that traditional load tests can be carried out on small scale piles of varying rib geometries. Results will be compared and discussed with respect to previous research into the behaviour of piles in stiff clay.

This thesis details the achievements of a two year research programme into the behaviour of high shear capacity ribbed piles in stiff clay. The research has been jointly funded by Expanded Piling Limited and the Geotechnical Engineering Research Group at City University London and carried out in collaboration with Arup Geotechnics.

CHAPTER 1: INTRODUCTION

1.1 Background

The design of pile foundations in stiff clays such as London Clay is always being pushed to further limits, with recent piles being constructed to more than 60m below ground level, and up to 3m in diameter. Alternative solutions that might make the pile more efficient, either by an increase in its shaft or bearing capacity, are constantly being investigated and perfected. For example, the base of a pile can be enlarged by under-reaming, giving the pile a vastly increased base capacity. There are currently, however, no widely used methods of significantly increasing the shaft capacity. It has been suggested that a suitable method may be through the construction of ribs along the length of a pile, enabling the shaft capacity to be considerably greater than that of a similar sized pile with a straight shaft.

1.1.1 Initial development of the rib-cutting tool

Piling contractors, Expanded Piling Ltd., have been investigating the construction of ribbed piles since 2003. They have developed and perfected a rib-cutting tool (Figure 1.1) that can be used in conjunction with a rotary bore piling rig, looking for the most accurate and efficient method of constructing the ribs in order to discover just how much higher the shaft capacity would be compared with a similar straight shafted pile. In the summer of 2003, their first rib-cutting tool was used to construct ribbed piles in boulder clay at their Lincolnshire depot, and subsequent field trials were carried out. The development of the rib-cutting tool was continued with further trial piles on the Radcliffe Hospital site in Oxford. Despite encouraging results from the pile tests carried out up to that stage, they were not reliable enough to make any definitive conclusions as seepages of water were encountered in both cases. An article was published later that same year in *Ground Engineering* (2003) showing the company's confidence and commitment to the development of the ribbed pile,

and their research continued in association with engineering consultants Arup Geotechnics. It was concluded that a trial pile would need to be constructed in controlled conditions with as much care as possible taken to cut the perfect ribs if the pile test results were to be conclusive.

1.1.2 Further development of the rib-cutting tool

It was decided that the test pile would be constructed in London Clay at a suitable site on Lime Street in the City of London where Expanded Piling and Arup Geotechnics were working on a job together. Two trial piles were designed as straight shafted piles and tested to failure, comparing the load at failure with that predicted. The straight shafted pile failed at the predicted load, showing that the soil strength model to be a fairly accurate representation of the actual soil. The ribbed pile failed at a load 40% higher than predicted for a similar sized pile with a straight shaft, confirming the assumption that the addition of ribs increased the pile's shaft capacity (Figure 1.2).

Despite care and time being taken to cut the ribs as accurately as possible, when the trial ribbed pile was taken out of the ground it was discovered that there were sections where part of the ribs were damaged. This is likely to be due to the requirement to pass a cleaning bucket down the open shaft after the cutting of the ribs to pick up spoil that has fallen to the base as a result of the ribs being cut. The tool is still being improved, and different ways of ensuring the ribs are not damaged during construction are being investigated.

1.1.3 Further research into the behaviour of the ribbed pile

As much of the focus of these load tests was on the efficiency of the rib-cutting tool itself, investigation into the optimal geometry of these ribs was not carried out. It was considered that such an investigation would benefit from an academic approach through the detailed analysis of laboratory experiments. The testing of small scale piles in a geotechnical centrifuge would make it possible to test many

piles to failure, and remove and examine the piles after testing. This would be extremely difficult and expensive to do with full scale piles in the field. After construction, the pile would have to be left for weeks before testing could be carried out due to the curing process, and furthermore exhuming a pile from the ground is a very costly process. The laboratory experiments in comparison can be carried out in about 3 weeks including setup, performing of the tests, and taking out the pile.

Laboratory experiments using the geotechnical centrifuge also have the advantage of using model soil. There is control over the consistency of the model soil and the properties as required to replicate a specific type of prototype soil, and the model can be reproduced for multiple tests.

1.1.4 Implications of the research in the construction industry

The construction of High Shear Capacity Piles would enable construction sites to be more environmentally aware as shorter piles could be used to carry the same load. Less concrete would need to be transported to site, and less spoil would need to be transported away from site. Though this should also make pile construction more cost efficient, the most important factor financially is time. If the time taken to construct the ribs of each individual pile exceeds the time saved by being able to construct shorter piles, it is unlikely this type of pile will become widely used. It is hoped this research project will help to clarify these details, and suitable uses suggested for the ribbed pile.

It has been suggested that this type of pile may be particularly useful for sites where it is necessary to have shorter piles, for example because below a certain level the material is difficult to work with or unsuitable for use as a load bearing material.

1.2 Objectives

This project aims to gain an understanding of the various factors affecting the capacity of a ribbed pile in stiff clay, in particular geometric details of the ribs such as:

- Outstand of the ribs (Figure 1.3)
- Thickness of the ribs (Figure 1.4)
- Distance between ribs (Figure 1.5)

This will primarily be investigated through physical modelling of the ribbed piles. Traditional pile tests will be simulated in the geotechnical centrifuge at the Geotechnical Engineering Research Group at City University London so as to evaluate the significance of various aspects of the rib geometry. Load test results will be compared and discussed with reference to previous research into the behaviour of piles in stiff clay.

1.3 Summary of the thesis

This thesis details the approach to the research and reasons behind it. Chapter 2 discusses literature on the behaviour of bored piles in stiff clay and different approaches to pile testing. General principles of centrifuge modelling and how testing in the centrifuge can be compared to full scale tests are presented in Chapter 3. The design and development of the experiments are discussed in Chapter 4, as well as the apparatus used to carry tests out. Chapter 5 outlines the testing procedure and Chapter 6 gives detail the experiments themselves and presents the results. The results are then discussed in Chapter 7 with conclusions and recommendation given in Chapter 8.

CHAPTER 2: LITERATURE REVIEW

2.1 Introduction

Pile foundations are widely used to support heavy buildings in areas such as London where the soil is stiff clay at practical depths for construction. For this reason there has been a vast amount of research into the behaviour of clay, ways of determining the capacity of pile foundations, and methods of load testing. These are explored and discussed in this chapter, and considered further in Chapter 7 with relation to conclusions drawn from test results.

2.2 Pile Design

It is well established that soil behaviour is governed by the stress history of the soil and the subsequent stresses acting on it. London Clay is, for example, a heavily overconsolidated clay. Overconsolidated relates to the stress history of the soil, meaning that it has been deposited and undergone a series of loading and unloading due to various geological processes such as redeposition of alluvial deposits, erosion of the soil, and changes in sea level. This causes a series of compression (or consolidation) and swelling of the soil, which it undergoes to reach its current state. As a result, the effective stresses in the soil vary with depth, which is an important factor in the design of any deep construction.

The maximum load that a pile foundation is capable of carrying can be defined by the sum of the shaft capacity and the end bearing capacity (Figure 2.1). Failure of the pile foundation, however, is related to settlement and so usually occurs at a lower load.

2.2.1 Shaft Bearing Capacity

The shaft capacity of the pile shaft, Q_{shaft} , can be given by:

$$Q_{\text{shaft}} = \alpha \cdot S_u \cdot A_{\text{shaft}} \quad \text{Formula 2.1}$$

Where α is the adhesion factor, S_u is the average undrained shear strength of the clay along the length of the pile, and A_{shaft} is the total surface area of the pile shaft (which is given by $\pi \cdot D \cdot H$, where D is the pile diameter and H is the pile length) (Skempton, 1959).

The adhesion factor, α , is defined as the ratio of the average adhesion between the clay and the pile shaft to the average undisturbed shear strength of the clay within the depth of penetration of the pile in the clay (Skempton, 1959). A typical value of α for overconsolidated clay would be 0.3 to 0.6, the higher value representing favourable geological conditions and careful workmanship. For cast-in-situ piles, the adhesion factor is largely affected by softening of the clay immediately adjacent to the pile-soil interface. This will be discussed in further detail in Section 2.3.

The undrained shear strength S_u of the soil is determined by obtaining soil samples from the ground in a suitable state such that it can be tested to assess the strength. Data acquired in this way enables a profile of the undrained shear strength of the soil to be created as it varies with depth.

2.2.2 End Bearing Capacity

The bearing capacity at the base end of the pile can be given by:

$$Q_{\text{base}} + W = (N_c \cdot S_u + \gamma \cdot H) \cdot A_{\text{base}} \quad \text{Formula 2.2}$$

Where W is the total weight of the pile, N_c is the bearing factor, S_u is the undrained shear strength of the clay at the base of the pile, γ is the unit weight of

the clay, H is the length of the pile in the clay strata, and A_{base} is the area of the base of the pile.

It can be assumed that, approximately:

$$W = \gamma \cdot H \cdot A_{\text{base}} \quad \text{Formula 2.3}$$

Thus Formula 2.2 can be reduced to:

$$Q_{\text{base}} = N_c \cdot S_u \cdot A_{\text{base}} \quad \text{Formula 2.4}$$

A bearing capacity factor of $N_c = 9$ is generally accepted for pile design in clay. It has been suggested that this factor may be lower for higher pile depth to diameter ratios as a higher load transferred from the shaft to the surrounding soil might cause larger settlements to occur in the soil around the base. There is little evidence to support this, however, probably because the settlements in the soil caused by loading on the shaft are relatively small compared to those caused by the base.

Many factors can affect soil strength and consideration should be given to which effects should be taken into account when calculating pile capacity. For example, the undrained shear strength of the clay can be greatly affected by fissures which are often found in London Clay at different levels. This effect depends how heavily fissured the clay is at the specific area the engineer is interested in. Whitaker (1966) proposed the introduction of a coefficient, ω , to be used in Formula 2.4 to quantify this affect and take it into account in fundamental pile design.

$$Q_{\text{base}} = N_c \cdot \omega \cdot S_u \cdot A_{\text{base}}$$

Where ω is the ratio of the fissured strength of the clay measured on shear planes of large area to the mean strength of a fissured clay determined by triaxial compression tests.

The problem with such factors involved in pile design is that the only way to quantify them accurately is through empirical methods, that is by testing piles in the field and analysing the results. It would of course be impractical to do this for every pile, but values can be taken from pile tests carried out in similar ground conditions and using similar construction methods. The inclusion of a safety factor should take into account any discrepancies in the values used for the factors.

2.2.3 Pile Settlement

It has been stated that the ultimate load of a pile foundation is reached when the pile first starts to continuously settle at a steady rate with a constant load applied. This does not, however, describe the failure load of a pile foundation which can be defined as the load at which a settlement of 10% of the pile base diameter takes place (Fleming, 1992).

It has been observed that the shaft is fully mobilised at very small settlements of around 0.5% of the pile diameter. In comparison, much larger settlements of around 10-15% of the pile diameter are required to develop a resistance at the base of $N_c = 9$ (Whitaker, 1966). Thus the shaft tends to be fully mobilised and settles at a constant rate long before failure occurs at the base (Figure 2.2). As pile failure is associated with a fully mobilised pile shaft, it is hoped that that high shear capacity ribbed pile will have a much higher shaft capacity relative to the base and therefore a much higher failure load than that of a similar straight shafted pile.

It is also important to consider long term factors affecting settlement, such as consolidation of the soil around the pile and redistribution of the load between pile shaft and base. Consolidation settlement of bored piles in stiff clay has been shown in the past to be comparatively insignificant in the vast majority of cases, though some settlement due to consolidation is inevitable, causing further load to be mobilised at the base. Assuming the load applied by the structure remains

constant, this will result in a reduction in the load carried by the shaft (Figure 2.3).

2.3 Pile-soil interface

The main concept of the ribbed pile is that it should have a significantly higher shaft bearing capacity than that of a similar straight shafted pile. Thus it is necessary to look at the factors affecting the pile shaft capacity, and the behaviour of the soil immediately adjacent to the pile-soil interface.

In the design of pile foundations it is the adhesion factor, α , that dictates how much the average undisturbed shear strength of the soil is reduced by the construction process in the area immediately adjacent to the pile surface. Disturbance and remoulding of the soil in this region will inevitably occur when constructing the borehole, though the main reason for reduction in the strength of the soil is an increase in water content which happens for a number of reasons. These can include high groundwater levels, water flows through fissures, migration of water through the clay due to decreased stress levels around the borehole, water used in boring to facilitate cutting-tool operation, and water exodus from concrete where a water-cement ratio higher than that needed for hydration is necessary. Although the effects of the majority of these can be kept to a minimum with quick and efficient construction methods, it is important to remember that some water movement in the soil is unavoidable and a rise in water content of just 1% can result in a decrease in the adhesion factor of up to 20%.

It has been shown that softening of the clay around the pile shaft takes place in a very thin region. In tests carried out by Skempton (1959), for example, it was found that where a water content increase of as much as 4% has occurred in this region, the soil 75mm away from the contact surface was unaffected. An example of measured water content and strength varying with distance from the pile surface is given in Figure 2.4 (Milititzky, 1980). It is thought that the construction of ribs on the pile shaft may cause shear failure to take place further

away from the pile shaft where the soil is less disturbed and less prone to softening (Figure 2.5).

It has been suggested that this rapid movement of water during construction and loading implies a drained behaviour in the area immediately adjacent to the pile shaft. However, there is no simple way of relating the drained strength to the undrained strength of the soil. Burland (1973) attempts to simplify this problem by using an effective stress approach to describe the pile behaviour. This relates the shaft friction to the horizontal effective stress acting on the pile and the effective angle of friction between the clay and the pile shaft. It can be assumed that the horizontal effective stress is proportional to the vertical effective overburden pressure, although this relies on being able to reasonably estimate a value for the coefficient of earth pressure at rest.

It has been pointed out that undisturbed lateral effective stresses are not maintained during the installation process and, even if they were, it would be extremely difficult and costly to determine the in-situ coefficient of earth pressure at rest (Clayton & Milititzky, 1983), particularly due to reconsolidation of the softened clay around the pile shaft which is caused by soil creep leading to horizontal effective stresses being re-established.

It has been observed on instrumented test piles that the mobilised shear strength along the length of the shaft of a pile in stiff clay does not increase with depth as the shear strength of the soil does (O'Neill & Reese, 1972). It is in fact parabolic and highly dependant on how much vertical load is being applied to the pile head, with no relation to either the undrained shear strength or the likely horizontal effective stresses in the soil immediately adjacent to the pile surface (Figure 2.6).

2.4 Pile testing

There are currently two main methods of carrying out load tests on piles in the field; the maintained load test, and the constant rate of penetration test. Many

varieties and combinations of these methods of load testing are used in the field depending on foundation type and ground conditions. Cyclic loading in some form is often included, firstly, to assess the effect of loading and unloading and even to attempt to separate the effects of shaft bearing and the end bearing.

2.4.1 Maintained Load Test

The most common load testing procedure, particularly in the UK, is the slow maintained load test. The pile is loaded in eight equal increments usually up to 200% of the design load. At each increment the load is maintained until the rate of settlement has decreased to 0.3mm/hr (equivalent to 0.05mm/hr) or for 2 hours, whichever is reached first. This method of testing is a time consuming process and can take up to 70 hours.

For this reason, variations on the standard method have been proposed in an attempt to speed up the process. These include allowing the load (jack pressure) to drop rather than being maintained by pumping (Mohan, 1967), or setting a much shorter time limit on each loading increment regardless of the rate of settlement that is reached (Housel, 1966). The latter aims to allow an analysis of movement with time, which is not possible using the standard method. Fellenius (1980) extends this idea by recommending a greater number of increments maintained at much shorter time intervals, the idea being that time dependant influences can be reduced as far as is possible to obtain an undrained test.

A pile that is supporting a structure, however, will in the long term be loaded under drained conditions. For this reason it may be desirable to investigate time dependant effects such as soil creep. A load test lasting 70 hours would be insufficient to study these effects and it is suggested that such a load test would need to take weeks or months, rather than hours.

2.4.2 Constant Rate of Penetration Test

A quick load testing procedure also commonly used is the constant rate of penetration test. The pile head is forced to settle at a fixed rate, usually 0.5mm/minute, and the load required to maintain a steady movement is recorded. The test is carried out to a maximum penetration of the pile head of 50-75mm, or to the maximum capacity of the reaction arrangement, with readings of the load taken every 2 minutes. This means the load test is completed within just two or three hours.

This testing procedure has the advantage of giving a better determination of the load-deformation curve than the maintained load test, particularly for friction piles where the load required for a constant rate of settlement decreases after a peak value has been reached. However, the requirement for a mechanical pump providing a constant and non-pulsing flow of oil and for simultaneous reading of all load and deformation gauges make the maintained load method preferable for instrumented piles. This test is also limited by the capacity of the plant to apply a suitably large load for sufficient data to be obtained. Whilst a peak load is often clearly achieved for friction piles in soft or loose soils, it is not so easily attained for stiffer soils.

2.4.3 Interpretation of Pile Test Results

The main objective when interpreting pile test results is to determine the ultimate load of the pile. There are many proposed methods of interpretation for each type of load test.

For constant rate of penetration tests where a peak value is reached, this peak value can be defined as representing the ultimate load. Identifying the “failure” load, however, is more difficult. A 90% criterion is presented by Brinch Hansen (1963), defining failure as the load giving twice the movement at the pile head as is recorded for 90% of that load. This criterion assumes that the test curve is

hyperbolic at failure, and is credited with providing reasonable results that are reproducible independent of the judgement of the interpreter.

Several methods have been suggested to identify the failure load for the slow maintained load test. For example, De Beer and Wallays (1972) use a double logarithmic diagram on which to plot the load-movement relationship. It has been shown empirically that the data can be separated into two straight lines, the intersection of which represents the failure value. It is made clear this interpreted value of the failure load is conservative though, and should not be confused with the ultimate failure load. Similar approaches of approximating some form of load-movement curve to two straight lines exist, whereby the failure load, sometimes called the “yield point” or “critical load”, is deduced in the same way.

Another method of determining the failure load from the shape of the load-movement curve, for example, is cited by Chellis (1961) and Fuller & Hoy (1970), whereby failure is defined as the load corresponding to the point on the curve where its gradient is equal to 0.14mm/kN.

Fellenius (1975) compares eight methods of defining pile failure including those previously mentioned, and, whilst it is accepted that all the methods examined are equally viable, there is shown to be a variation in interpretation of the failure value in the order of 40%.

Pile testing method for this project is discussed in Chapter 6.

2.5 Conclusions

This project focuses on the pile shaft capacity, which is given by:

$$Q_{\text{shaft}} = \alpha \cdot s_u \cdot A_{\text{shaft}}$$

where Q_{shaft} is the shaft capacity, α is the factor of the soil strength, s_u is the undrained shear strength of the clay, and A_{shaft} is the area of the shaft.

Standardised values of the factor α can vary hugely, even in the same formation. For example, values used in pile design in London Clay are usually in the range of 0.4 to 0.6. These values were established in the 1950s and 1960s when a large amount of research was carried out in this area and are thought to depend on a variety of factors, such as the presence of fissures in London Clay. A significant increase in the value of α is expected through the addition of the pile ribs, as they should move the failure zone away from the soil-pile interface where the soil is less disturbed. It is hoped that through carrying out equivalent pile tests on ribbed piles and straight shafted piles, a better understanding can be gained of how much the value of α can be increased by and the effect of rib geometry on that increase, as well as how these α values may be used in conjunction with those currently used in pile design. Test results should also enable some assessment of the viability of ribbed piles, with a view to give design engineers guidance as to the value of α for the design of this type of pile.

CHAPTER 3: THE CENTRIFUGE MODEL

3.1 Introduction

The idea of using a centrifuge to physically model real engineering problems at a small scale was first suggested as early as 1869 by French engineer Edouard Phillips. But it was not until some sixty years later that this idea came to fruition, the first major developments in centrifuge modelling taking place in the USSR and some papers being published in the USA during the 1930's. With the coming of the Second World War, closely followed by the Cold War, and the development of digital technology, the centrifuge seemed to be left on the shelf for another three decades. Finally, in the late 1960's, papers relating to centrifuge modelling were published by Mikasa et al. in Japan, Schofield and Avgherinos in England, and Ter-Stepanian and Goldstein in the USSR. Centrifuge modelling in engineering research continued to develop aided in particular by advancements in instrumentation and, as limitations of numerical solutions to engineering problems became recognised, the centrifuge had by the mid 1980's become a much more widespread tool in engineering research (Craig 1995).

The centrifuge was initially recognised as a particularly useful tool in modelling geotechnical problems involving gravity-induced hydraulic gradients or soil self-weight. It is now commonly used in many academic research institutions, with new applications rapidly becoming apparent and being developed, such as loading due to sudden impact or vibrations, and new construction techniques. This is particularly evident in Japan which has the largest proportion of the world's geotechnical centrifuges, and uses them widely in industry as well as academia.

3.2 Principles of Centrifuge Modelling

In physical modelling of construction in the ground, the governing factors of soil behaviour to be considered are the strength and stress history of the soil. The naturally occurring stresses in the ground that vary with depth require modelling, which means stress distribution in the soil needs to be reproduced before any kind of construction can be simulated. Through the use of a consolidation press, in-situ stress distributions can be replicated in a relatively short period of time. Kaolin clay, for example and in the case of this research, is often used to model overconsolidated clays such as London Clay as its high permeability enables minimal time for preparation of the sample.

The soil sample is contained in a steel tub or strongbox which is placed on a swing at the end of a centrifuge arm. When the centrifuge is spun up, the model is subjected to an inertial radial acceleration field, which simulates Earth's gravity. This radial acceleration, combined with the soil density, determines the values up to which the stresses in the soil increase with depth from zero at the surface (Figure 3.1).

Vertical stress at a depth h_m (m) in a centrifuge model that is subjected to an inertial acceleration field N times Earth's gravity, will correspond to the vertical stress at a prototype depth of h_p (m), so that:

$$h_p = N \cdot h_m \quad \text{Equation 3.1}$$

According to Newton's laws of motion, a mass being pulled out of a straight path into a radial curve will be subjected to an acceleration toward the centre of the curve. This can be expressed in terms of the radius of the curve, r (m) and the angular velocity, ω (rad/s), where a is the acceleration (m/s^2):

$$a = \omega^2 \cdot r \quad \text{Equation 3.2}$$

Since the effect of the radial acceleration in the centrifuge is to increase the self weight of the model in the direction of its base, it therefore follows that the radial

acceleration, a (m/s^2) can be related to Earth's acceleration due to gravity, g (m/s^2) using N from equation 3.1 as such:

$$a = N \cdot g \quad \text{Equation 3.3}$$

Thus a prototype can be accurately simulated, with careful model preparation, whereby a model that is N times smaller than the prototype will be put into a centrifuge with a radial acceleration that is N times acceleration due to gravity (Taylor 1995).

3.2.1 Scaling Laws

Appropriate scaling laws can be used to relate information about the prototype with that of the model. Reproducing the soil stresses of the prototype in the model is a fundamental principle of centrifuge modelling, so that the vertical stress in the model σ_{vm} at a depth h_m is equal to the vertical stress σ_{vp} in the prototype at a depth h_p :

$$\sigma_{vm} = \sigma_{vp} \quad \text{Equation 3.4}$$

The vertical stress in the model σ_{vm} can be expressed in terms of the soil density ρ , the depth at that vertical stress is acting h_m , and the scale of Earth's gravity $N \cdot g$, to which the soil is subjected:

$$\sigma_{vm} = \rho_m \cdot N \cdot g \cdot h_m \quad \text{Equation 3.5}$$

In the same way, the vertical stress σ_{vp} in the prototype can be expressed as:

$$\sigma_{vp} = \rho_p \cdot g \cdot h_p \quad \text{Equation 3.6}$$

Assuming the density of the soil in the model ρ_m is the same as that of the prototype ρ_p , and the vertical stresses are equivalent, the following applies:

$$\rho \cdot N \cdot g \cdot h_m = \rho \cdot g \cdot h_p \quad \text{Equation 3.7}$$

and can be reduced to:

$$h_p / h_m = N \quad \text{Equation 3.8}$$

Thus the scaling law for length is $1/N$. This will affect geometrical properties of all components of the model.

The scaling law for length can be used to derive scaling factors for other properties of the model. For example, consolidation of the sample can be expressed in terms of a dimensionless factor, T_v :

$$T_v = [c_v \cdot t] / H^2 \quad \text{Formula 3.9}$$

where c_v is the coefficient of consolidation, t is time, and H is a distance related to the drainage path.

For the same consolidation to be represented by the model as exists in the prototype, the dimensionless factor, T_v , should be the same, giving:

$$c_{vm} \cdot t_m / H_m^2 = c_{vp} \cdot t_p / H_p^2 \quad \text{Formula 3.10}$$

Given that the scaling law in Formula 3.8 holds, it follows that:

$$H_m^2 / H_p^2 = 1 / N^2 \quad \text{Formula 3.11}$$

which gives:

$$t_m = [1 / N^2] \cdot [c_{vp} \cdot t_p / c_{vm}] \quad \text{Formula 3.12}$$

Thus the scaling factor for consolidation is $1/N^2$, assuming the same soil is used in the model and prototype, and there is no reason for the coefficients of consolidation to differ. This makes it possible to simulate long term effects in a

timescale that is practical to carry out a centrifuge test. For example, a year long period would last 5 and half hours during a centrifuge test with a scale factor of 40, and a period of a month less than half an hour.

3.2.2 Errors in Centrifuge Modelling

No method of modelling is perfect, and this is no different in the case of the centrifuge model. There are inevitable errors that need to be taken into account. One of the main differences between the model and the prototype is the inertial acceleration field and Earth's naturally occurring gravity. Gravity is uniform for the practical range of soil depths in civil engineering problems. In the centrifuge, however, acceleration is a function of the radial velocity, ω , and the radius of rotation, r . As depth in the model is along the axis of the radius (Figure 3.2), there is an increase in acceleration from the top of the model to the base. This causes several different errors in modelling the prototype that will be considered in this section.

3.2.2.1 Vertical Acceleration Field

The variation in the inertial acceleration field through the model results in a non linear relationship between vertical stress in the model, σ_{vm} , and depth, h_m . Thus, in modelling the prototype, there will be an understress at the soil surface of the model and an overstress at the base, and care must be taken to keep these within acceptable limits (Figure 3.3).

To find the acceleration required for the least variation between the stresses in the prototype and the model, expressions can be given for the ratios of understress and overstress in the model to the stress at the same depth in the prototype:

$$\sigma_{vp} = \rho \cdot g \cdot h_p = \rho \cdot N \cdot g \cdot h_m = \sigma_{vm} \quad \text{Equation 3.13}$$

where $N \cdot g = a$ Equation 3.14

thus $N \cdot g = a = \omega^2 \cdot R_e$ Equation 3.15

where $R_e =$ effective centrifuge radius of the model (i.e. where $\sigma_{vm} = \sigma_{vp}$ is true).

Given that $R_t =$ centrifuge radius to the top of the model, it follows that:

$$\sigma_{vm} = \int \rho \cdot \omega^2 \cdot (R_t + z) dz = \rho \cdot \omega^2 \cdot z \cdot (R_t + z/2)$$
 Equation 3.16

and $R_e = R_t + h_i/2$ Equation 3.17

where $h_i =$ depth of the model z at the effective centrifuge radius of the model R_e .

It can be shown that the ratio of understress r_u can be expressed as:

$$r_u = h_i / 4R_e$$
 Equation 3.18

Similarly, the over stress ratio r_o is given by:

$$r_o = (h_m - h_i) / 2R_e$$
 Equation 3.19

Where the understress and over stress ratios are equal, the depth of the model at which exact correspondence with the stress in the prototype occurs can be found:

$$r_u = r_o$$
 Equation 3.20

$$h_i / 4R_e = (h_m - h_i) / 2R_e$$
 Equation 3.21

This can be reduced to:

$$h_i = 2h_m/3$$
 Equation 3.22

giving expressions for the understress and overstress ratios as such:

$$r_u = r_o = h_i / 6R_e \quad \text{Equation 3.23}$$

Putting Equation 3.22 back into Equation 3.17 gives the location of the effective radius R_e at 1/3 of the soil depth of the model:

$$R_e = R_t + h_m/3 \quad \text{Equation 3.24}$$

3.2.2.2 Radial Acceleration Error

There is also a difference in the direction of the acceleration field in the model and gravity in the prototype that needs to be taken account. At all points of the prototype gravity will act vertically. In the model, however, the acceleration field will act towards the centre of rotation. Therefore it will only act exactly vertically at the very centre of the model, along the axis of rotation. Elsewhere within the model the direction of the acceleration will have a horizontal component which will increase with distance from the axis of rotation. It is considered good practice to keep the model as close to the axis of rotation as possible in order to keep this radial acceleration error to a minimum. Where the model is furthest from this axis, the magnitude of the radial error must be checked to make sure that it is small enough to be considered insignificant.

See Section 4.2.3 Model Geometry for radial acceleration error check for these tests.

3.2.2.3 Alignment of Model Piles

For efficient testing of the model piles it was decided two should be tested at a time, thus they had to be located away from the central axis of rotation. As previously mentioned, this causes the model foundation to be out of line with the resultant acceleration. A possible solution to this error is to align the model piles

with the resultant acceleration at their location. In this model, however, this correction would cause further errors as the piles would then be out of line with the direction of consolidation and swelling of the soil. If the piles are kept in line with this direction rather than that of the resultant acceleration, and providing the axial loading of the foundations is kept in line with the vertical axis of the pile, the subsequent horizontal component of the acceleration will be relatively insignificant.

3.2.2.4 Boundary Effects

The model is limited also by the relative size of container in which the prototype is being modelled. The effect of the friction of the side wall of the containers must be considered. For the centrifuge tests being carried out in this project, the model is contained in a stainless steel drum with an inner diameter of 420mm and an inner depth of 400mm. The side walls are covered in grease to reduce the friction effect, though it is important to remember that side wall friction is always present to some extent (Phillips, 1995). The container should be suitably sized relative to the model such that the effect of the side wall friction does not have a significant impact on the tests carried out. It is suggested that, in order to sufficiently minimise the boundary effect, there is a minimum distance of 5 pile diameters between the model piles and the side wall of the container.

3.2.2.5 Soil Errors

Before the model itself is constructed and placed on the swing platform in the centrifuge, the soil sample is prepared in a consolidation press. It is subjected to a vertical pre-consolidation pressure, p'_{max} , at the top, which is reduced to a lower pressure, p'_c , when the stresses in the sample have reached equilibrium. The new pressure, p'_c , will be constant with depth in the model, whereas it will increase with depth in the prototype. After construction of the model, the sample will be further consolidated under the acceleration field in the centrifuge in order to attempt to replicate the variation of stress with depth in the prototype.

However, as p'_c is likely to be lower in the model than in the prototype at depth, there is likely to be a higher specific volume leading to a lower stiffness and lower undrained strength.

This can be shown using critical state soil mechanics to determine failure on the critical state line. Undrained shear strength can be defined as:

$$S_u = (M/2) \cdot \exp [(\Gamma - v) / \lambda]$$

where M is the gradient of the critical state line on the q' (effective deviator stress) – p' (mean normal effective stress) plane, Γ is the specific volume of the soil on the critical state line at $p' = 1.0$ kPa, v is the specific volume, and λ is the slope of the normal consolidation and critical state lines. A higher specific volume will therefore result in a reduction in undrained shear strength. Assuming the undrained shear strength in the model and prototype are the same at the surface, this error will increase with depth in the soil sample.

This will also affect the permeability of the Speswhite Kaolin Clay used in the model as it is a function of the voids ratio. The higher specific volume, and therefore voids ratio, will result in the reduction of permeability with depth to be reduced in the model compared with the prototype.

3.2.2.6 Summary

There are many ways in which the geotechnical centrifuge model is not the same as the prototype, though most can be reduced so that they are relatively insignificant or at least kept to a minimum. Providing these differences are known and quantifiable, and the model is sufficiently representative of the prototype that tests can be carried out to obtain meaningful results obtained, any subsequent errors can be managed. It is important to acknowledge these errors and understand how they may affect the test when analysing the results.

CHAPTER 4: METHODOLOGY (APPARATUS DESIGN AND DEVELOPMENT)

4.1 The Geotechnical Centrifuge

Testing for this project uses the Acutronic 661 (Figure 4.1 and 4.2) in the Geotechnical Engineering Research Centre at City University. At one end of the rotor, the model is placed on a swing platform which has a usable height of 960mm and overall dimensions of 500mm by 700mm. The platform is located on a 1.8m swing arm, giving a working radius of 1.5m to 1.6m from the centre of rotation. The swing arm and platform are balanced by a 1.6 tonne counterweight that can be moved radially by a screw mechanism. The centrifuge can accelerate up to 200 times gravity, giving a maximum rotation speed of 345rpm. It is a 40g/tonne machine, meaning that at an acceleration of 200g (or 5 x 40g), a package weight of 200kg (or 1/5 tonne) can be accommodated, and this weight will increase linearly as the acceleration is reduced.

Signals from four strain-gauged sensors are monitored continuously to detect out-of-balance of the centrifuge base. If a pre-set maximum out-of-balance of 10kN is exceeded the machine shuts down automatically enabling safe unmanned overnight running of the centrifuge. It is enclosed in an aerodynamic shell, which is surrounded by a block wall, and that by a reinforced concrete structure providing safe and effective containment.

A series of slip rings are available at the swing platform to supply electrical and hydraulic connections to the model. In total, 55 electrical connections are available, some of which are used to transmit transducer signals, others to communicate video images, supply power to lights, or operate solenoids or motors. These signals are converted from analogue to digital by the on-board computer and can be amplified as necessary prior to transmission in bits. Also available are 5 fluid connections (15 bar capacity) for water, oil or air.

4.2 Model Design

4.2.1 Model Container

The model is contained in a cylindrical stainless steel tub with an internal diameter of 420mm, an internal height of 400mm, and a 20mm thick base for drainage (Figure 4.3). Access ports enabling the installation of pore pressure transducers (PPTs) are located at a distance above the base of 5mm, 50mm, 100mm, 150mm, 180mm, 200mm, and 250mm. These are used for periodically recording measurements of pore water pressure at specific points in the model during each test. In the context of these centrifuge tests, pore water pressure was deemed to be of significance only for observing equilibrium in the model soil before loading and any changes associated with this equilibrium. It was recognised that no more than three PPTs would be necessary and, for this reason, access ports at 50mm, 150mm and 250mm were used for these tests. Further details of PPTs used for these tests are discussed in Section 4.3.2.3, and installation of PPTs in Section 5.2.2.

4.2.2 Model Preparation

Centrifuge testing in clays usually uses kaolin owing to its high permeability. This enables the stress history of prototype soil to be simulated by consolidation of the soil in the lab over a relatively short period of time.

In preparation for construction of the model piles, the model soil was placed in the steel tub as a clay slurry with a water content of 120%, approximately twice the liquid limit of the model soil. By placing this in a consolidation press (Figure 4.4), a vertical pressure could be applied. This pressure was increased incrementally to a pressure of 500kPa before being swelled back to 250kPa. This stress history was chosen as it has been shown to successfully replicate the characteristics of overconsolidated clays such as London Clay in previous centrifuge tests (Qerimi 2010).

When the soil was at 250kPa and consolidation complete, which was possible to recognise by observing reduction in swelling of the sample, the PPTs could be installed through the access ports in the side of the steel tub. The model preparation process is discussed in further detail in Section 5.2.

Due to the type of piles that needed to be constructed it was identified that construction of model piles would need to be carried out at 1g, in between removal from the press and spin up of the model in the centrifuge. With the sudden release of 250kPa on removal from the press, the sample would inevitably be subject to negative pore pressure during model construction. Thus it was necessary that this process be carried out in as short a time as possible to minimise changes in the soil stress profile of the sample and prevent drying out of the clay surface. Further consolidation in the centrifuge would create the required soil stress profile.

4.2.3 Model Geometry

Geometry of the centrifuge model test is shown in (Figure 4.5). It was designed such that two piles could be tested in one centrifuge spin up. Having decided on a pile diameter of 15mm and pile depth of 200mm (reasons for these dimensions this will be discussed later in this chapter), it was easy to fit more than one pile in the tub, boundary conditions stating that the model piles should be 5 pile diameters (75mm) from the side of the tub and each other. It was decided that no more than 2 piles could reasonably be tested at a time, to ensure there would be enough space for the loading apparatus which would be located above the piles during testing, sitting on top of the tub.

Checking for maximum radial acceleration error at the furthest possible distance of the model piles from the centre of rotation ($5d$, or 75mm, from the sample boundary), and assuming the model acceleration acts at a distance of two thirds the length of the pile from the pile head (for minimum under or over stress due to vertical acceleration error see Section 3.2.2.1 Vertical Acceleration Field), the

maximum overstress for this model geometry would be 0.7% which is sufficiently negligible.

4.3 Apparatus Design and Development

New apparatus were required to create the model piles and to carry out loading tests in flight. As the soil sample is prepared before the piles are constructed, it was decided the best way to install them would be to first bore a hole and then cut ribs into the profile. In this way, it would be necessary to obtain a liquid material that could be poured down the hole and set to reliably take the shape of the pile.

The first problem was to choose a suitable factor of g . Due to the small size of the ribs, this factor needed to be low enough to ensure the size of the model would be large enough to be constructed at model scale. However, to get meaningful results from the experiments, the piles had to be loaded to failure in the centrifuge. For this reason, they couldn't be so large that their ultimate capacity would be too high for the loading equipment to be able to cause failure.

4.3.1 Pile Installation

In constructing the model ribbed pile, it was decided the only way to form the correct shape would be to cut a borehole and rib profile, the pile then being cast using a resin that could be poured down the borehole. Mixing of the resin could not be done in the centrifuge, so construction of the piles had to be carried out at $1g$ before putting the model into the centrifuge. The soil sample needed to be moved from the consolidation press to the centrifuge in as short a time as possible to prevent any significant changes in soil stress and to avoid drying out of the clay. For this reason, it was considered the simplest way to create the ribbed pile borehole would be first to cut a straight pile borehole through the conventional method of using a thin-walled steel tube. The rib profile would then be cut using a separate rib-cutting tool. To make the cutting of the rib

profile as quick and efficient as possible, it was decided the tool should be the length of the pile shaft with teeth located along that length, creating the profile by being flicked out to cut into the clay surface and rotated around inside of the borehole. Thus a guide was required for both the pile-cutting and rib-cutting tools, and a mechanism needed to be designed for the control of movement of the rib-cutting teeth from outside the borehole.

4.3.1.1 The Pile Cutting Tool

The main limitation in choosing the diameter of the thin-walled steel tube, and therefore the model pile diameter, was availability from the manufacturer. The diameter of the pile would dictate the rib dimensions, which needed to be large enough to be constructible at model scale yet small enough to represent realistic prototype dimensions. Ribbed piles constructed in the field were 750mm core diameter, 20m deep, and had rib dimensions of up to 100mm outstand, 75mm thickness, 250mm spacing. In the early stages of apparatus design, it was thought reasonable to assume that it would not be possible to guarantee reliable construction of model ribs with a dimension of less than 1mm outstand. 750mm diameter ribbed piles constructed at prototype size with 50mm ribs had an outer (rib) to inner (pile) diameter ratio of 1.133. To be able to reproduce similar rib to pile diameter ratios at model scale, and assuming a preliminary rib outstand dimension of 1mm, the model pile diameter required was 15mm.

The largest diameter stainless steel tube available from the chosen manufacturer, and also available with a sufficiently thin wall thickness to be able to use to cut into the clay, was 15mm in diameter and had a wall thickness of 0.3mm. With this and the preliminary rib outstand dimension in mind, a factor of g had to be chosen for the tests such that the model piles could simulate the size of the ribbed pile at prototype scale, and a reasonable size load would be sufficient to cause failure of the pile.

The chosen thin wall steel tube was attached to a wider, thicker section of brass tubing with a bar handle at the end (Figure 4.6). All handling of the tool could

then be done using this stronger section, the steel section being quite fragile due to its thinness. For this same reason a plastic tube was chosen that could be used as casing to protect the tool when it was not in use. Finally, a metal bar was adapted to clean the cutting tool out of the clay that would inevitably get stuck inside it when cutting into the soil sample.

4.3.1.2 The Rib Cutting Tool

A tool was needed to cut the shape of the ribs quickly and efficiently once the hole had been bored. With this in mind, a mechanism was designed so that the tool could be put down the borehole without touching the sides, and, once in place, the cutting teeth could be flicked out into the clay and rotated so as to cut the rib profile (Figure 4.7 and 4.8). Using this method, the minimum dimensions of the ribs could be reduced to 0.5mm in thickness and outstand so as to ensure they were constructible, lower than originally envisaged. This in turn dictated the gravity scale so that the dimensions could be similar to the prototype piles that had already been tested in the field. The result is a model pile of 15mm diameter and 200mm length, with the factor of g chosen to be 50. This represents a pile of 750mm diameter and 10m depth at prototype scale. With this size model pile, ribs of 1mm outstand and 1mm depth would represent ribs of 50mm outstand and 50mm depth at prototype scale. The initial pile cutting tool was designed to cut model ribs of 1mm outstand, 2mm depth and 8mm centre spacing (50mm outstand, 100mm thickness, and 400mm spacing at prototype scale).

To check that the mechanism would cut the ribs cleanly and that no other aspects of the tool would cause unforeseen problems with their construction, a preliminary version of the tool was constructed. This initial pile cutting tool was used to cut a short borehole without a guide in a spare sample of clay and the preliminary rib cutting tool was then put down the borehole manually and the mechanism tested. The teeth of the rib cutting part of the tool cut into the clay with ease, and rotating it around the inside of the borehole could be done manually without using much force. It was observed that if the tool was rotated

anticlockwise such that the teeth followed the vertically moving part of the tool around, the clay that was cut away from inside the borehole would be caught in the gap where the vertically moving part was narrower compared to the other plates. Once the ribs were cut, resin was poured down the ribbed borehole and left to set before being cut out to observe the result. The ribs were found to be even and well formed (Figure 4.9).

4.3.1.3 The Guide

To cut the pile profiles efficiently and accurately, a guide was required to make sure the boreholes were cut vertically, to the correct length, and in the correct location for the loading apparatus to be able to transfer load to the centre of the pile head. It was decided the guide would be incorporated into an aluminium plate that could be attached to the top of the tub to keep it in the exact same location for each test. The guiding part of the apparatus would then consist of two holes located above the pile locations, with a tube between the base of the plate and the surface of the clay to keep the pile cutter in line as it passes through. As the exact height of the sample would not be known until after consolidation was complete, the height of the guide needed to be adjustable. Thus the guiding tubes were made to screw into the holes in the plate so that they could be moved up and down as necessary. Screw fittings located above and below the hole were added to tighten the tubes to the plate once they were at the correct height (Figure 4.10).

As it became apparent that the thin wall steel tube of the pile cutting tool was fairly fragile, and that a great deal of force would be needed to cut into 200mm of such stiff clay, it was decided to cut the borehole in two stages. The thin wall steel tube was attached to a thicker and thus much sturdier brass tube, which was also slightly wider in diameter. By attaching fittings that only the thin wall steel tube could pass through to the bottom and top of the guide, the pile cutting tool could be guided into the clay sample halfway, the wider brass section being stopped on reaching the top fitting. Having rotated the pile cutting tool and taken it out of the sample, a metal bar was adapted to use for cleaning out the clay

inside it, ready for cutting the second section. To do this, the top fitting could be taken off and the tool guided back through the bottom fitting, that being the diameter of the thin wall steel tube. With the top fitting taken off, the brass section of tube would then reach the top of the guiding tube which would be the same diameter as this brass section, and the tool could then be guided through to cut the rest of the length of the pile.

With the straight borehole cut, the guiding apparatus would then need an attachment to adapt it to guide the rib cutting tool. This tool was designed to be the length of the pile, so there would be 200mm length of rib cutting tool to pass down through the guide before the straight section of the tool would reach the top of the guiding tube. For this reason, an attachment was created that could be screwed into the top of the guiding tube in the plate. This would extend the guiding tube upwards so that the bottom of the tool would not reach the top of the borehole before the bottom of the guidable part of the tool had reached the top of the now extended guiding tube. This is shown in Figure 4.11, with the guide extension indicated in red, and the rib-cutting tool in blue. The guidable part of the tool is shown in two positions; (b) at the point where it first passes through the guiding tube, and (c) at the point where the tool reaches the bottom of the borehole.

4.3.1.4 Casting The Piles

Due to the intricate nature of casting the profile of the pile shaft, it was decided a resin would be the most suitable material with which to cast the piles. Sika Biresin G27, a two part “fast cast” polyurethane resin was chosen due to its suitability to forming small intricate shapes such as the model pile ribs, and its ability to set quickly as the model piles would need to be solid before being subject to the stresses due to radial acceleration in the centrifuge.

4.3.2 The Test

The piles were intended to be loaded to failure, that generally being considered to be a settlement of 10% pile diameter for axial loading, the point at which the base is fully mobilised (Burland & Cooke, 1974). Loading was then to be continued beyond failure, particularly as it was unsure whether to consider the pile diameter to be the inner diameter of the pile surface or the diameter of the ribs. In carrying out the tests, sufficient apparatus was needed to apply and measure the required load to reach failure. A suitable method of measuring the pile settlement was also needed.

4.3.2.1 Loading Apparatus

It was decided the simplest and most reliable way to load the piles axially would be by locating a reservoir directly above each pile. Once the model is in the centrifuge and the pore pressures in equilibrium, the reservoirs can be filled with water and a loading pin located below each one transfers the load of the water to the pile below. A similar method had been previously employed at City University London (Qerimi 2010) (Figure 4.12). Thus, adapting existing pile loading apparatus was considered for use in this research project.

The first consideration was capacity of the reservoirs. The maximum amount of water that could fill the reservoirs without risk of overflow was little more than a litre. At 50g this would give a maximum load of 613N (Table 4.1 and Figure 4.13), though this was likely to be closer to a 40g value of 491N due to the reservoir's distance from the centre of rotation. This was thought unlikely to be sufficient to cause failure of the piles in these tests, and, subsequently, ways of increasing the reservoir capacity were considered. The weight of the existing reservoirs was also taken into consideration as they were already quite heavy (0.726kg, or 363N at 50g), and it was preferential to make sure this weight was not increased in creating a larger capacity reservoir, or better still reduced. This was because a heavier reservoir would require a stiffer spring to prevent any significant increase in the downward movement required to position the loading

apparatus correctly for loading in the centrifuge, the correct position being just above the pile head. The apparatus was designed to require a small amount of movement before the loading pin made contact with the pile and this would be achieved by starting to fill the reservoirs to further compress the spring. With a less stiff spring, less water would be required in the reservoir to reach this position and thus a greater proportion of the reservoir volume would be available to fill with water for loading of the pile. Given calculations of predicted shear strength in the soil (Tables 4.2 and 4.3, and Figure 4.14) and subsequent likely shaft capacities (Tables 4.4, 4.5, 4.6, and 4.7, and Figure 4.15), it was important to maximise the loading capability of the reservoirs.

Undrained shear strength S_u was calculated using critical state soil mechanics as outlined in A. M. Britto & M. J. Gunn (1987) in order to give the predictions for likely shaft capacities and thus aid with sizing of the reservoirs, and design of the springs.

Undrained shear strength can be defined as half the deviator stress:

$$S_u = \frac{1}{2} q'_f \quad \text{Equation 4.1}$$

In critical state soil mechanics, the deviator stress is equal to the average effective shear stress factored by a mobilisation factor:

$$q'_f = M \cdot p'_f \quad \text{Equation 4.2}$$

This can then be substituted back into Equation 4.1, giving:

$$S_u = \frac{1}{2} M \cdot p'_f \quad \text{Equation 4.3}$$

Where q'_f is the deviator failure stress, p'_f is the average effective shear stress and M is a mobilisation factor on the soil strength which is constant for a given soil. M is 1.00 for Kaolin Clay (Table 4.2).

The generic loading-unloading lines for any undrained soil as defined in the $\ln(\text{effective stress}) - \text{specific volume}$ plane ($\ln(p') - V$) are given by the following formula:

Compression or loading line (for normal consolidation):

$$V_\lambda = V - \lambda \cdot \ln(p') \quad \text{Equation 4.4}$$

Swelling or unloading line (for overconsolidation):

$$V_\kappa = V - \kappa \cdot \ln(p') \quad \text{Equation 4.5}$$

Where V gives the location of the line on the $\ln(p')$ - V plane, and $-\lambda$ or $-\kappa$ give the slope of the line. These general equations can be used in specific loading situations for soils with specific properties.

The specific equation for the isotropic normal consolidation line is given by:

$$V_c = N - \lambda \cdot \ln(p'_c) \quad \text{Equation 4.6}$$

Where N defines V_c at $\ln(p'_c) = 0$, and is 3.26 for Kaolin Clay in these tests, and p'_c is the effective stress at the end of normal consolidation, also defined as the maximum stress applied to the sample.

The swelling line is given by:

$$V_\kappa = V_c - \kappa \cdot \ln(p'_c) = V_0 + \kappa \cdot \ln(p'_0) \quad \text{Equation 4.7}$$

Where V_c and p'_c are the specific volume and effective shear stress at the end of normal consolidation, and V_0 and p'_0 are the specific volume and effective shear stress at the end of overconsolidation.

The critical state line, for shear failure of the soil is then given by:

$$V_0 = \Gamma - \lambda \cdot \ln(p'_f) \quad \text{Equation 4.8}$$

Where Γ is a constant, 3.14 for Kaolin Clay in these tests.

The critical state line equation can be rearranged to give:

$$p'_f = \exp [(\Gamma - V_0) / \lambda] \quad \text{Equation 4.9}$$

And Equation 4.7 used to V_0 substitute into Equation 4.9:

$$p'_f = \exp \{ [\lambda \cdot \ln(p'_c) - \ln(N) + \ln(\Gamma) - \kappa \cdot \ln(p'_c) + \kappa \cdot \ln(p')] / \lambda \} \quad \text{Equation 4.10}$$

By substituting Equation 4.10 into Equation 4.3, the undrained shear strength was calculated, (Table 4.3):

$$S_u = \frac{1}{2} \cdot M \cdot \exp \{ [\lambda \cdot \ln(p'_c) - \ln(N) + \ln(\Gamma) - \kappa \cdot \ln(p'_c) + \kappa \cdot \ln(p')] / \lambda \} \quad \text{Equation 4.11}$$

Table 4.3 was used to provide a predicted shear strength profile for the clay sample (Figure 4.14). This was used to calculate the range of potential shaft and bearing capacities for the model piles, and thus design and develop suitable loading apparatus.

Due to the constrictions in the size of the piles previously mentioned, the maximum possible load estimated for shaft capacity was fairly high (Table 4.8 and Figure 4.15). To make sure the reservoirs would load the piles sufficiently, possible capacities were calculated and it was decided that a container with a minimum volume of 3 litres would be necessary, which would give a maximum load of over 1000N (Table 4.1 and Figure 4.13).

As the reservoirs become heavier in the centrifuge's acceleration field, springs of a suitable stiffness and size to compress under this increase in weight were acquired for the reservoirs to sit on. Due to this increase in weight, the reservoirs needed to remain relatively light compared with their capacity. For this reason, PVC tubing was first considered as a suitably light material for their construction. It was found to be an expensive material, and, being only available as tubing, a suitable bottom for container would need to be created and attached. Other materials were considered until, eventually, manufactured plastic bottles were suggested as a reservoir container. It was found that 3 litre containers existed and a sample bottle was tested to check it could take the hydraulic pressure associated with 300mm head at approximately 40g, that being equivalent to 12m head at 1g, or 120kPa. The bottle was attached to a pressure transducer applying a controllable air pressure that could be gradually increased. This was done until failure of the bottle, which occurred at approximately 600kPa, much higher than the expected hydraulic pressure for maximum loading of the piles. Holes were drilled in the centre of the bottom of each bottle, and piping attached and connected to solenoid valves so that they could be drained to unload the piles if necessary (Figures 4.16). These were also used to empty the bottles after each test. A simple guide was constructed to hold the bottles vertically in place as they move downwards during testing (Figure 4.17).

In choosing an appropriate compression spring on which to place the reservoirs, it was decided that the load transferred to it from the reservoirs due to the acceleration field would need to be close to its capacity, so that when water flows into the reservoirs they start to load the piles virtually straight away, rather than the springs.

Loading pins were attached underneath the fitting for draining the reservoirs, extending through the middle of the spring and a hole into the aluminium plate on which the reservoirs sit, and down to the head of each pile. The apparatus was designed such that the increased weight of the reservoirs would compress the springs causing the reservoir and loading pin move down by the same distance by which the length of the spring was reduced. At this point, before loading, it was required that the loading pin would be located just 3-5mm above the pile head, so that loading of the piles could start as soon as possible after water is released into the reservoirs, and the loading capacity of the reservoirs kept to a maximum. The spring design to achieve this maximum loading capacity can be seen in Tables 4.9, 4.10 and 4.11.

To check that the calculated downward movement of the loading pin was correct for the springs chosen, the apparatus were bolted onto a tub before the first test with a camera and light attached to observe the movement as the centrifuge was spinning up. This check confirmed that the movement was as expected. Flow rates into the reservoirs were also tested during this spin up to make sure the rate of loading would be the same for each of the two pile tests in any one centrifuge test. In the preliminary test using existing loading apparatus, it had become apparent that this was not the case, so this gave the opportunity to change the rate of the inflow in the centrifuge control room and make sure the water flowed at the same rate.

4.3.2.2 The Water Table

A variable standpipe was used to control the water table in the model soil during testing in the centrifuge (Figure 4.18). The height of the standpipe can be changed to suit the height of the soil sample, which may not be exactly the same for each test. The standpipe is connected to the bottom of the tub where a drainage plate (Figure 4.19) enables control of the hydrostatic pressure by applying a predetermined head of water. In these tests, the soil sample was designed to be 300mm in depth and fully saturated. Thus a head of approximately 150 kPa, at 50g, needed to be applied by the variable standpipe

giving a hydrostatic pore pressure distribution through the height of the sample and a water table about 5mm below the clay surface in the centre of the sample due to the radial acceleration field in the centrifuge.

4.3.2.3 Instrumentation

Three types of instrumentation were used in these tests for gathering relevant data; pore pressure transducers (PPTs), linearly variable differential transformers (LVDTs), and load cells.

The PPT type used in these tests was PDCR 81. They are fitted with a porous ceramic front element to measure pore pressures at different levels in the soil sample. This was specifically of use before the loading stage, so that the change of the pore pressures in the sample when it is put in the centrifuge could be seen. Before loading could take place, the stresses in the soil sample needed to be in equilibrium with the radial acceleration such that no further change in stress was visible, and it could be seen where this occurs at different levels within the sample from the data recorded by the PPTs. Similarly, a PPT with the porous stone removed was used to monitor the water level in the standpipe to check the correct head of water was being applied to the sample to simulate the water table.

The load cells were Strain Gauge Load Cells. Located within the loading pin, they were used to measure the load applied at the pile head. They can measure up to 2.5 kN in tension and compression.

The LVDT type used was Solatron DC05 ± 5 mm. These were used to measure the pile settlement and movement of the soil at the surface. Two LVDTs were located above a thin aluminium plate which is connected to the pile head, one on either side of the pile head (Figure 4.20), and an average of the readings recorded by the two was taken.

Calibration and installation of all instrumentation is discussed further in Section 5.1.

CHAPTER 5: TESTING PROCEDURE

5.1 Preparation of instrumentation

Before each test, all instrumentation was calibrated using arm mounted junction boxes in the centrifuge with filters and amplification, slip rings, and logging system. PPTs were calibrated using a pressure transducer which is regularly calibrated against dead weight system. LVDTs were calibrated using a micrometer. Load cells were calibrated using a Budenberg.

5.1.1 PPTs

The PPTs were inserted into a calibration chamber filled with distilled water (Figure 5.1), which was then de-aired using a vacuum pump before calibration of the PPTs. To calibrate the PPTs, they were each connected to a different channel in the arm mounted junction box in the centrifuge (Figure 5.2), with the centrifuge computer reading an output as a number between 0 and 63500. In these tests, channels 22, 23, and 24 were chosen for the PPTs for the sample, and channel 25 for the standpipe PPT. The calibration chamber was connected to a pressure transducer which is regularly calibrated against a dead weight system. Known pressures were applied to the PPTs via the calibration chamber, and their outputs at these pressures noted. By plotting this data on a graph, an equation for the line of best fit could give a gradient and intersect. These were inputted into the centrifuge computer before the each test so that the output could be converted directly and recorded on the computer in KPa.

5.1.2 Load Cells

The load cells were connected to pre-decided channels in the arm mounted junction box, just as the PPTs were. Channels 29 and 30 were chosen for these tests. The load cells were calibrated individually with loads applied

incrementally up to 1000N using a Budenburg (Figure 5.3). Just as with the PPTs, each load corresponds to an output on the centrifuge computer and these could be plotted giving the information required for the centrifuge computer to be able to convert the output of these load cells to a measurement of load in Newtons during the test.

5.1.3 LVDTs

Two LVDTs were used to take measurements of the pile head settlement of each pile, and a fifth LVDT to take measurements of the level of the clay surface in the centre of the sample. Each of these were calibrated using a micrometer for a range of 11mm, with care taken to ensure the pin stayed in the 0 to 63500 output range for the entire distance. Plotting of the distance against these outputs gave information that could be inputted into the centrifuge computer as with calibration of the PPTs and load cells, so that data recorded during the test was in micrometres.

5.2 Preparation of the sample

Preparation of the soil sample was a lengthy process compared with the time taken to construct the model and carry out the test, taking up to two weeks. This time was largely taken up by the consolidation process.

5.2.1 Consolidation of the clay sample

Consolidation of the clay took place in a consolidation press, going in as a slurry at 120% water content. This was created by mixing the correct proportions of kaolin clay powder with distilled water in a ribbon blade mixer, and carefully poured into the steel tub to avoid air bubbles being trapped. The volume of this clay slurry was much greater than that of the model sample which should have a water content of 40% by the end of the consolidation process. For this reason, a

300mm extension was bolted to the top of the steel tub so that all the slurry could fit without overflow.

Before the slurry was put into the tub, a 3mm sheet of porous plastic with the exact diameter of the tub was put into the bottom of the tub. This prevented clay from getting into the drainage channels cut into the base of the tub which will ensure clear flow of water out of the sample during consolidation, and from the standpipe to the sample during the test. Above this, a piece of filter paper was placed to stop the clay from sticking to the porous plastic. The sides of the tub and extension were then spread with Ramonol, white grease, so that there could be ease of movement of the clay along these surfaces during consolidation, and the effect of boundary conditions on the centrifuge test could be minimised. After the tub and extension had been prepared, the slurry could be put into the tub up to the required level so that the sample was the correct depth for the designed experiment when the consolidation process is complete. On top of the clay slurry another piece of filter paper was placed, followed by a second sheet of porous plastic, again with the exact diameter of the tub. This second sheet of porous plastic ensured clean contact between the clay slurry and the piston of the consolidation press without the slurry seeping out on the first application of low pressures, the piston being very slightly smaller than the diameter of the tub. Before any pressure was applied to the clay surface via the piston, the two valves at the bottom of the tub, which were closed while the clay slurry was being put into the tub, were then opened and plastic tubes connected to each one with the opposite ends put into a bucket. This enabled water to exit the soil from the bottom of the sample during consolidation, and from the top of the sample through the tiny gap between the edge of the piston and the side of the tub.

As the clay slurry was well over its liquid limit, it was important to raise the pressure applied by the piston in the consolidation press very little and very slowly to start with. In general, the pressure initially applied was no more than 10kPa, and increased at regular intervals (25kPa, 75kPa, 125kPa, 250kPa, 500kPa), usually twice a day so that it would take 3 or 4 days to reach the maximum pressure of 500kPa. A displacement transducer was located above the piston to observe vertical movement of the sample. Consolidation could be

observed to be complete when the data recorded by this transducer showed no further vertical movement. It would normally take 2 or 3 days to reach this zero vertical movement. The consolidation pressure could then be reduced gradually to 250kPa, usually over the space of a day, and again the vertical movement due to swelling was observed using the displacement transducer. The overconsolidation process did not normally take longer than a day. The sample was then ready for installation for the PPTs.

5.2.2 PPT Installation

PPTs were kept in the calibration chamber between calibration and installation so as to prevent air from getting into the porous stone. Specially adapted apparatus were used for installation of the PPTs. Before beginning, a syringe was filled with clay slurry and, to prevent clay drying out at the tip of the syringe, it was placed in a plastic wallet also filled with clay slurry.

After taking out the bolt covering the installation port in the steel tub, the guide was screwed on in its place. The clay cutter, which was a steel tube, was then inserted up to the correct depth. A line was marked before inserting the clay cutter so that the end of the cutter reached the centre of the sample. The cutter was rotated so that the clay it has cut into was sheared at the end of the cutter, and when the cutter was withdrawn the clay came out with it. As soon as the cutter was taken out, the hole that was left in the soil would start to close up due to the pressure of 250kPa still being applied at the top of the sample by the consolidation press. For this reason it was important to carry out the installation of the PPT in as short a time as possible.

The guide was removed from the installation port, and a specially adapted fitting attached. The PPT was then taken out of the consolidation chamber and inserted into the installation tool; a half tube with a handle at one end. A tiny amount of clay slurry was applied to top of the PPT to avoid air getting into the porous stone, and it was put at the end of the half tube with the cable inside its length. The installation tool was then inserted into the installation port through the

fitting, the PPT going first into the cut hole to the centre of the sample. When the centre was reached, the installation tool was removed leaving the PPT inside the sample. The syringe was then taken out of the plastic wallet and inserted into the hole until it reached the back of the PPT. Great care was taken to ensure the tip of the syringe did not touch the sides of the hole as it was inserted, as this can cause clay from the sample to get stuck at the tip and block it. When the back of the PPT was reached, the syringe was gradually withdrawn at the same time as injecting clay slurry into the sample, so that eventually the tip of the syringe would reach the fitting at the installation port and the hole would be filled with clay slurry. The fitting located on the cable of the PPT was then screwed into the fitting at the installation port, closing it up, and installation of the PPT was complete.

5.2.3 Preparation for model construction

When swelling of the sample, calibration of all instrumentation was complete and all PPTs were installed, the sample was ready to be taken out of the consolidation press for construction of the model and, ultimately, carrying out of the test. It was important to keep the time between taking the sample out of the consolidation press and putting the completed model into the centrifuge to a minimum to avoid significant changes in the soil stresses, and particularly to prevent drying out of the sample. For this reason, all equipment required for construction of the model were made ready before the taking the sample out of the consolidation press.

The first step in taking the sample out of the consolidation press was to remove the water sitting on top of the piston of the consolidation press. The tubes that allow flow of water out of the sample were then disconnected and the valves closed. The pressure was reduced to zero and the piston taken up above the top of the extension so that the tub could be taken out. The extension was then removed from the tub and the porous plastic on the surface of the sample taken out. The filter paper under the porous plastic was peeled off manually, using a scraper where necessary. The surface of the clay sample was then spread with a

thin layer of oil, and grease applied where the surface meets the side of the tub. This is done to prevent drying out of the sample, in particular shrinking away of the sides of the clay sample from the inside of the tub. The sample was then now ready for construction of the model.

5.3 Construction of the model

5.3.1 Construction of the model piles

Before construction of the model piles could take place, the exact distance of the top of the sample from the top of the tub was measured. The model was designed for a sample depth of 300mm, but as it can be difficult to measure the exact depth of the clay slurry when it is put into the tub before consolidation, this depth is not always achieved. The actual depth achieved varied between 295mm and 305mm so, once the exact depth was known, the guide for the pile cutting apparatus was adjusted to ensure model piles of the correct length were constructed.

The plate of the guide was bolted to the top of the tub to keep it in place during construction of the model piles. Fittings were attached to the top and bottom of the guide, guiding the pile cutting tool to cut half the length of the pile. The tool was rotated to ensure the clay that was being cut was sheared off at the bottom. The clay that was extracted was then cleaned from the tool before the fitting at the top of the guide was removed to enable the full length of the pile to be cut.

Once both the straight boreholes were cut, the fittings at the bottom of the guide were also removed and a further attachment to guide the rib-cutting tool was connected to the top of the guide. The rib-cutting tool was passed through the guide and into the borehole, and screwed into the top of the guide attachment to lock it into place. The handle at the top of the rib-cutting tool was then pushed down, forcing the teeth of the tool into the side of the borehole, and rotated anticlockwise to cut the rib profile. When the rib profile was cut the handle was

pulled up again so that the teeth retract, and the tool was unlocked and taken out. Once the profiles of both piles were complete, the plate of the guide was removed from the tub, and the boreholes were ready for the forming of the piles.

The resin was prepared before the tub was taken out of the consolidation press. 50g of filler and of each part of the resin were weighed out in plastic cups and left ready for mixing. After the cutting of the piles was complete and the guide removed from the tub, the resin could be mixed for the forming of the piles. Part A was first mixed with the filler, then Part B mixed in. The 2 parts start reacting straight away so the resin was mixed thoroughly and quickly in order to pour as soon as possible. The resin was poured directly into the borehole, slowly and steadily so as to avoid air bubbles forming while the resin set.

After the resin was poured into both boreholes, the pile head attachments were placed into the centre of each pile, the spacers connected to the aluminium plates to hold the attachments in place until the resin was set. The resin took approximately 5 minutes to set completely. In the meantime the model was prepared for testing.

5.3.2 Preparation of the model for testing

The LVDT apparatus was bolted to the tub (Figure 5.4) and the LVDTs adjusted so that there was plenty of space for the pins to move up and down. The tub was then weighed, as was the loading apparatus before being put on top of the tub over the LVDT apparatus. Care was taken to ensure all cables coming out of the apparatus from instrumentation were kept safe from getting in the way of the loading pins or getting stuck between the apparatus and the side of the tub, also with enough cable kept loose to enable movement of the instrumentation in the case of the load cells. The counterweight at the opposite end of the swing arm to the swing was then adjusted so that it would be balanced with the weight of the swing when the centrifuge was spun up.

The tub was then mounted onto the centrifuge swing and bolted onto the swing through its base plate. A camera and light were bolted onto the tub with the loading apparatus. The instrumentation was plugged into the corresponding channels on the junction box, and all loose cables tied down, including the stoneless PPT which was put into the standpipe. The plastic tube for flow into the standpipe and the inflow plastic tubes to the reservoirs of the loading apparatus were also plugged into the corresponding connections and tied down. The standpipe tube was connected to the valve at the bottom of the tub that is next to it and the valve on the opposite side was opened. The valve for controlling water flow into the standpipe, which is in the centrifuge control room, was then opened until water flowed cleanly out of the valve on the opposite side of the tub to the standpipe. This cleaned out the base of the tub. Lastly, 850ml of silicone oil was poured onto the surface of the sample via a funnel through a tiny gap in the apparatus attached to the top of the tub. This was to prevent drying out of the clay surface as the surface of the water table curves with the curvature of the centrifuge's rotation, leaving up to 15ml depth of clay unsaturated in the centre of the sample. The standpipe valve was now opened again and left open, and the centrifuge was ready to be turned on.

5.4 The Centrifuge Test

To turn on the centrifuge, the factor of gravity and the distance from the centre of the centrifuge at which that factor should act had to be inputted into the centrifuge control computer. Once this was done and the centrifuge door locked, the centrifuge was turned on using the centrifuge control computer.

5.4.1 Further consolidation of the sample

The centrifuge was left spinning for around 24 hours until the pore pressures in the soil sample have reached equilibrium. All data being recorded from the instrumentation could be observed on the centrifuge computer in either graphical

or numerical form. By observing the PPT data during this time, it could be seen when equilibrium was achieved.

5.4.2 Loading the model piles

When the stresses in the soil sample reached equilibrium, the loading test could begin. The piles were loaded one at a time by opening the valve in the centrifuge control room that corresponded to the correct reservoir in the loading apparatus. This allowed water to flow into the reservoir, the weight of which was then transferred to the pile head via the loading pin. The valve was closed when the pile had failed. Before the valve was opened, the time interval of data logging was reduced to 1 second, as overnight it was generally left on the maximum time interval of 5 minutes to keep the size of the data logging file on the centrifuge computer from being excessively large and therefore unable to fit on a floppy disc.

5.4.3 Dismantling the model

When both piles were loaded to failure, the inflow valve for the standpipe in the centrifuge control room was closed. The centrifuge was turned off using the centrifuge control computer and data logging from the instrumentation stopped.

The instrumentation and inflow pipes were disconnected from the junction box, and the bolts connecting the base plate of the tub to the swing were taken out. Any ties attaching cables or pipes to parts of the swing were taken off, and the tub and apparatus could be taken off the swing. The reservoirs were emptied and the loading and LVDT apparatus were taken off the tub. The pile heads were then observed to see in what position they had ended up, as were the pile head attachments, and photographs taken. Then the tub was emptied using clay cutters and scrapers, care being taken to extract the piles without damaging them. When the tub was empty, the sheet of porous plastic in the base was taken out and all the inside surfaces are wiped clean ready for the next test.

CHAPTER 6: EXPERIMENTAL WORK & RESULTS

Despite describing a well defined and specific testing procedure in Section 5.1, these methods and tools were continuously developed and modified during the testing period. New difficulties were encountered at different parts of the testing procedure during different tests, which had an inevitable influence on the test results and helped to refine the apparatus and overall testing procedure for following tests. Details of these difficulties and refinements will be described in this section, along with the test results.

Table 6.1 shows pile geometries for each test and results are shown in the figures for this chapter. These include:

- Pore water pressure-time graph:

This shows pore water pressures approach equilibrium as the sample consolidates in the centrifuge. Figure 6.1 shows the location of each transducer in the sample with the corresponding channel number relating to the results shown in the rest of the figures for this Chapter.

- Displacement-time graph

This shows movement of the soil with consolidation in the centrifuge.

- Load-time graph

This shows the rate of loading if each pile.

- Load-settlement graphs

These show the individual channel outputs for LDVTs recording settlement and average settlement for each pile.

Tested profiles were chosen with a view to comparison of specific geometric properties of the ribs. These will be discussed in more detail in Chapter 7.

6.1 Test JW01

The first proposed test was to load one straight pile (JW01_SP), and one ribbed pile (JW01_RP) with rib dimensions of 1mm outstand, 2mm thickness, and 8mm spacing, referred to as [1.2.8].

6.1.1 Sample Preparation

The sample was consolidated over two weeks as described in the testing procedure. Two PPTs were installed 50mm and 150mm above the base to observe change in pore pressure and assess equilibrium during consolidation of the sample in the centrifuge.

6.1.2 Model Construction

On taking the tub out of the consolidation press, it was found that the surface of the clay was slightly above the required level, despite being scraped down. For this reason, it was difficult to attach and detach the fitting for the bottom of the guiding tube to guide the pile cutter during construction of the model without disturbing the clay surface, the end of the guiding tube being much closer to the clay surface than anticipated.

It was also observed that the guide attachment for the rib cutting tool was too short, so that for a distance of approximately 20mm the tool had to be put down the borehole unguided. As it went down, the bottom of the tool reached the top of the borehole before the bottom of the guided part of the tool reached the guide, and so for 20mm guidance of the tool was relying on a steady hand. It was decided that this could easily be avoided by making the guide and guided part of the tool longer, so that it would be in the guide before the bottom of the tool reached the top of the borehole. Despite these problems, the piles were constructed successfully and the instrumentation and apparatus for testing were attached, and the model was put onto the centrifuge as in the testing procedure.

6.1.3 Centrifuge Test:

Estimates of the maximum possible capacities of both piles were made but, as it was not known exactly what the capacities would be, the testing procedure had to take this into account and it was decided to increase the load step by step simulating a traditional maintained load test. Potential capacities of the piles were calculated based on dimensions, average shear strength of the clay and possible adhesion factors, and it was found that the shear capacity should not exceed 1037N, though it would be unlikely to reach this value. Using a conservative α value of 0.8, and using the rib diameter to calculate capacity, this shaft capacity would be 830N giving an overall capacity of 996N when including the calculated end bearing capacity of 166N, well within the calculated 1177N loading capacity of the plastic bottle reservoirs (see Section 4.321). Thus it was decided the incremental loading would be eight equal steps to 1000kPa stopping at each step to let the pile settle enough to show it required more load to settle further (Table 6.2).

The two PPTs installed for this test did not give readings so it was not possible to check the water table level within the sample or assess when equilibrium had been reached. The centrifuge was stopped soon after starting up to check the PPT connections to the junction box. Connections external to the model container appeared to be set up correctly and thus the cause was assumed to be an error in PPT installation. The standpipe PPT, however, showed a maintained head of water of 125kPa (Figure 6.2), and equilibrium was instead gauged from the output of LVDT displacement (Figure 6.3). This was done by observing movement of the sample surface due to swelling during consolidation in the centrifuge until no further change in LVDT output was apparent.

The piles were loaded at increments of 125N (Figure 6.4), and with a maximum 1000N load possible, the piles failed at around 380N and 760N, the latter being reached by the ribbed pile (Figures 6.5, 6.6 and 6.7). A photograph of the settled pile heads after the model was taken out of centrifuge test be seen in Figure 6.8, and a photograph of the water levels in the bottle reservoirs of the loading apparatus after the test can is shown in Figure 6.9.

6.2 Test JW02

It was decided to carry out a second straight pile test. With this in mind, every other tooth was taken out of the cutting part of the existing rib cutting tool, so that a second ribbed pile would be tested with double the rib spacing of that tested in Test JW01; [1.2.16].

6.2.1 Model Construction

The sample was taken out of the consolidation press, and prepared for model construction as described in the testing procedure. The guide was attached to the tub and the boreholes were cut without problems. The guiding tube had been shortened so the end fitting for guiding the pile cutting tool could easily be attached and detached without damaging the top of the borehole or the clay surface.

After Test JW01, the rib cutting tool was taken apart and the guided part of the tool was replaced with a longer brass tube, long enough to be guided by a new guiding attachment that would guide the tool before entering the borehole. In replacing the brass tube, the moving parts inside the guided part of the tool were also replaced with sufficiently long parts. This altered rib cutting tool was successfully used in conjunction with the new guiding attachment to cut the ribs for this test.

The guide was removed and the resin mixed, however, it was found that the resin was not mixing as usual. Bubbles were present as the resin was mixed up, and when it was poured into the boreholes the resin expanded dramatically. Subsequently, the setting resin rose up out of the top of the boreholes and the piles were not formed properly. It was decided this must be due to the pots of resin being open for too long, and so new pots would be opened for the next test.

Despite the problems with the setting of the resin, the excess resin was wiped away and the aluminium pile heads were placed over the top of the borehole and

what resin was left formed around them. The LVDT and loading apparatus were weighed and bolted to the tub as described in the testing procedure, and the package was attached to the swing arm before turning on the centrifuge.

6.2.2 Centrifuge Test

After spinning overnight, the output from the PPTs seemed to show the water table to be lower than expected (Figure 6.10). The 0 kPa level appeared to be located between the top and middle PPTs, implying that the water table was below the top access port. The standpipe PPT, however, showed an output of 125 kPa, indicating that there should be a head of around 250mm. It was concluded the most likely reason for this lowered water table must be due to a leak from one or more of the access ports. The centrifuge was stopped and the access ports investigated. The middle access point was indeed leaking. This was due to the PPT screw fitting being too small for the connection fitting on the tub. It appeared that the fitting had been used successfully in the past by being forced on. This time, however, it did not work properly and would have to be replaced with a fitting at the correct size for the next test. The only possible solution for this test was to tighten the fitting as much as possible and restart the centrifuge. As the PPTs approached equilibrium, the outputs showed that the water table had been raised and was just above the level of the highest PPT.

Figure 6.11 shows displacement of the soil sample during consolidation in the centrifuge.

The piles were loaded, but they had not been formed properly and the resin was soft in texture and full of air bubbles. This meant the aluminium pile heads were not held rigidly by the resin, and while one took no load, the other failed to make contact vertically with the loading pin and after being loaded to approximately 300N it was pushed over (Figure 6.12, 6.13 and 6.14). As a result, the test yielded no useful results. Figure 6.15 shows the pile heads on removal of the sample after the test, including residue resin on the clay surface.

It was also noted after the test when the apparatus had been removed from the tub that the sample had been subject to shrinkage. A tiny gap between the soil and tub wall was visible all the way around the sample, and barely any of the surface oil was left. This was most likely caused by an insufficient spread of oil on the clay surface during model construction, and a note was made to check this during model construction of the next test.

6.3 Test JW03

Due to the difficulties encountered, Test JW03 was a repeat of Test JW02.

6.3.1 Model Construction

Once the consolidation process was complete, the sample was taken out of the consolidation press, and the surface was scraped down and spread with oil as described in the testing procedure. The guide was attached and the boreholes and ribs were cut with the corresponding apparatus.

New pots of resin were in storage in the centrifuge lab, ready to be opened and used for this test. When these pots were opened and a small amount mixed to test the resin before use in the test, it was found that the mixture bubbled slightly whilst setting. It was discovered that all the pots of resin stored in the lab had a “use by” date on them that was hidden by the distributor’s label. The rest of the resin available in storage was checked, but it was found that they had all been bought at the same time and had a shelf life of around three months, so the entire batch was out-of-date. With the sample ready to come out of the consolidation press, there was not enough time to order new resin for this test and the out-of-date resin had to be used. It was mixed thoroughly before pouring to minimise the presence of bubbles. This was done fairly successfully, but it was later discovered, when the piles were cut out of the sample after the test, that although the surface of the pile shafts appeared smooth, inside the piles the resin had set with lots of small, evenly distributed air bubbles.

The resin having been poured and set around the aluminium pile heads, the LVDT and loading apparatus were weighed and attached to the tub. The package was installed on the swing arm and the instrumentation was connected as described in the testing procedure in preparation for the test.

6.3.2 Centrifuge Test

When all preparation was complete and the package was ready, the centrifuge was started up and left overnight for the pore water pressure in the sample to reach equilibrium. It was immediately apparent that one of the three PPTs in the sample was not giving any output in range, although it had given good readings during calibration. On leaving the sample overnight, another of the PPTs showed extreme fluctuations in its output and was not approaching any kind of equilibrium. As it was giving output in range, and had given good readings during calibration, the most likely explanation was that air had become trapped in the sample during installation of the PPT, and so measurements were not representative of pore water pressure in the sample. Fortunately, the remaining PPT located near the top of the sample was working properly and giving reasonable readings. With only data from this PPT to observe the pore water pressure, the output implied a water table at the correct level (Figure 6.16). Equilibrium was also observed from the LVDT displacement (Figure 6.17).

The piles were loaded as described in the testing procedure and the straight pile appeared to fail just below 300N. The ribbed pile was loaded to 400N before appearing to be suddenly unloaded (Figures 6.18, 6.19, 6.20 and 6.21). When the test was stopped and the pile head observed it was evident that the aluminium pile head of the ribbed pile had twisted with loading. With this in mind and given the output from the load cell, the sudden drop in load was most likely due to the loading pin slipping off the loading point of the aluminium pile head. When the piles were taken out of the sample they were found to be broken, revealing the air bubble texture within so the result of the failed straight pile could not be regarded as a valid result either. Figure 6.22 shows the pile heads as observed on removal from the centrifuge after the test.

6.4 Test JW04

With new resin having been bought, the planned test for Test JW02 was now carried out a last time.

6.4.1 Model Construction

The sample was taken out of the consolidation press as described in the testing procedure, and the clay surface scraped down and spread with oil. The straight and ribbed pile boreholes were cut using the relevant apparatus as described in the previous two tests. New resin had been bought for this test, and it was opened and a test sample mixed before model construction to check it was mixing and setting as expected. It appeared to be working well, and was successfully mixed and poured into the boreholes. The aluminium pile heads were immediately placed at the top of the boreholes, sitting on the spacers, and the resin set around them.

As the sample came out of the press slightly lower than expected at a height of 290mm rather than 300mm, the variable standpipe had to be lowered to accommodate a lower than usual water table. It was found, however, that the bolts connecting the upper variable part of the standpipe to the lower part that is attached to the base plate had become rusty and lost their shape. They could no longer be unwound using a spanner so the standpipe had to be sawn down for this test, and a new upper variable part would need to be created with new bolts for further tests.

The LVDT and loading apparatus were weighed and attached to the tub as described in the testing procedure, and the package installed onto the centrifuge swing arm.

6.4.2 Centrifuge Test

As soon as the centrifuge was spun up it was evident that the standpipe PPT must have been installed incorrectly as it was giving an output much lower than would be expected at the bottom of the standpipe. Also immediately visible was that the same PPT that had given outputs out of range in the previous test was again out of range despite having had the wire re-connected and a reasonable output being recorded during calibration. It was later concluded that this must be because the PPT's thinner and therefore more fragile wire required additional rubber reinforcement to protect the vulnerable connection to the back of the PPT.

As the two PPTs in range settled into equilibrium it became apparent that they were approaching pore pressures lower than anticipated, suggesting that the required head of water was not being maintained (Figure 6.23). It was later found this was due to leaking at the PPT access ports. LVDT readings of displacement during consolidation in the centrifuge were also observed in as shown in Figure 6.24.

One load cell was giving results out of their range. The test was stopped after the first pile was loaded to see if changing the gain would bring it back into range, but when the centrifuge was spun up again, the load cells showed no change in output. After the test, both load cells were tested and found to be not working properly due to problems with the internal wiring. New load cells would be required to carry out further tests. Figures 6.25, 6.26 and 6.27 show the results of loading.

On taking the model out of the centrifuge, it was found that the aluminium pile head of the pile that was loaded and then appeared to become unloaded had cracked on one side (Figure 6.28) probably resulting in the loading pin slipping from the loading point on the pile head.

6.5 Test JW05

Test JW05 had to be delayed until new load cells could be sourced and purchased that were suitable for use in the centrifuge and capable of loads within the range required for these load tests. By the time the new load cells were delivered, the second rib cutting tool was also ready for use and two ribbed piles could be constructed in the same test for the first time.

6.5.1 Model Construction

With the new rib cutting tool finally ready in time for use in this test, two ribbed piles were constructed for the first time. JW05_RPa used the original rib cutting tool to cut a profile of [1.2.16]. JW05_RPb was cut to a profile of [$\frac{1}{2}$ $\frac{1}{2}$ 8]. The new rib cutting tool proved to be slightly stiffer than the original, and the profile of the cutting part of the tool seemed to scrape away part of the cut borehole surface as well as the rib profile. It appeared that mechanism forced the cutting part of the tool out slightly further than was required to cut the ribs.

6.5.2 Centrifuge Test:

As the PPTs approached equilibrium, it was observed that they were showing measurements lower than anticipated, except the standpipe which gave readings as expected. The readings also showed a gradual drop in the water table implying that although the correct head of water was being applied via the standpipe, water must be leaking from the sample. The centrifuge was stopped and water and oil appeared to be leaking from the top two access ports. On closer inspection it was observed that the rubber stoppers within the bolt connections on the access ports had split. The gap in the lower of the two was plugged with a small piece of wood, whilst the higher access port was taped up to avoid water leaking. When the centrifuge was spun up, the PPT graph showed a stable water table, though lower than required with a reading of 0kPa showing for the highest PPT. This access port continued to leak, sustaining the water at

the same level. The PPT readings at equilibrium are shown in Figure 6.29, though an issue with size of the data logging file meant that only the final 30 minutes of recorded data have been recovered. This was also the case for LDVT displacement data which is shown in Figure 6.30 for completeness.

The piles were both loaded successfully. The aim was to keep the loading rate as similar as possible for each test and whilst a steady loading rate was maintained for pile test JW05_RPa, the loading rate of pile test JW05_RPb seemed to reduce slightly as the test progressed (Figure 6.31).

From the load settlement curves it can be seen that two of LVDTs measuring settlement of the pile head showed no movement for sections of the test during loading. This is most likely because they were out of range, so average settlements recorded do not give a fully representative result. For pile test JW05_RPa, channel 44 showed no movement until a load of 700N was reached, whilst the other LVDT giving output to channel 45 had already settled by 750 μ m (Figure 6.32). It is most likely that the LVDT giving output to channel 44 was indeed settling with that connected to channel 45, but movement was only registered as it came into range.

A similar problem occurred in recorded settlement for pile test JW05_RPb. Channel 47 initially showed movement in the opposite direction to Channel 48 implying a slight twisting of the aluminium bar on which the LVDTs sit. However, after a settlement of -350 μ m, no further movement was observed despite the output from channel 48 showing significant movement (Figure 6.33). It is thought that this too has occurred due to the LDVT moving out of range beyond this value.

The affect of these will be taken into account when discussing the results. Resulting load-settlement curves are shown in Figure 6.34.

Figures 6.35 shows the level of water in the reservoirs on being taken out of the centrifuge after the pile tests and Figure 6.36 shows the end position of the pile heads. Some resin residue can be seen on the clay surface around the pile heads

in Figure 6.37. This could have caused some strengthening the soil around the pile head, and whilst this will be taken into account when commenting on the results, it is not expected that this would affect the recorded failure loads.

6.6 Test JW06

With the second rib cutting tool available and the new load cells attached to the loading equipment, this test required less time to prepare. Two new profiles were created for the cutting part of the tool. The PPT fittings were checked thoroughly ahead of this test, and new rubber stoppers attached where necessary to replace those that were split.

6.6.1 Model Construction

With two rib cutting tools now usable, two new profiles were cut for this test were [1.1.8] for pile test JW06_RPa and [2.2.16] for JW06_RPb. It was ensured that the problem of the cutting part of the rib cutting tool making contact with the borehole surface between the ribs, which was encountered in construction of model pile for test JW05_RPb, was not repeated. The new cutting part was made to be narrower with just the teeth protruding far enough to cut into the inner surface of the borehole.

Construction of the model piles was completed successfully. All apparatus and the package were weighed and installed onto the centrifuge arm as described in the testing procedure before turning on the centrifuge.

6.6.2 Centrifuge Test

The centrifuge was left overnight for the model to consolidate, but it was found that the PPTs in the sample were approaching equilibrium at a lower value than that expected, even though the standpipe PPT appeared to show the required

head of water being applied by the standpipe (Figure 6.38). Shrinkage at the clay surface (Figure 6.39) also implied a low water table.

Piles were loaded until settlement could be seen to be accelerating from the numerical output data on the centrifuge computer in the centrifuge control room, implying a fully mobilised shaft. Loading rates for the two pile test were similar but, as seen in the previous test, JW06_RPb was slightly lower and seemed to reduce slightly on loading (Figure 6.40).

Load-settlement curves showed no output from channel 44. It is assumed that this LDVT remained out of range for the entire test and so it has not been included in the results for average pile settlement for test JW06_RPa (Figure 6.41). The consequences of this will result be taken into account when discussing the results in Chapter 7. All other LDVTs performed as expected and JW06_RPb produced successful results despite twisting of the aluminium plate occurring yet again (Figure 6.42 and 6.43).

Figure 6.44 shows the water levels in the bottle reservoirs after the test was carried out and the equipment removed from the centrifuge, and Figure 6.45 and 6.46 show the final pile head positions.

CHAPTER 7: OBSERVATIONS & DISCUSSION

7.1 Observations

After each test, the model piles were taken out of the sample to observe how well they had formed when cast in the clay. Great care was taken during construction of the model piles to cut the bore and ribs cleanly without leaving excess clay in the borehole. Pouring of the resin to form the piles was also carried out slowly and steadily to ensure flow into the rib profile, which was as small as 0.5mm by 0.5mm for one of the tests. Despite this, it could not be guaranteed that every pile would form exactly as expected, so a visual inspection was required to understand how the size and shape of the formed pile relative to the design might affect the results.

The diameter of each pile shaft was measured with a micrometer in two locations; close to the top of the pile and close to the bottom. None of the formed pile shafts were a perfect cylinder, so two measurements were recorded at each of these locations; a maximum and minimum diameter. An average pile diameter was taken from the four recorded measurements, so that analysis of the expected capacity associated with these dimensions could be compared to the test results. A similar procedure was adopted for measurement of the rib diameter, or “effective” pile diameter.

Measurements taken and the subsequent calculations can be seen in Table 7.1. Failure loads from the pile tests carried out in the centrifuge are shown in Table 7.1 as “measured pile capacity from centrifuge test”. These are taken from the load-settlements curves in Figure 7.1. Only the model piles that yielded useful test results have been included for discussion in the chapter.

7.1.1 JW01_SP

Pile test JW01_SP was the only straight pile test to successfully yield a result. With a measured diameter of 16.22mm, compared to a design diameter of 15.00mm, the formed pile was considerably wider than the design pile (Figure 7.2). From Table 7.1, the calculated shaft capacity was found to be 922N by calculating the pile shaft surface area and multiplying by the average shear strength, assuming the average adhesion between the clay and pile shaft was equal to the average undisturbed shear strength of the clay and so α was equal to 1). The test result showed the pile to fail at 380N (Figure 7.1), and the calculated end bearing capacity was 194N. Assuming the difference gives the shaft load failure, or “Test shaft capacity” as shown in Table 7.1, this gives a shaft capacity of 186N, considerably lower than 922N. If the ratio between is taken to be α for this pile, then $\alpha = 0.20$. This is substantially lower than the literature would suggest, particularly comparing with London Clay in which α tends to lie between 0.3 and 0.6. This difference may relate to a difference in the way the resin surface interacts with the clay compared to concrete.

Given that these tests all use resin piles, the results can be compared with a view that the material interaction with the soil should be similar for all tests with the main difference being the rib geometry. A reduced average shear strength and therefore pile capacity could be explained by a lowered water table, which occurred to some degree in all tests.

7.1.2 JW01_RP

Pile test JW01_RP was the first successful ribbed pile load test with a profile of [1.2.8]. This pile disappeared from the lab after being left on display for a tour of visiting academics, and therefore could not be measured. To give a more accurate representation, an average of the measurements taken of the other tested ribbed piles was used to calculate shaft and end bearing capacity for this pile. This gave an assumed pile shaft diameter of 16.31mm. A similar approach was

used to give the outer diameter of the ribs, or “effective” diameter. Measurements were taken from test piles JW05_RPa and JW06_RPa and averaged, these being the two other test piles with a design rib outstand of 1mm. The result was an effective diameter of 17.76 implying the outstand of the ribs was 0.72mm, less than the design.

In the same way a value for α was calculated for test pile JW01_SP, this was calculated for JW01_RP using two different measurements of pile diameter and therefore giving two potential α values (Table 7.1). The first α was calculated using the smaller internal pile shaft diameter giving a value of 0.60. By using the larger external rib diameter or effective diameter, a second value of α was calculated to be 0.55.

7.1.3 JW05_RPa

Test pile for test JW05_RPa was constructed using the same cutting plate as JW01_RP, the only difference being that every other tooth had been taken out effectively doubling the rib spacing (Figure 7.3). This gave a profile of [1.2.16]. Using the same method as for previous tests, the two α values were established; 0.64 using the internal pile diameter, or 0.59 using the effective diameter. The failure load was 800N.

7.1.4 JW05_RPb

A profile of [1/2.1/2.8] was cut for pile test JW05_RPb, the first using the second rib cutting tool. On removing the model pile from the sample after the test, however, it was noted that the shape of the pile shaft was somewhat distorted (Figure 7.4). The ribs had also not formed all the way around the pile shaft and appeared to be considerably smaller than the 0.5mm thickness and outstand as designed. This was confirmed when the diameters measurements showed the average outstand to be 0.2mm, less than half the design outstand.

The measured diameters varied considerably, the internal shaft diameter varying from 15.78mm to 17.79 and the effective diameter from 16.27mm to 18.08mm. The non-uniform profile around the shaft was taken into consideration when calculating and commenting on the α values. From the failure load of 730N an α value of 0.55 was calculated using the average internal pile diameter of 16.66mm, and an α value of 0.53 was calculated using the average effective pile diameter of 17.07mm.

7.1.5 JW06_RPa

Pile test JW06_RPa loaded a pile with profile [1.1.8], cut using the original rib cutting tool. On removal from the sample after the centrifuge test, the pile was found to be well formed with just a few small gaps visible where the resin had not quite filled the profile of the ribs (Figure 7.5). With a recorded failure load of 670N, the average measured pile diameter, 16.15mm, gave an α value of 0.54, and the average measured effective pile diameter gave an α value of 0.47.

7.1.6 JW06_RPb

Pile test JW06_RPb tested the first and only pile with a 2mm outstand, the profile being [2.2.16]. This was also the second profile cut using the second rib cutting tool. The formed pile was observed to have poorly formed ribs in several locations with air bubbles forming and narrowing the pile shaft diameter where ribs should be widening it (Figure 7.6). It is most likely this was caused by a lack of care when pouring the resin into the borehole to form the pile.

The measured dimensions take into account only the formed ribs so the capacity is likely to be less than that calculated. Assuming the failure load of 690N would be higher were the ribs better formed, the value of α could also be expected to be higher than calculated. The α values calculated were 0.54 using the internal pile diameter, and 0.47 using the effective pile diameter (Table 7.1).

7.2 Geometry comparison

All ribbed piles tested as part of this project have shown a huge increase in overall pile capacity relative to the equivalent straight shafted pile, that increase varying from 76% to 122%. The calculated values of α indicate the relative difference in shaft capacity. The highest calculated value of α , 0.64 for JW05_RPa, is three and half times that for the similar straight shafted pile, 0.2.

The pile tests were designed such that it was possible to compare each rib geometry independently as tests were carried out on model piles with similar geometries apart from a single geometrical aspect which would be different. These will be discussed here.

7.2.1 Rib outstand

To compare the effect of the rib outstand dimension, pile test JW05_RPa with profile [1.2.16] and test JW06_RPb with profile [2.2.16] were considered. These two piles share the same rib dimensions, the only difference being the outstand. The pile tested for JW05_RPa failed at 800N, and that for JW06_RPb at 690N. The pile with the larger outstand failed at a lower load. The calculated values of α are also higher for the 1mm outstand pile at 0.64 or 0.59, compared with 0.54 or 0.47 for the 2mm outstand. As described in Section 7.1.6, it may be expected that the model pile from test JW06_RPb would have a higher capacity and therefore higher value for α than recorded in this test, though the results would imply that a larger effective diameter does not necessarily offer a pile a greater shaft capacity.

7.2.2 Rib thickness

Model piles of 8mm design spacing and 1mm design outstand were tested for pile tests JW01_RP and JW06_RPa, the only variable in rib geometry being the thickness. This was designed to be 2mm for test JW01_RP, which failed at

760N, and 1mm for test JW06_RPa, which failed at 670N. Both piles were well formed so it can be assumed that these are comparable results. The failure loads suggest that a thicker rib offers the pile a higher capacity, in this case an overall increase of 13% due to a doubled rib thickness. Assuming this increase in capacity is taken by the shaft only, the implication is in fact a 19% increase in shaft capacity. This is also shown by the higher α values of 0.60 and 0.55 for test JW01_RP compared with 0.52 and 0.48 for test JW06_RPa.

7.2.3 Rib spacing

For comparison of rib spacing, model piles from tests JW01_RP and JW05_RPa were considered. The design dimensions of 1mm outstand and 2mm rib thickness were the same for both tests while the design spacing was 8mm for JW01_RP which failed at a load of 760N, and 16mm for JW05_RPa which failed at 800N. The pile with half as many ribs, or double the rib spacing failed at the higher load with α values calculated to be 0.64 or 0.59 compared with 0.60 or 0.55. This implies a 7% higher shaft capacity for the pile with 16mm rib spacing.

Given that the pile with 8mm rib spacing has a higher proportion of its shaft surface area at the outer surface relative to that of the 16mm rib spacing, it might be expected that the pile with the smaller rib spacing would have a higher shaft capacity. Reasons behind the test results showing the opposite may be due to a greater proportion of the shear failure along the length of the pile occurring within the soil between ribs where a greater friction force could be required for mobilisation relative to that near to the resin pile surface.

7.2.4 Other geometrical comparisons

In addition to comparison of specific individual rib dimensions, other comparisons of the pile profile could be made. For example, the pile tested in JW06_RPa has half the rib dimensions to that test in JW06_RPb, [1.1.8]

compared with [2.2.16]. Interestingly, they appear to fail at a similar load with similar α values. JW06_RPa failed as 670N with α values of 0.52 and 0.48, and JW06_RPa failed at 690N with α values of 0.54 and 0.47. Given that a higher rib thickness and higher rib spacing have shown a higher shaft capacity in other piles, it would be expected that the pile of profile [2.2.16] would have a substantially higher capacity. Having observed that the pile and ribs were not formed well in places, it may be that a better formed pile of the same dimensions would have failed at a considerably larger load.

7.3 Other observations and comments

In the case of all piles, the load-settlement curves showed failure to occur well before a settlement of 10% pile diameter had been reached so this criterion does not seem to be valid for these tests. This may be due to material properties of the resin and how it interacts with the clay at the pile-soil interface. This could also explain the low α value of 0.2 for the straight shafted pile. It may be that some testing of the resin-clay surface may be required to understand this fully, in a shear box for example. It would also be worth taking in flight measurement of undrained shear strength of the model soil, to compare against that calculated and give better informed test results.

CHAPTER 8: CONCLUSIONS AND RECOMMENDATIONS

The experiments carried out in this research project have been developed to produce comparable test results, the later tests finally producing successful results. The six successful test results have been observed and compared, offering some better understanding of the effect of the rib geometry on the pile capacity. To understand this effect in more detail and what the implications could be in the field, further testing would need to be carried out with a view to investigate the pile-soil interface of the resin piles and how their behaviour compares with that of concrete piles at prototype scale. This could be pursued through laboratory observations and experiments such as shear box or shear ring tests,, as well as numerical modelling of the material properties. Shear vane tests of the model soil during centrifuge tests would help to offer a more accurate value of undrained shear strength, particularly given the varying level of the water table in each test. Developing a test pile that could be constructed with a false pile bottom would also help to give more accurate results by reducing the bearing resistance to virtually zero and giving a direct value of shaft resistance.

With substantially more tests carried out, a far greater understanding of the behaviour of the high shear capacity pile could be gained. The apparatus could be developed to rotate by 90° offering the opportunity to construct and test a further two piles per centrifuge run, perhaps with one straight pile in each to give a directly relevant comparison. During the centrifuge test, the reservoirs would need to be enabled to empty during flight of the centrifuge so that they could rotate and start loading the second pair of piles from zero after loading of the first pair of piles.

In choosing rib geometry to test, testing for extreme cases would be a good way to understand the limits between which further tests could be expected to lie, and the different mechanisms of failure that apply as ribs are spaced closer together. For example, a test with ribs closely spaced together along the length of the pile could be compared to a pile of similar internal diameter with just one rib at the top and one at the bottom. The number of geometrically similar ribs could then

to be increased gradually, with equal spacing along the length regardless of number of ribs. By carrying out a substantial number of load tests, an overall comparison could be made, and hopefully relationship concluded, as the number of ribs increase and the rib spacing decreases. It might also be possible to observe at what point the failure of the pile shaft changes from acting in the vicinity of the internal pile surface between ribs along the pile length, and starts to become a linear action at the outer surface of the ribs.

With some basic relationships established, further tests could include profiles with ribs only for a certain length of the pile shaft and at different depths. Given that the main implication for this type of pile being used in construction is related to time saving, an aim of future testing would be to optimise the location along the pile shaft at which ribs should be profiled so that substantially fewer can be constructed for little loss of shear capacity compared to ribs being profiled along the entire pile length. Optimising the number of ribs and location along the length of the pile would be key to the commercial and technical success of high shear capacity pile.

REFERENCES

- Atkinson, J. H. (1993). An introduction to the Mechanics of Soils and Foundations.
McGraw Hill Book Company Europe.
- Brinch-Hansen, J. (1963). Hyperbolic stress-strain response: cohesive soils. Discussion.
ASCE Journal of Soil Mechanics and Foundation Engineering, Vol. 89, SM4, pp241-242.
- Britto A. M. and Gunn, M. J. (1987). Critical state soil mechanics via finite elements.
Ellis Horwood Limited.
- Brown, M. J., Hyde, A. F. L. & Anderson, W. F. (2006). Analysis of a rapid load test on an instrumented bored pile in clay.
Geotechnique 56, No. 9, pp627-638.
- Burland, J. B. (1973). Shaft friction of piles in clay – a simple fundamental approach.
Ground Engineering 6, No. 6, pp30-42.
- Burland, J.B. and Cooke, R.W. (1974). The design of bored piles in stiff clay.
Ground Engineering 7, No. 4, pp 28-35.
- Chandler, R. J. and Martins, J. P. (1982). An experimental study of skin friction around piles in clay.
Geotechnique 32, No. 2, pp119-132.
- Chellis R.D. (1961). Pile foundations.
Second Ed., New York: McGraw-Hill.
- Clayton, C. R. I. and Milititsky, J. (1983). Installation effects and the performance of bored piles in stiff clay,
Ground Engineering 16, No. 2, pp17-22.
- Craig, W. H. (1995). Chapter 1 in Geotechnical centrifuges: past, present and future. Geotechnical centrifuge technology, Taylor, R. N. (Ed).
Blackie Academic and Professional, Glasgow.
- Coop, M. R. and Wroth, C. P. (1989). Field studies of an instrumented model pile in clay.
Geotechnique 39, No. 4, pp679-696.

- De Beer, E.E. and Wallays, M. (1972). Forces Induced in Piles by Unsymmetrical Surcharges on the Soil around the Pile. In Proc. 5th European Conf. On Soil Mechanics and Foundation Engineering, Madrid. Vol. 1, pp325-332.
- Fellenius, B. H. (1980). The analysis of results from routine pile load tests. Ground Engineering, September 1980, pp19-31.
- Fellenius, B. H. (1975). Reduction of negative skin friction with bitumen coated slip layers. Discussion. American Society of Civil Engineers, ASCE, Journal of the Geotechnical Division, Vol. 101, GT4, pp412-414.
- Fleming, W. G. K. (1992). A new method for single pile settlement prediction and analysis. Geotechnique 42, No. 3, pp411-425.
- Fuller, F. M. and Hoy, H. E. (1970). Pile Load Tests Including Quick Load Test Method, Conventional Methods, and Interpretations. Research Record No. 333, Highway Research Board, Washington, D.C., pp74-86.
- Housel, W. S. (1966). Pile load capacity, estimates and test results. Proc. ASCE, Vol 92, SM4, pp1-30.
- McNamara, A.M. (2001). Influence of heave reducing piles on ground movements around excavations. PhD thesis, City University London.
- Mohan, D., Jain, G. S. and Sharma, D. (1967). Bearing capacity of multi under-reamed bored piles. Proc. 3rd Asian Reg. Conf. SMFE, Haifa (Israel), pp103.
- Milititsky, J. (1980). Large bored piles in clay – design and behaviour. University of Surrey, Civil Engineering Department, Internal Report, pp130.
- O'Neill, M. W. and Reese, L. C. (1972). Behaviour of axially loaded shafts in Beaumont Clay. Journal of Soil Mechanics and Foundation Division, ASCE, 98(2), pp195-213.
- Phillips, R. (1995). Centrifuge modelling: practical considerations. In R.N. Taylor (ed.), Geotechnical Centrifuge Technology, Glasgow: Blackie Academic & Professional, pp34–59.
- Pellew, A. (2002). "Field investigations into pile behaviour in clay" PhD thesis, Imperial College London.

Poulos, H. G. (1982). The influence of shaft length on pile load capacity in clays.
Geotechnique 32, No. 2, pp145-148.

Powrie, W. (1997). Soil Mechanics Concepts and Applications.
E & FN Spon.

Qerimi Begaj, L. (2010). "Geotechnical centrifuge model testing for pile foundation re-use"
PhD thesis, City University London.

Skempton, A. W. (1959). Cast in-situ bored piles in London Clay.
Geotechnique 9, No. 4, pp153-173.

Taylor, R. N. (1995). Chapter 2 in Geotechnical Centrifuge Technology; Centrifuges in modelling: principles and scale effects.
Blackie Academic & Professional, Taylor, R.N. (Ed) Glasgow, pp19-33.

Unwin, W. and Jessep, R. A. (2004). Long-term testing in London Clay: a case study.
Ground Engineering 157, Issue GE2, pp57-63.

Whitaker, T. and Cooke, R. W. (1966). An investigation of the shaft and base resistances of large bored piles in London Clay.
Large bored piles, London: Institution of Civil Engineers, pp7-49.

TABLES

Table 4.1

Volume: (litres)	Load [50g] (N)	Load [40g] (N)	Load [35g] (N)
1.20	589	471	412
1.25	613	491	429
1.30	638	510	446
1.35	662	530	464
1.40	687	549	481
1.45	711	569	498
1.50	736	589	515
1.55	760	608	532
1.60	785	628	549
1.65	809	647	567
1.70	834	667	584
1.75	858	687	601
1.80	883	706	618
1.85	907	726	635
1.90	932	746	652
1.95	956	765	670
2.00	981	785	687
2.05	1006	804	704
2.10	1030	824	721
2.15	1055	844	738
2.20	1079	863	755
2.25	1104	883	773
2.30	1128	903	790
2.35	1153	922	807
2.40	1177	942	824
2.45	1202	961	841
2.50	1226	981	858
2.55	1251	1001	876
2.60	1275	1020	893
2.65	1300	1040	910
2.70	1324	1059	927
2.75	1349	1079	944
2.80	1373	1099	961
2.85	1398	1118	979
2.90	1422	1138	996
2.95	1447	1158	1013
3.00	1472	1177	1030
3.05	1496	1197	1047
3.10	1521	1216	1064

Table 4.2

		<u>kaolin</u>	<u>(london clay)</u>			
	M	1.00	0.89			
	N	3.26	2.68			
	λ	0.19	0.16			
	0.028 κ	0.0494	0.0624	where $\Lambda = \frac{1}{1 - (\kappa / \lambda)}$		
	κ / λ	0.26	0.39			
bulk unit weight	γ	17.44 kN/m ³			Gs	1.778
	Γ	3.14	2.54		w	40.0%
	ϕ	25	23	and $p'f = p' \cdot R^\Lambda \cdot e^{-\Lambda}$	v	1.711
unit weight of water	γ_w	9.81 kN/m ³				1845.43
	R_0	1.436509				
earth pressure coefficient	K_{0nc}	0.577382		and $S_u = \frac{p'f \cdot M}{2}$	and $p'f = \exp \left\{ \frac{[\lambda \cdot \ln p'c - \ln N + \ln \Gamma - \kappa \cdot \ln p'c + \kappa \cdot \ln p']}{\lambda} \right\}$	
max stress applied	p'_c	359.1				
max vertical stress applied	σ'_{vc}	500				
	Λ	1.35				

Table 4.3

sample depth (cm)	z (soil) (mm)	total vertical stress Σv (kPa)	Water depth (cm)	pore pressure u (kPa)	effective vertical stress $\sigma'v$ (kPa)	R_0	earth pressure coefficient K_0	effective horizontal stress $\sigma'h$ (kPa)	average effective stress p' (kPa)	effective over-consolidation ratio R	average effective Failure Stress $p'f$ (kPa)	deviator failure stress $q'f$ (kPa)	undrained shear strength S_u (kPa)
0	0	0.00	-1	-4.91	4.91	101.94	4.076	19.9921	14.96	24.00	129.02	129.02	64.51
1	10	8.72	0	0.00	8.72	57.34	3.196	27.8698	21.49	16.71	141.75	141.75	70.87
2	20	17.44	1	4.91	12.54	39.89	2.742	34.3664	27.09	13.26	150.55	150.55	75.28
3	30	26.16	2	9.81	16.35	30.58	2.450	40.0645	32.16	11.17	157.42	157.42	78.71
4	40	34.88	3	14.72	20.17	24.80	2.243	45.2218	36.87	9.74	163.11	163.11	81.56
5	50	43.60	4	19.62	23.98	20.85	2.084	49.9801	41.31	8.69	168.01	168.01	84.01
6	60	52.32	5	24.53	27.80	17.99	1.958	54.4273	45.55	7.88	172.33	172.33	86.17
7	70	61.04	6	29.43	31.61	15.82	1.855	58.6230	49.62	7.24	176.21	176.21	88.10
8	80	69.76	7	34.34	35.43	14.11	1.767	62.6095	53.55	6.71	179.73	179.73	89.87
9	90	78.48	8	39.24	39.24	12.74	1.693	66.4182	57.36	6.26	182.98	182.98	91.49
10	100	87.20	9	44.15	43.06	11.61	1.628	70.0733	61.07	5.88	185.98	185.98	92.99
11	110	95.92	10	49.05	46.87	10.67	1.570	73.5938	64.69	5.55	188.79	188.79	94.39
12	120	104.64	11	53.96	50.69	9.86	1.519	76.9951	68.23	5.26	191.42	191.42	95.71
13	130	113.36	12	58.86	54.50	9.17	1.473	80.2899	71.69	5.01	193.90	193.90	96.95
14	140	122.08	13	63.77	58.32	8.57	1.432	83.4884	75.10	4.78	196.25	196.25	98.13
15	150	130.80	14	68.67	62.13	8.05	1.394	86.5997	78.44	4.58	198.49	198.49	99.25
16	160	139.52	15	73.58	65.95	7.58	1.359	89.6312	81.74	4.39	200.62	200.62	100.31
17	170	148.24	16	78.48	69.76	7.17	1.327	92.5895	84.98	4.23	202.67	202.67	101.33
18	180	156.96	17	83.39	73.58	6.80	1.298	95.4801	88.18	4.07	204.62	204.62	102.31
19	190	165.68	18	88.29	77.39	6.46	1.270	98.3081	91.34	3.93	206.50	206.50	103.25
20	200	174.40	19	93.20	81.21	6.16	1.245	101.0777	94.45	3.80	208.31	208.31	104.16
21	210	183.12	20	98.10	85.02	5.88	1.221	103.7928	97.54	3.68	210.06	210.06	105.03
22	220	191.84	21	103.01	88.84	5.63	1.198	106.4569	100.58	3.57	211.75	211.75	105.87
23	230	200.56	22	107.91	92.65	5.40	1.177	109.0731	103.60	3.47	213.38	213.38	106.69
24	240	209.28	23	112.82	96.47	5.18	1.157	111.6441	106.58	3.37	214.96	214.96	107.48
25	250	218.00	24	117.72	100.28	4.99	1.139	114.1725	109.54	3.28	216.50	216.50	108.25
26	260	226.72	25	122.63	104.10	4.80	1.121	116.6606	112.47	3.19	217.99	217.99	108.99
27	270	235.44	26	127.53	107.91	4.63	1.104	119.1104	115.38	3.11	219.44	219.44	109.72
28	280	244.16	27	132.44	111.73	4.48	1.088	121.5239	118.26	3.04	220.85	220.85	110.42
29	290	252.88	28	137.34	115.54	4.33	1.072	123.9028	121.12	2.97	222.22	222.22	111.11
30	300	261.60	29	142.25	119.36	4.19	1.058	126.2487	123.95	2.90	223.56	223.56	111.78

$\Sigma Su = 1899.34$
 Mean $S_u = 90.44$ kPa

Table 4.4

prototype		model			
	α		0.6		
10	m	L	200 mm		
750	mm	\emptyset	15 mm		
	Su		90.44 kN/m ²		
	shaft cap:	0.51145	kN		
		511.45	N	>	straight shafted pile
50	mm	rib depth:	1 mm	50	mm
50	mm	rib thick:	1 mm	50	mm
300	mm	rib space:	6 mm	300	mm
	α		0.93		
	effective \emptyset :		17 mm		
	shaft cap:	0.9017	kN		
		902	N	>	ribbed pile
	α		1.00		
	effective \emptyset :		17 Mm		
	shaft cap:	0.9661	kN		
		966	N	>	ribbed pile

Table 4.5

α	0.6		α	0.6	
L	10 m		L	10 m	
\emptyset	750 mm		\emptyset	850 mm	
Su	90.44 kN/m ²		Su	90.44 kN/m ²	
shaft cap:	1278.63 kN	> straight shafted pile	shaft cap:	1449.12 kN	> straight shafted pile

	rib spacing			rib outstand			rib thickness					
rib depth:	100	100	100	100	100	100	25	50	75	100	125	150
rib thick:	100	100	100	50	100	150	100	100	100	100	100	100
rib space:	250	500	750	500	500	500	500	500	500	500	500	500
α	0.84	0.92	0.95	0.96	0.92	0.88	0.92	0.92	0.92	0.92	0.92	0.92
effective \emptyset :	850	850	850	850	850	850	775	800	825	850	875	900
shaft cap:	2029	2222	2286	2319	2222	2125	2026	2091	2157	2222	2287	2353

Table 4.6

α	0.6		α	0.6	
L	200 mm		L	200 mm	
\emptyset	15 mm		\emptyset	17 mm	
Su	90.44 kN/m ²		Su	90.44 kN/m ²	
shaft cap:	0.511 kN 511.45 N	> straight shafted pile	shaft cap:	0.580 kN 579.65 N	> straight shafted pile

	rib spacing			rib thickness			rib depth					
rib depth:	2	2	2	2	2	2	0.5	1	1.5	2	2.5	3
rib thick:	2	2	2	1	2	3	2	2	2	2	2	2
rib space:	5	10	15	10	10	10	10	10	10	10	10	10
α	0.84	0.92	0.95	0.96	0.92	0.88	0.92	0.92	0.92	0.92	0.92	0.92
effective \emptyset :	19	19	19	19	19	19	16	17	18	19	20	21
shaft cap:	0.907	0.993	1.022	1.037	0.993	0.950	0.837	0.889	0.941	0.993	1.046	1.098
	907	993	1022	1037	993	950	837	889	941	993	1046	1098

Table 4.7

Model end bearing capacity:

base area:	0.00018 m ²
su at base:	104.16 kPa
N:	9
Bearing capacity:	166 N

Table 4.8

straight pile:

length:	200 mm		
diameter:	15 mm		
alpha:	0.6	0.8	1.0
Su:	90.44 kN/m ²		
shaft cap:	0.511453 kN 530 N	0.681937 kN 700 N	(alpha=1) 0.852421 kN 871 N

high capacity pile:

length:	200 mm			
diameter:	15 mm			
alpha:	1			
Su:	90.44 kN/m ²			
rib outstand: (mm)	0.5	1	1.5	2 Mm
effective dia: (mm)	16	17	18	19 Mm
max shaft cap: (kN) (with alpha = 1.0) (N)	0.909 928	0.966 984	1.023 1041	1.080 1098 kN N
max shaft cap: (kN) (with alpha = 0.8) (N)	0.727 746	0.773 791	0.818 837	0.864 882 kN N
max shaft cap: (kN) (with alpha = 0.6) (N)	0.546 564	0.580 598	0.614 632	0.648 666 kN N
Su at 200mm depth:	104.16 kPa			
base capacity:	0.165653 165.7 N			

Table 4.9

Spring rate: The force required to produce unit deflection, F/d.

Outer dia	Coil dia	Inner dia	Wire dia	Spring index	Spring rate	Max defl	No coils	Max load	Shear Modulus
Do	D	Di	d	C	k	δ_{max}	Nt	Pmax	G
D+d	(Do+Di)/2	D-d		D/d	(Gdexp4)/8Dexp3Na	Lo-Ls		k* δ_{max}	E/(2(1+v))
30.4	27.76	25.12	2.64	10.5151515	4.180128808	43.7	7.5	182.6716	81000

	Plain ends	Closed ends	Plain ends ground	Closed ends ground					
Pitch	p	(Lo-d)Na	505.2	(Lo-3d)/Na	11.28727273	Lo/(Na+1)	9.333333	(Lo-2d)/Na	10.58545455
Free length	Lo	Na*p+d	70	Na*p+3d	70	(Na+1)p	70	Na*p+2d	63.5
Solid length	Ls	(Na+1)d	22.44	(Na+1)d	17.16	(Na+1)d	19.8	(Na+2)d	19.8
Active coils	Na	Nt	7.5	Nt-2	5.5	Nt-1	6.5	Nt-2	5.5

Table 4.10

weight / load of:	kg	kg (at 40g)	N (at 40g)
reservoir	0.057	2.280	22.3668
valve fitting	0.185	7.400	72.594
load connection	0.045	1.800	17.658
load pin	0.024	0.960	9.4176
apparatus total	0.311	12.440	122.036
			60.635 N
			capacity left in spring at 40g
water	3.000	120.000	1177.2
	3.311	132.440	1299.236

Table 4.11

Rate = 4.18013 N/mm

Capacity:	Load left in spring	Displacement left in spring	Actual Displacement	Displacement due to apparatus weight:
At 40g =	60.635 N	14.51 mm	29.194 mm	66.81%
At 35g =	75.787 N	18.13 mm	25.570 mm	58.51%

Table 6.1 Table of Tests

Test	Outstand (mm)	Thickness (mm)	Spacing (mm)
JW01_SP	0	0	0
JW01_RPa	1	2	8
JW02_RPa	0	0	0
JW02_RPb	1	2	16
JW03_RPa	0	0	0
JW03_RPb	1	2	16
JW04_RPa	0	0	0
JW04_RPb	1	2	16
JW05_RPa	1	2	16
JW05_RPb	1/2	1/2	8
JW06_RPa	1	1	8
JW06_RPb	2	2	16

Table 6.2

total load: 1000 N

flow is: L: 10.833 ml/s
R: 10.667 ml/s

	Apparatus load (N)		Dist from swing	centrifuge arm (m)					
	50.0	@	187 mm	1.613					
bottom of bottle	40.3	@	501 mm	1.299	estimated increment for 125N load	actual increment	vol water:	L time:	R time:
	39.4	@	530 mm	1.270					
1	38.6	@	554 mm	1.246	30.39 mm	30 mm	322.5 ml	29.8 S	30.2 s
2	37.7	@	584 mm	1.216	31.06 mm	31 mm	333.3 ml	30.8 S	31.2 s
3	36.7	@	615 mm	1.185	31.85 mm	32 mm	344.0 ml	31.8 S	32.3 s
4	35.7	@	647 mm	1.153	32.71 mm	33 mm	354.8 ml	32.8 S	33.3 s
5	34.7	@	680 mm	1.120	33.64 mm	34 mm	365.5 ml	33.7 S	34.3 s
6	33.7	@	714 mm	1.086	34.66 mm	35 mm	376.3 ml	34.7 S	35.3 s
7	32.6	@	749 mm	1.051	35.78 mm	36 mm	387.0 ml	35.7 S	36.3 s
8	31.5	@	785 mm	1.015	37.01 mm	37 mm	397.8 ml	36.7 S	37.3 s
Total:					267.1 mm	268 mm	2881.4 ml		

Table 7.1

Average undrained shear strength = **90.44** kPa or kN/m²
 Undrained shear strength at pile base = **104.16** kPa or kN/m³

	JW01_SP		JW01_RP		JW05_RPa		JW05_RPb		JW06_RPa		JW06_RPb	
Loading Rate (N/s):	2.46		3.02		3.63		2.85		3.71		3.12	
Design outstand (mm):	-		1		1		1/2		1		2	
Design thickness (mm):	-		2		2		1/2		1		2	
Design spacing (mm):	-		8		16		8		8		16	
Pile diameter (mm):												
Top	16.42	16.30	-	-	16.70	16.15	17.79	16.57	16.40	16.24	16.42	16.14
Bottom	16.17	16.00	-	-	16.48	16.19	16.50	15.78	16.08	15.87	16.11	15.83
Average pile diameter (mm):	16.22		16.31		16.38		16.66		16.15		16.13	
Design pile diameter (mm):	15.00		15.00		15.00		15.00		15.00		15.00	
Effective pile diameter (mm):												
Top	-	-	-	-	18.11	17.94	18.08	16.69	18.24	18.06	19.53	18.64
Bottom	-	-	-	-	18.04	17.84	17.23	16.27	17.02	16.79	18.12	17.80
Average effective pile diameter (mm):	16.22		17.76		17.98		17.07		17.53		18.52	
Design effective pile diameter (mm):	15.00		17.00		17.00		16.00		17.00		19.00	
Effective diameter as a proportion of pile diameter:	1.00		1.09		1.10		1.02		1.09		1.15	
Average rib outstand (mm):	0.00		0.72		0.80		0.20		0.69		1.20	
Design rib outstand (mm):	0.00		1.00		1.00		0.50		1.00		2.00	
Measured pile length (mm):	200		202		201		203		202		202	
Design pile length (mm):	200		200		200		200		200		200	
Pile surface area (mm ²):	10193		10348		10343		10625		10247		10233	
Design pile surface area (mm ²):	9425		9425		9425		9425		9425		9425	
Effective pile surface area (mm ²):	10193		11267		11355		10885		11123		11754	
Design effective pile surface area (mm ²):	9425		10681		10681		10053		10681		11938	
Effective surface area as a proportion of pile surface area:	1.00		1.09		1.10		1.02		1.09		1.15	

Table 7.1 continued

	JW01_SP	JW01_RP	JW05_RPa	JW05_RPb	JW06_RPa	JW06_RPb
Not including α						
Calculated pile capacity (N):	922	936	935	961	927	925
Design pile capacity (N):	852	852	852	852	852	852
Effective pile capacity (N):	922	1019	1027	984	1006	1063
Design effective pile capacity (N):	852	966	966	909	966	1080
Calculated end bearing capacity (N):	194	196	198	204	192	191
Design end bearing capacity (N):	166	166	166	166	166	166
Measured pile capacity from centrifuge test (N): Q_m	380	760	800	730	670	690
Test shaft capacity = Q_m – calculated end bearing	186	564	602	526	478	499
α ratio Q_m : calculated Q	0.20	0.60	0.64	0.55	0.52	0.54
α ratio Q_m : calculated effective Q	0.20	0.55	0.59	0.53	0.48	0.47

FIGURES

Figure 1.1 Photograph of the Expanded Piling rib-cutting tool

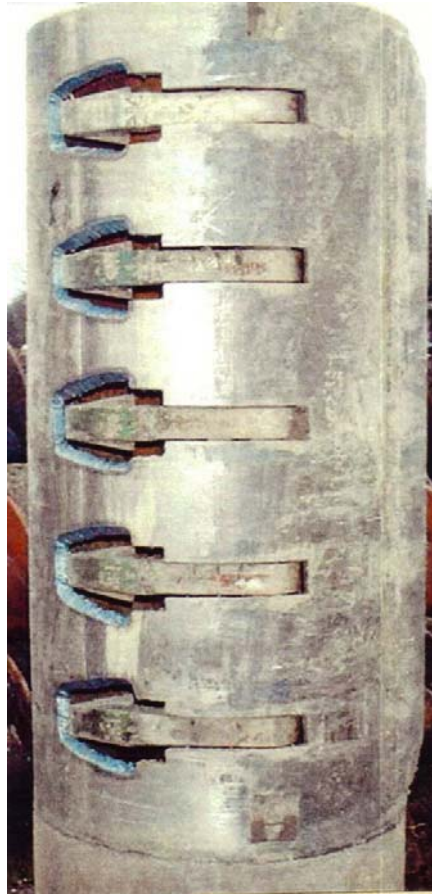
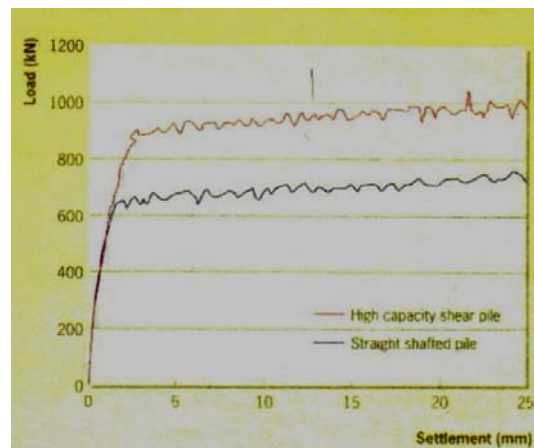


Figure 1.2 Outcome of pile tests at Lime Street



Comment [JW1]: Reference to add (as mentioned previously in Comment [JW1] – Ground Engineering 2003)

Figure 1.3 Outstand of the pile ribs

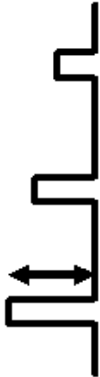


Figure 1.4 Depth of the pile ribs.



Figure 1.5 Spacing between the pile ribs



Figure 2.1 Diagram showing components of pile capacity

Pile capacity, $Q_{ult} = \text{shaft bearing capacity, } Q_{\text{shaft}} + \text{base bearing capacity, } Q_{\text{base}}$

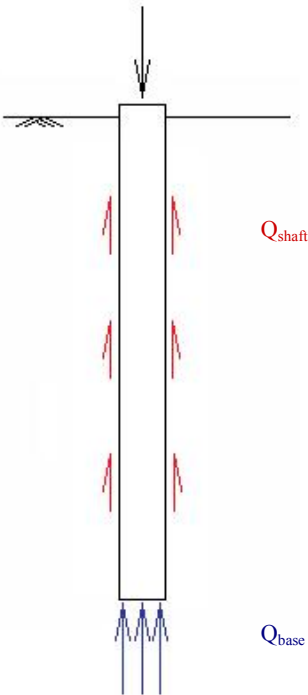


Figure 2.2 Short term distribution of the pile load between shaft and base (Burland & Cooke, 1974)

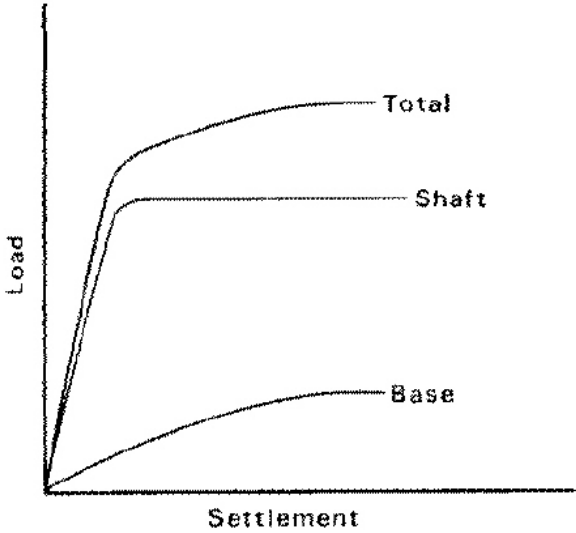


Figure 2.3 Long term distribution of the pile load between shaft and base (under reamed pile)
(Burland & Cooke, 1974)

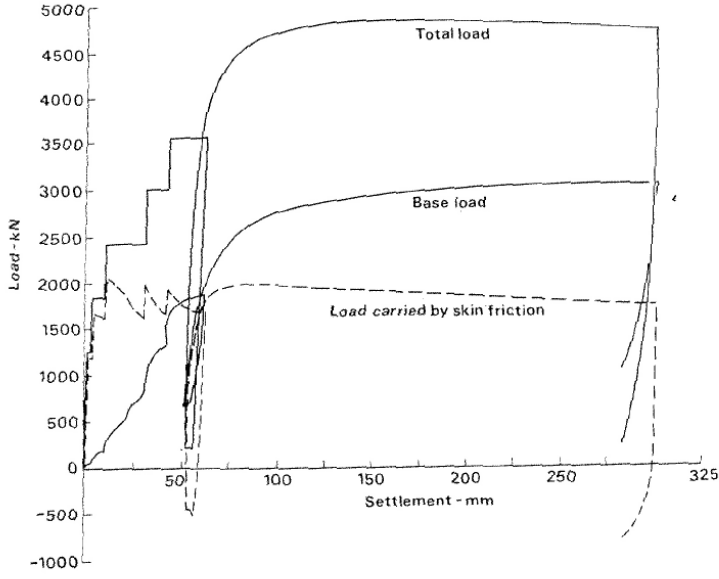


Figure 2.4 Moisture content and penetration resistance adjacent to Pile No. 29, Monument Street, City of London (Milititzky, 1980)

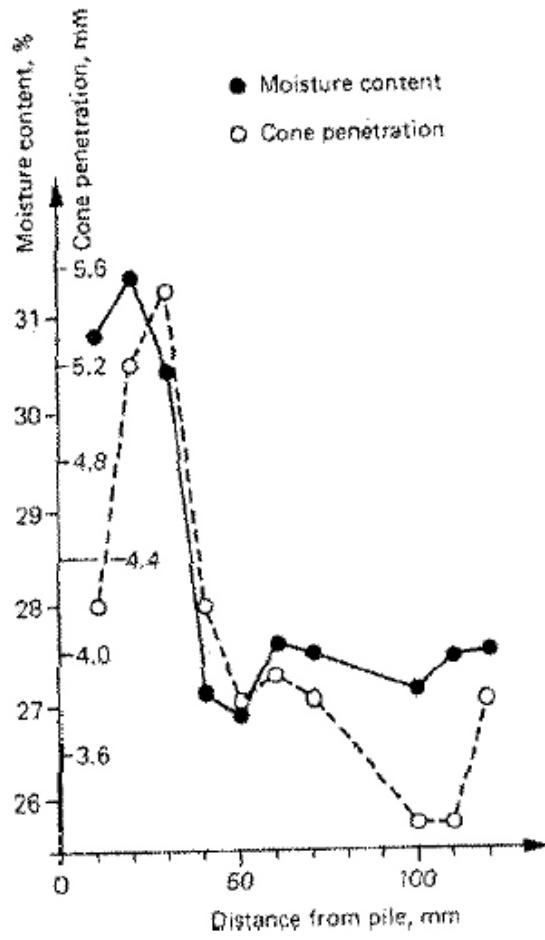


Figure 2.5 High shear capacity pile concept

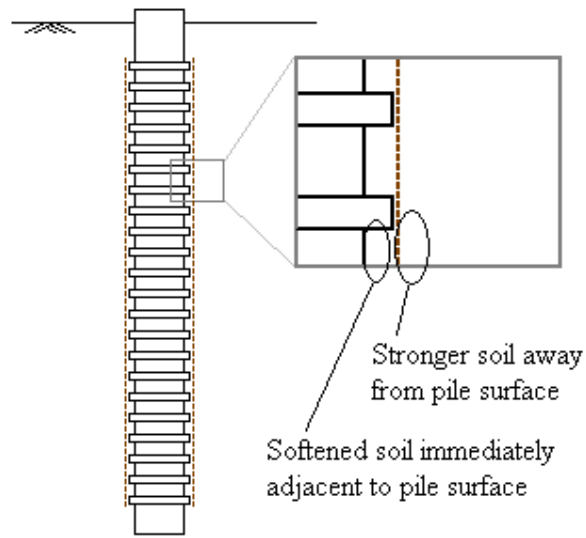


Figure 2.6 Distribution of shear stress on the shaft of a bored pile (O' Niell & Reese, 1972)

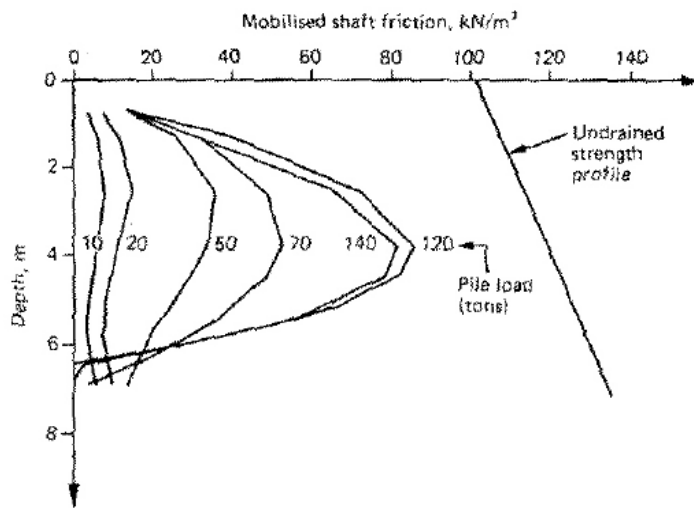


Figure 3.1 Inertial stresses in the model correspond to gravitational stresses in the prototype (Taylor, 1995)

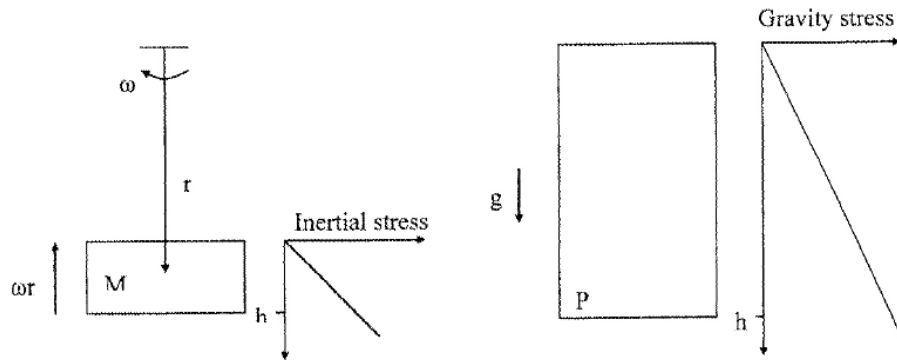


Figure 3.2 Diagram showing the geometry of the centrifuge arm and swing for use in calculating of acceleration errors (Taylor, 1995)

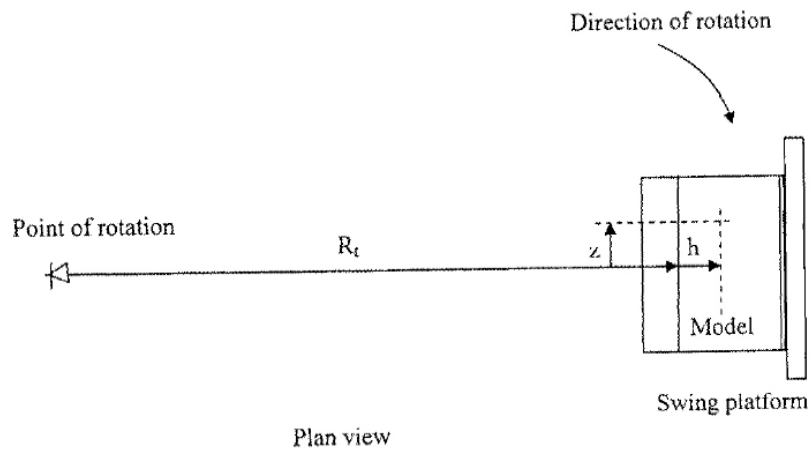


Figure 3.3 Stress variation with depth in the centrifuge model (Taylor, 1995)

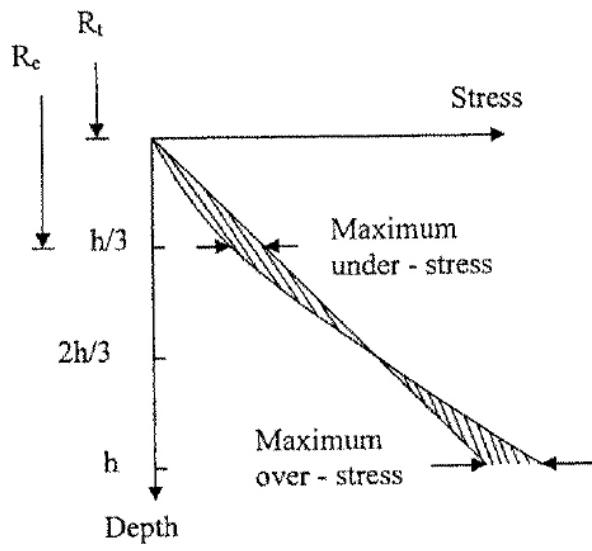


Figure 4.1 Schematic diagram of the Acutronic 661 in the Geotechnical Research Centre at City University (Schofield & Taylor, 1988)

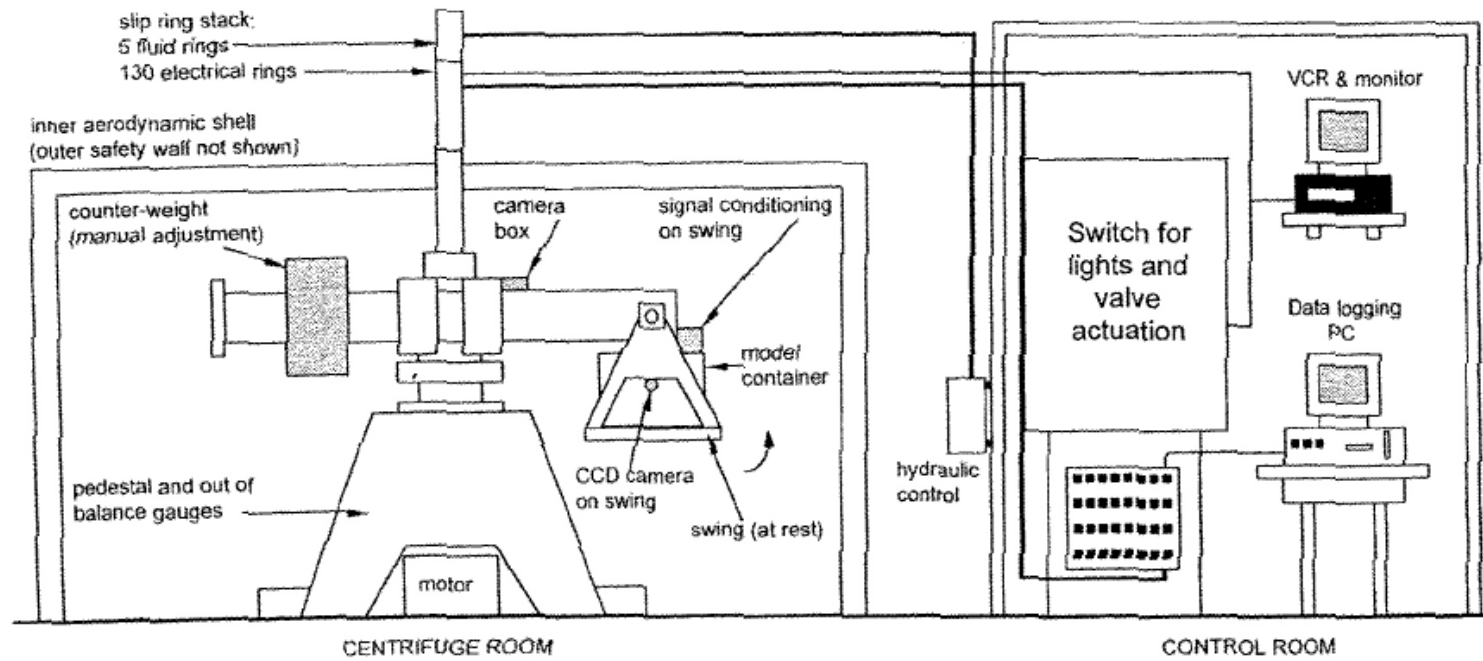


Figure 4.2 Photograph of the Acutronic 661 in the Geotechnical Research Centre at City University



Figure 4.3 Stainless Steel Tub in which the soil sample is prepared and the model piles are constructed



Figure 4.4 Photograph of a soil sample being prepared in the consolidation press



Figure 4.5 Diagram showing the geometry of model in the steel tub

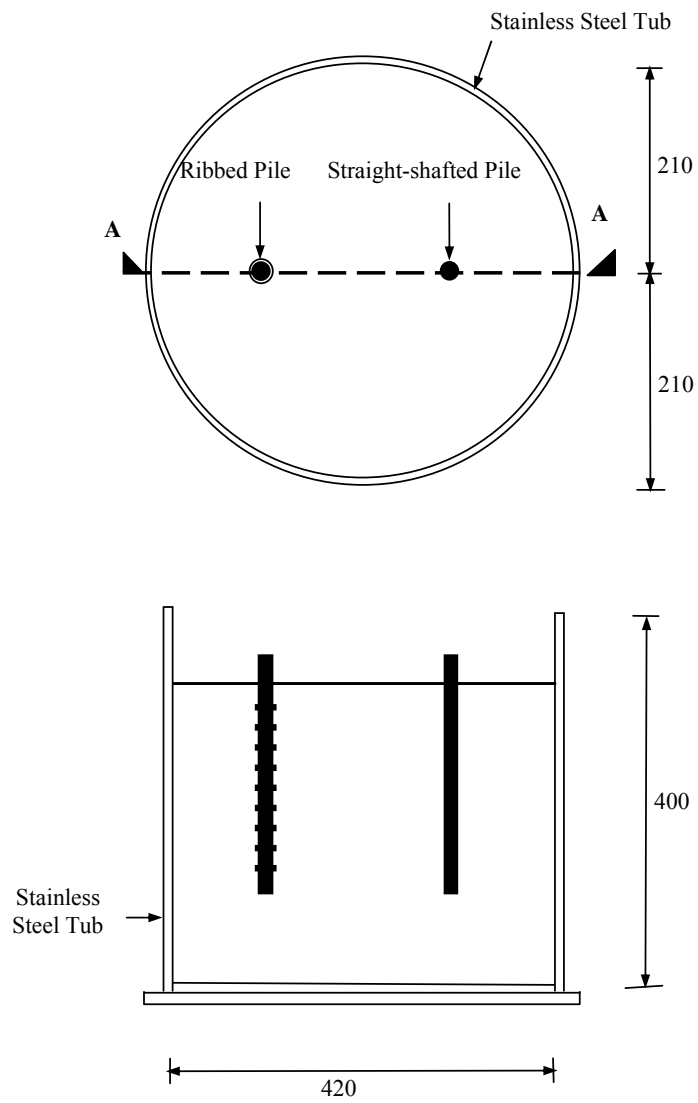


Figure 4.6 Diagram of pile cutting tooling

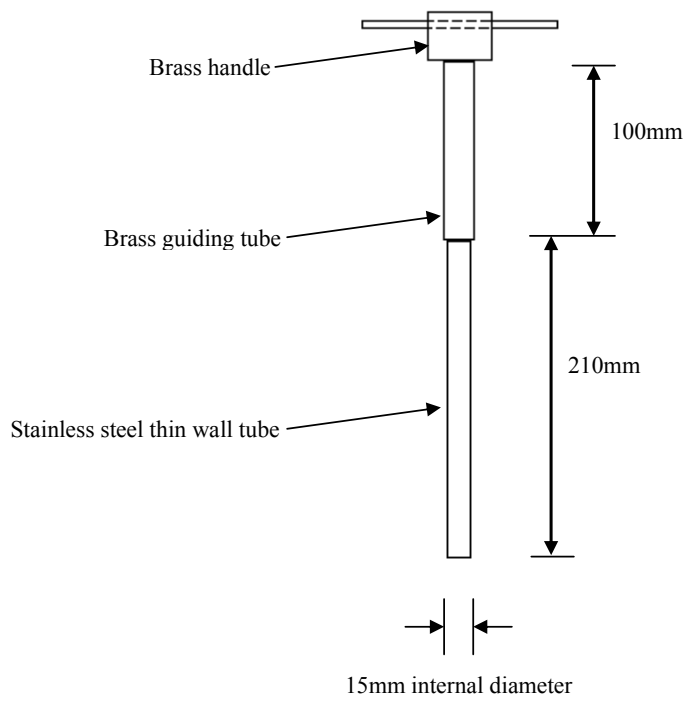


Figure 4.7 Moving parts of the rib-cutting tool separated to show mechanism

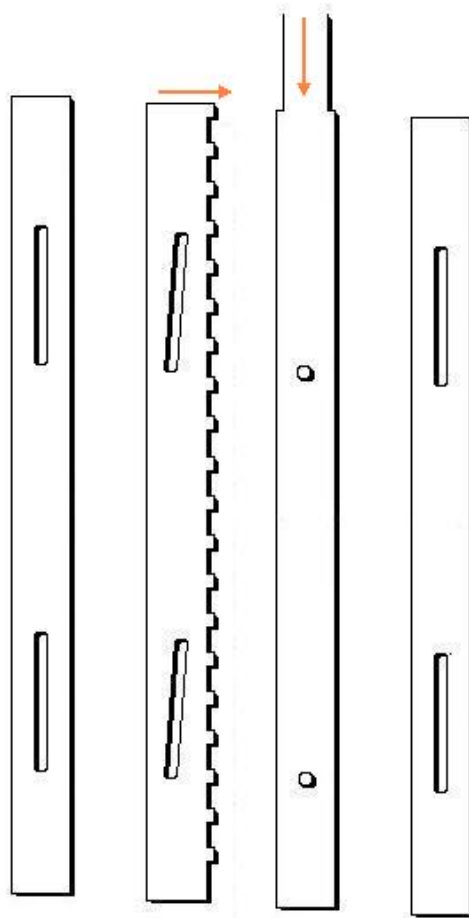


Figure 4.8 Photograph of complete rib-cutting tool



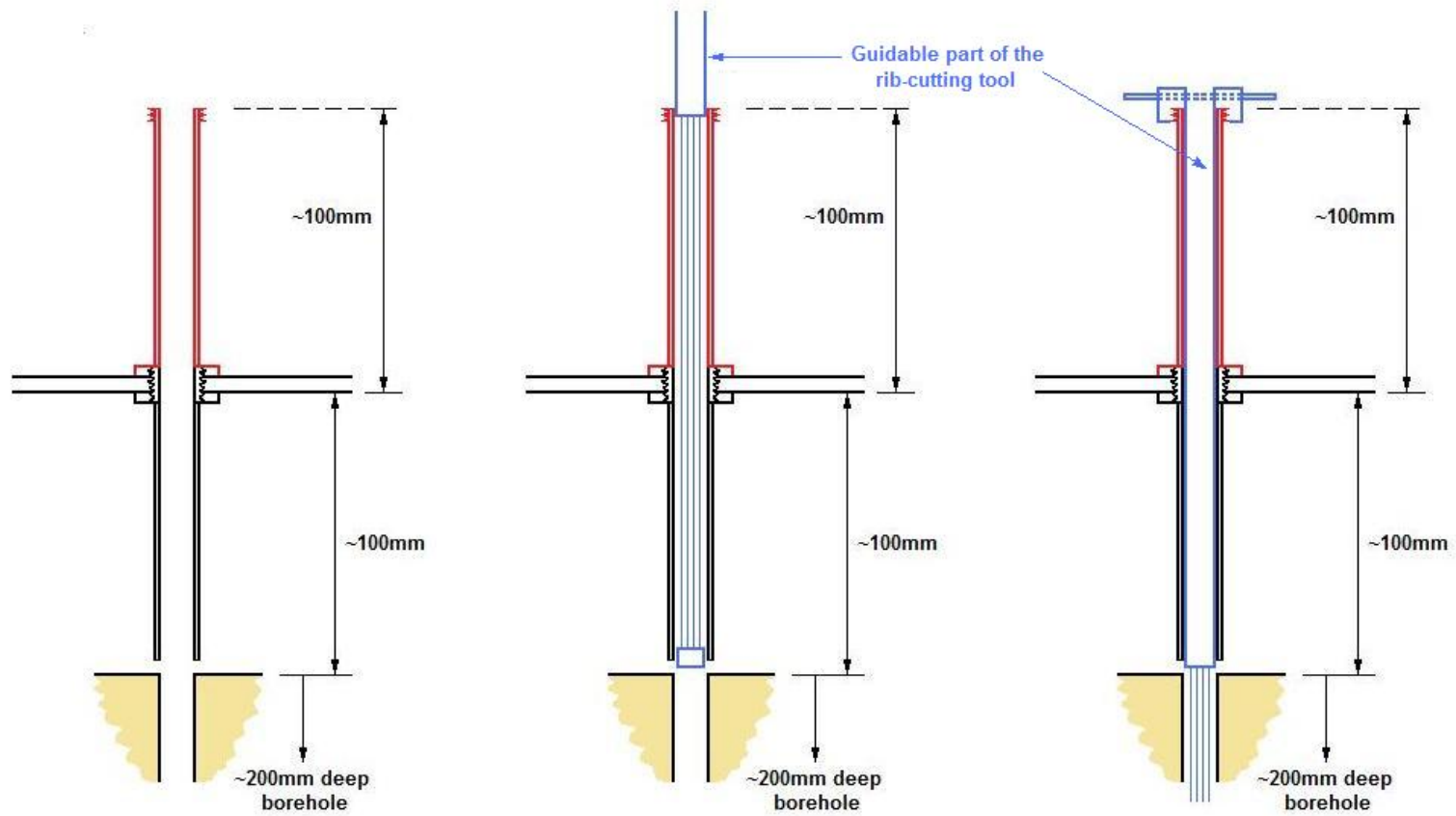
4.9 Photograph showing resin pile formed by first test of rib cutting mechanism



Figure 4.10 Photograph of guide apparatus for the pile cutter



Figure 4.11 Rib-cutting tool guide concept



(a) guide extension attached

(b) guidable part of rib-cutting tool reaches guide extension

(c) rib-cutting tool reached bottom of borehole

Figure 4.12 Loading apparatus used in centrifuge tests for L. Begaj Qerimi's PhD research project: "Geotechnical centrifuge model testing for pile foundation re-use"

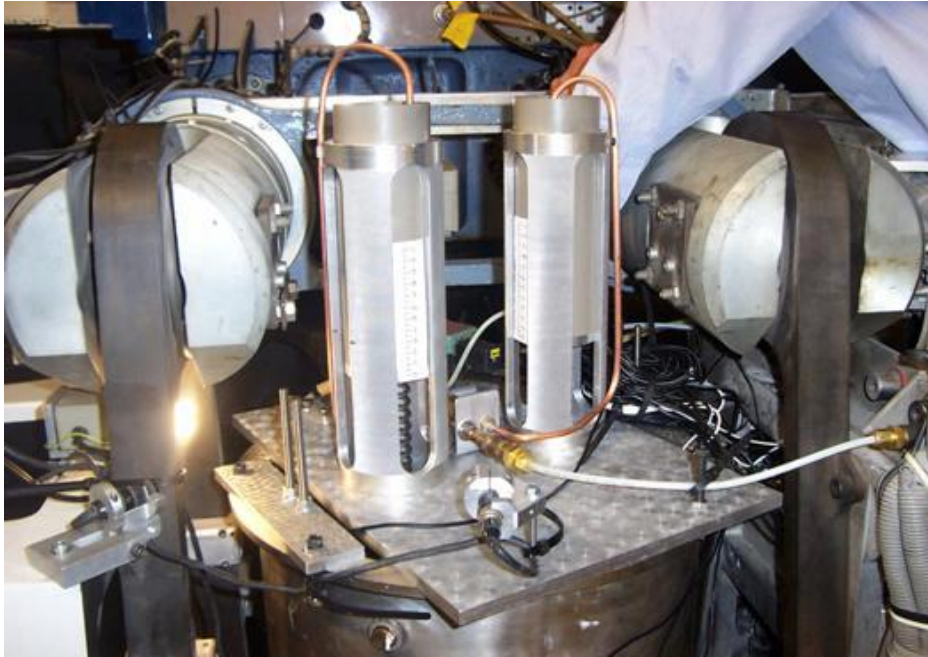


Figure 4.13 Loading capability of different volumes of reservoirs (to be read in conjunction with Table 4.1)

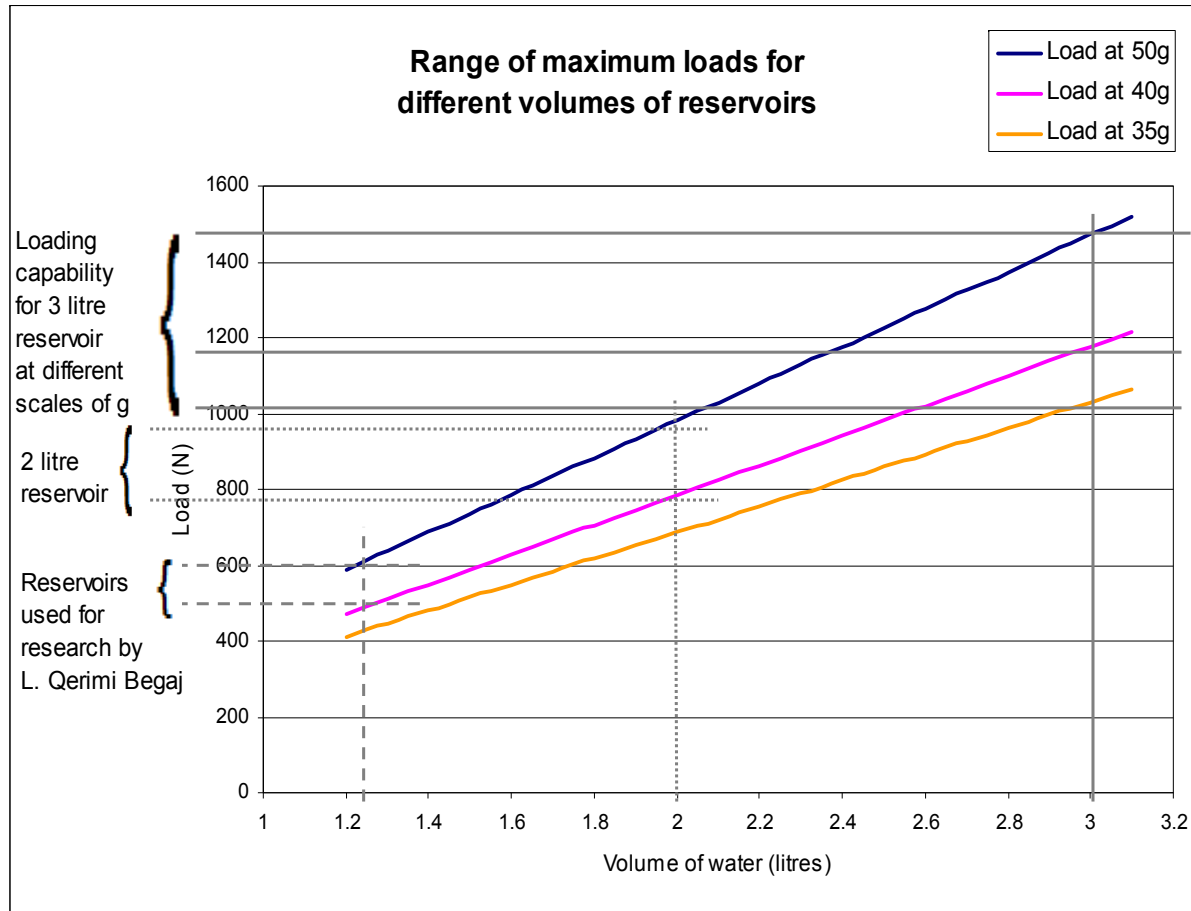


Figure 4.14 Graphical representation of stresses in the model soil with sample depth

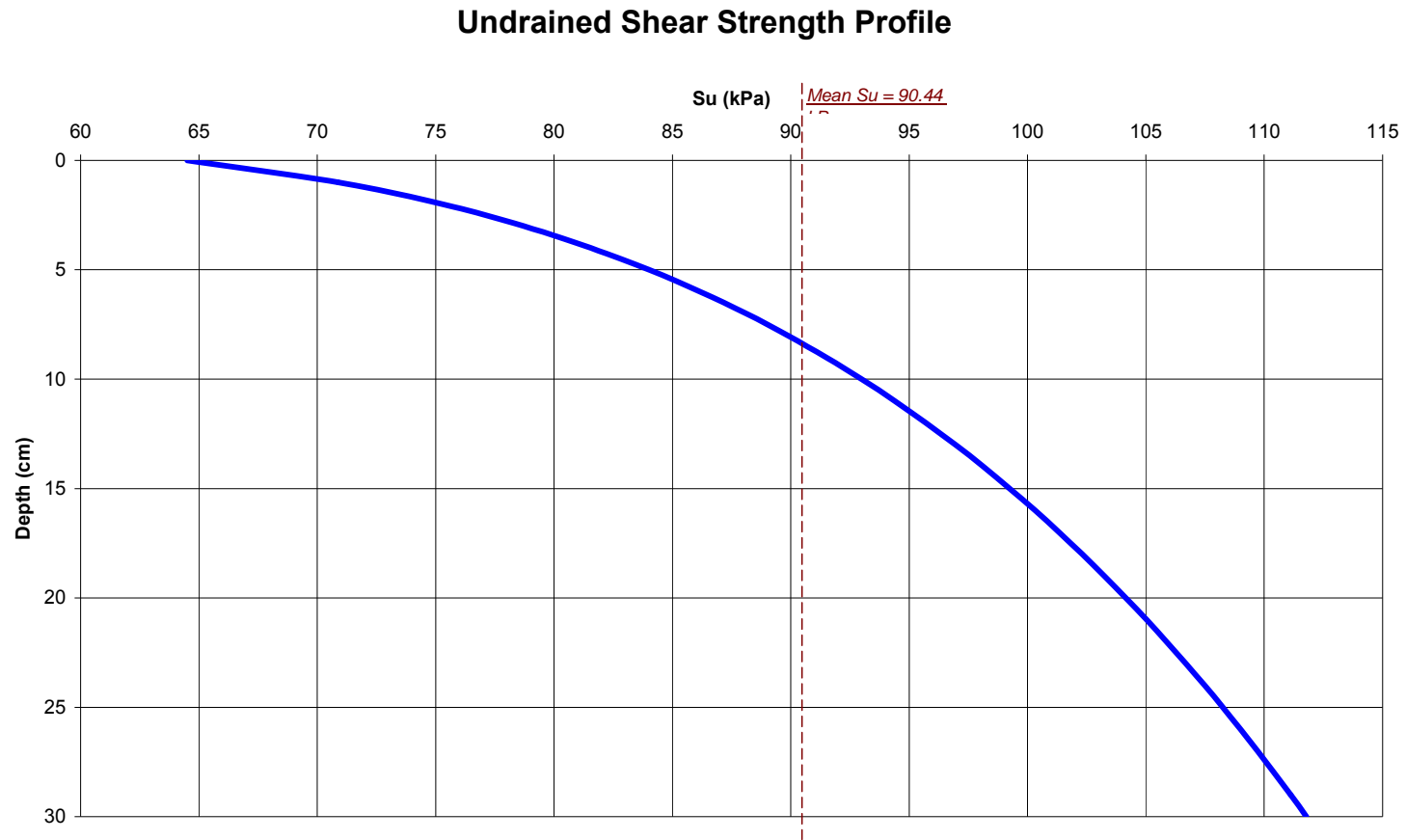


Figure 4.15 Possible pile capacity using diameter of ribs as pile diameter

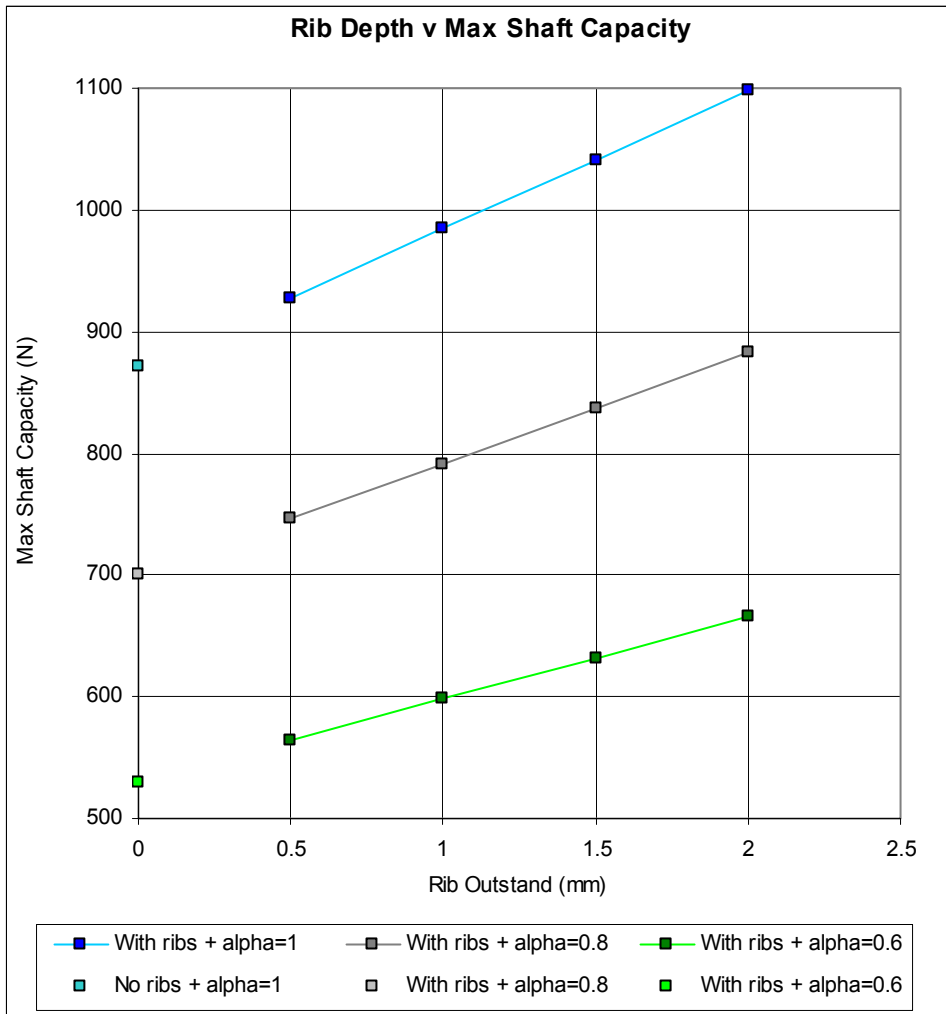


Figure 4.16 Diagram showing loading apparatus

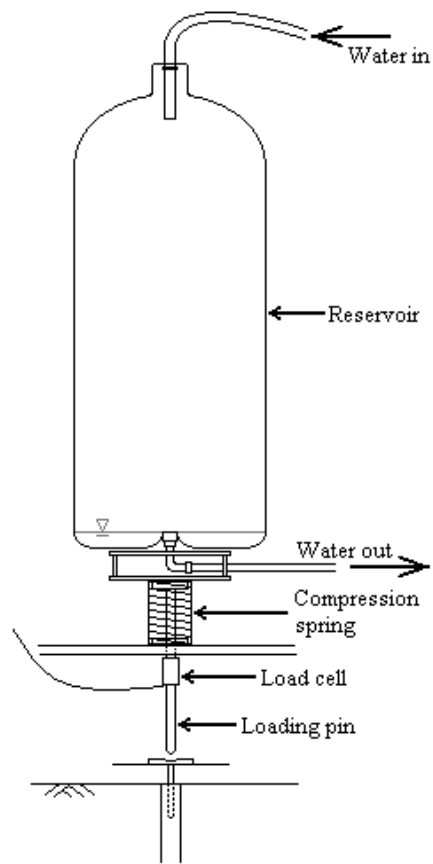


Figure 4.17 Photograph showing loading apparatus.



Figure 4.18 Photograph showing the variable standpipe

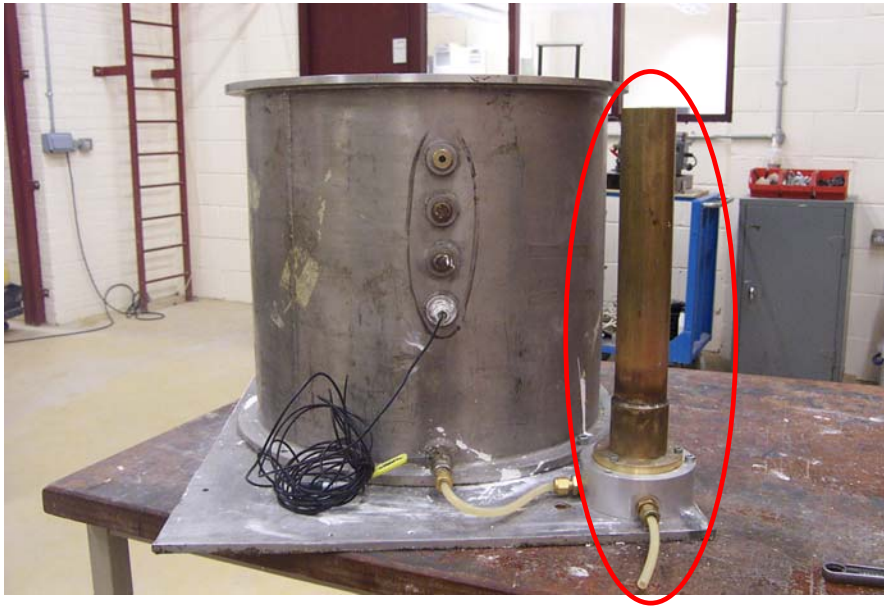


Figure 4.19 Drainage plate in the base of the tub

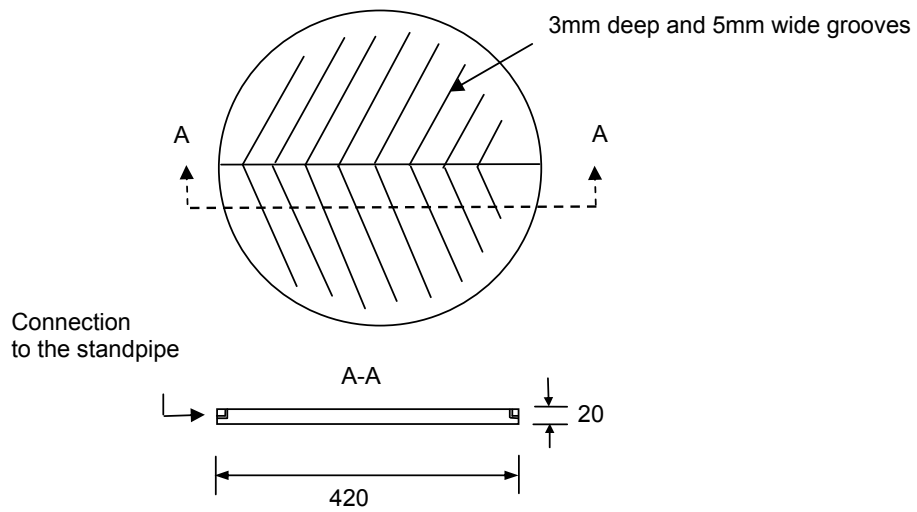


Figure 4.20 Photograph showing location of the LVDTs above the model

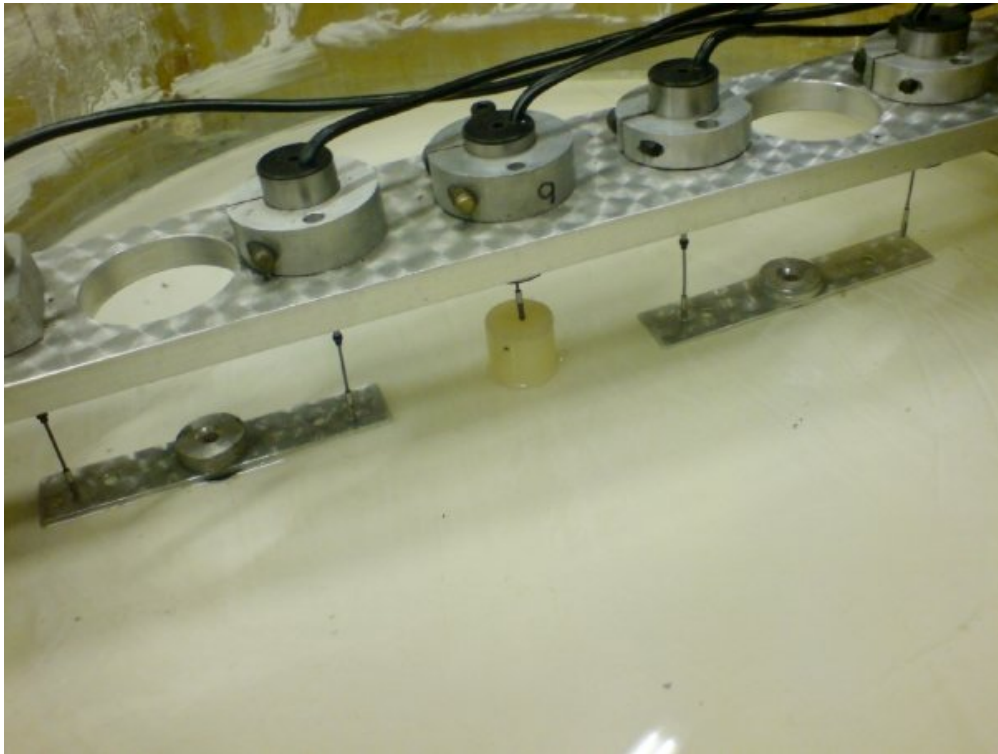


Figure 5.1 Calibration chamber for PPT calibration



Figure 5.2 Photograph showing location on centrifuge arm of junction box, used for connection of all instrumentation

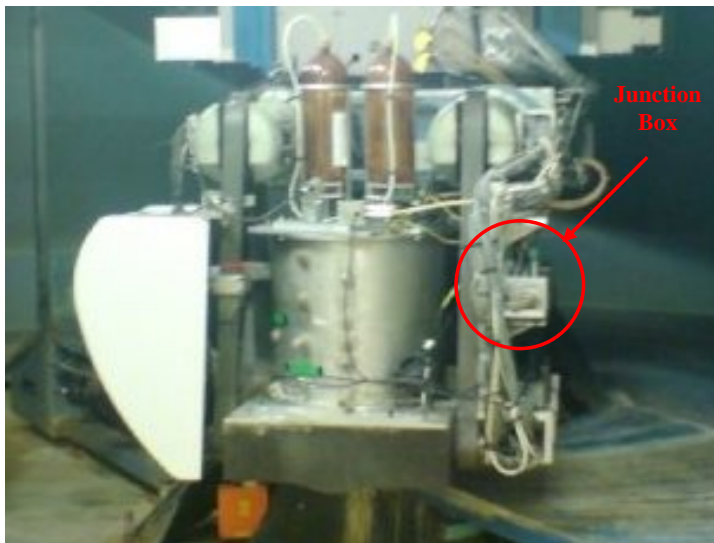


Figure 5.3 Photograph of the Budenberg for calibration of the load cells



Figure 5.4 LVDT apparatus bolted to the tub

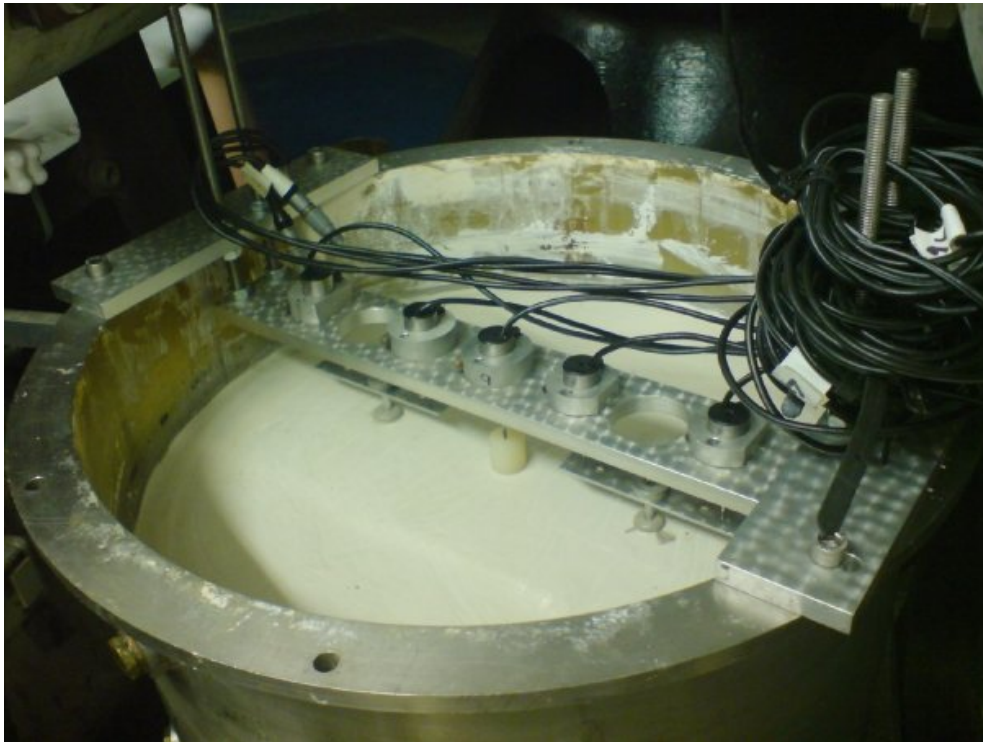


Figure 6.1 Location of pore pressure transducers in the sample and corresponding Channel Number

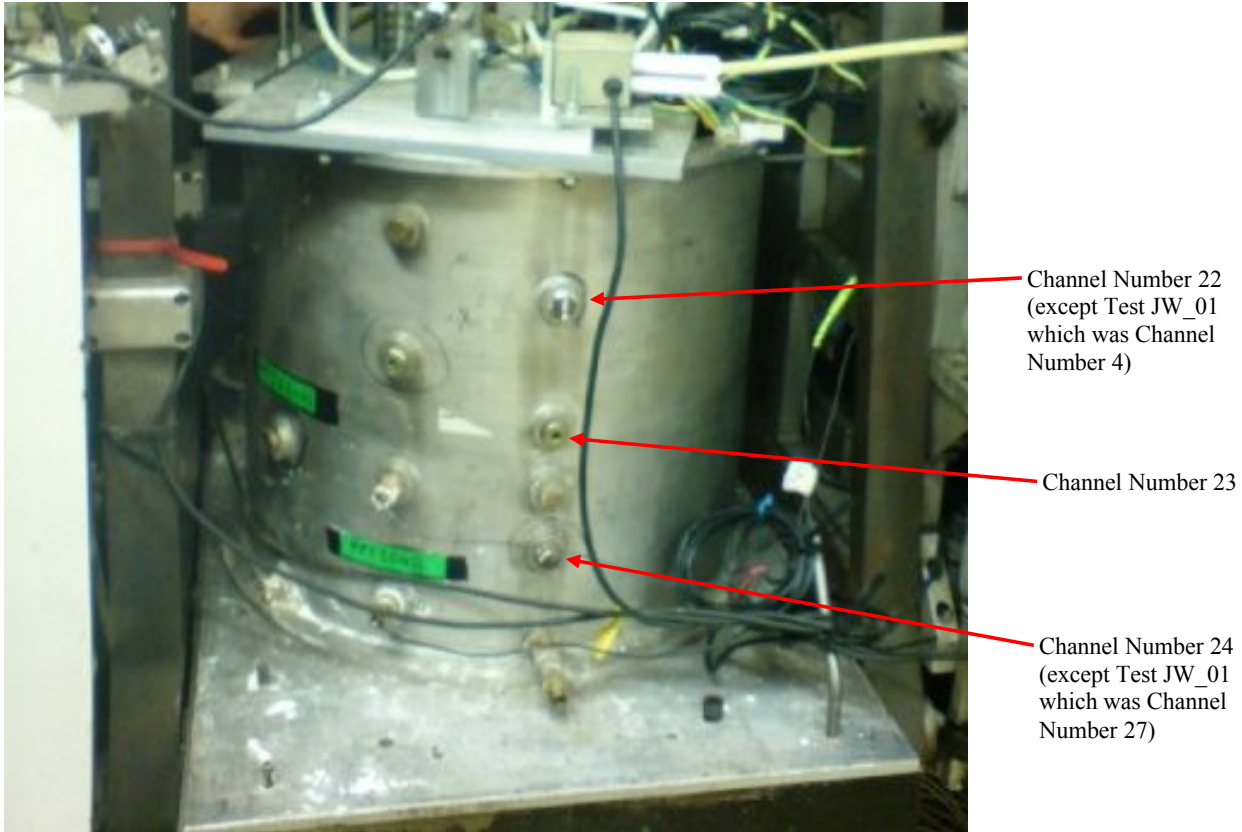


Figure 6.2 Test JW01: Pore Water Pressure-Time Graph

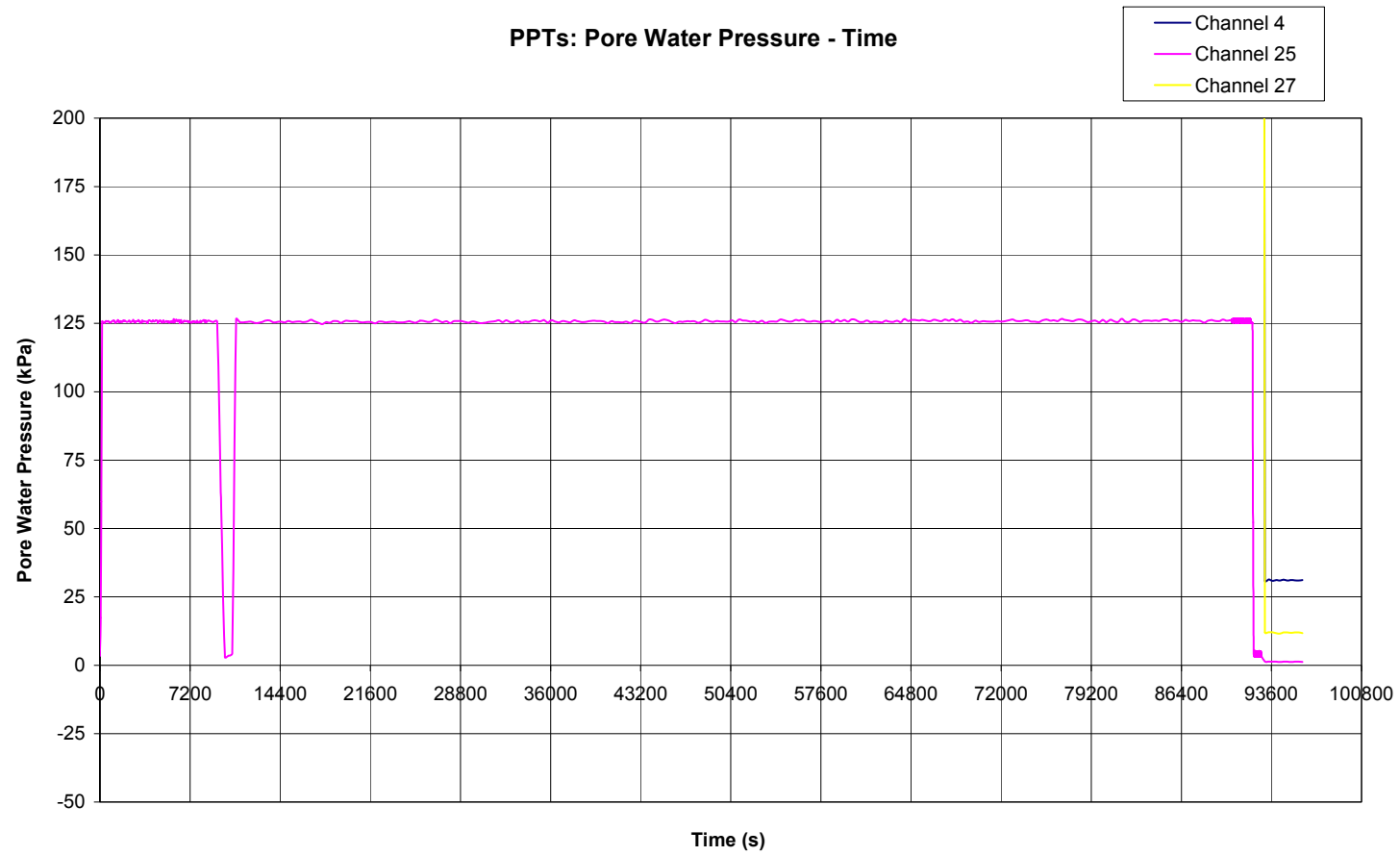


Figure 6.3 Test JW01: Displacement – Time Graph

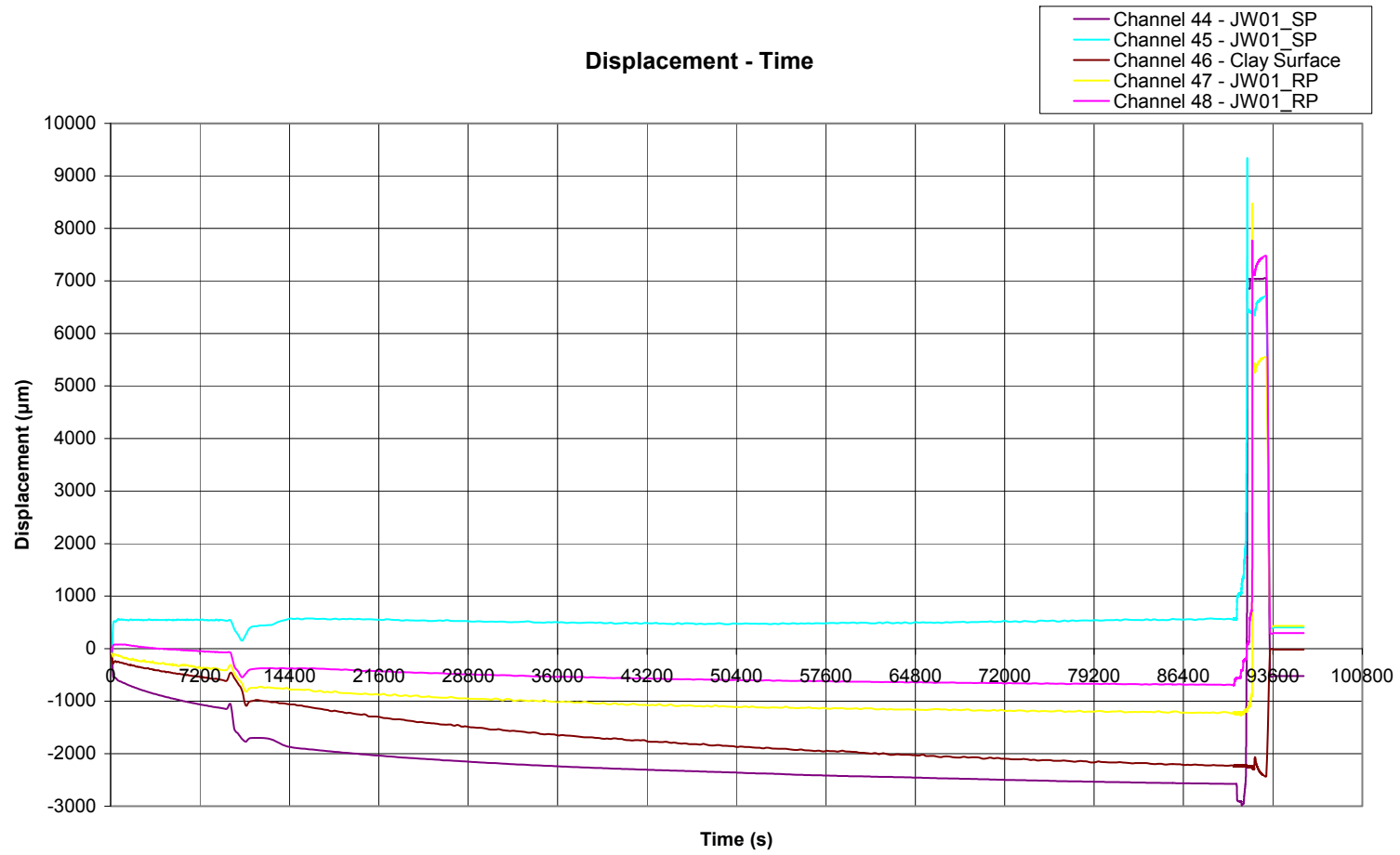


Figure 6.4 Test JW01: Load-Time Graph

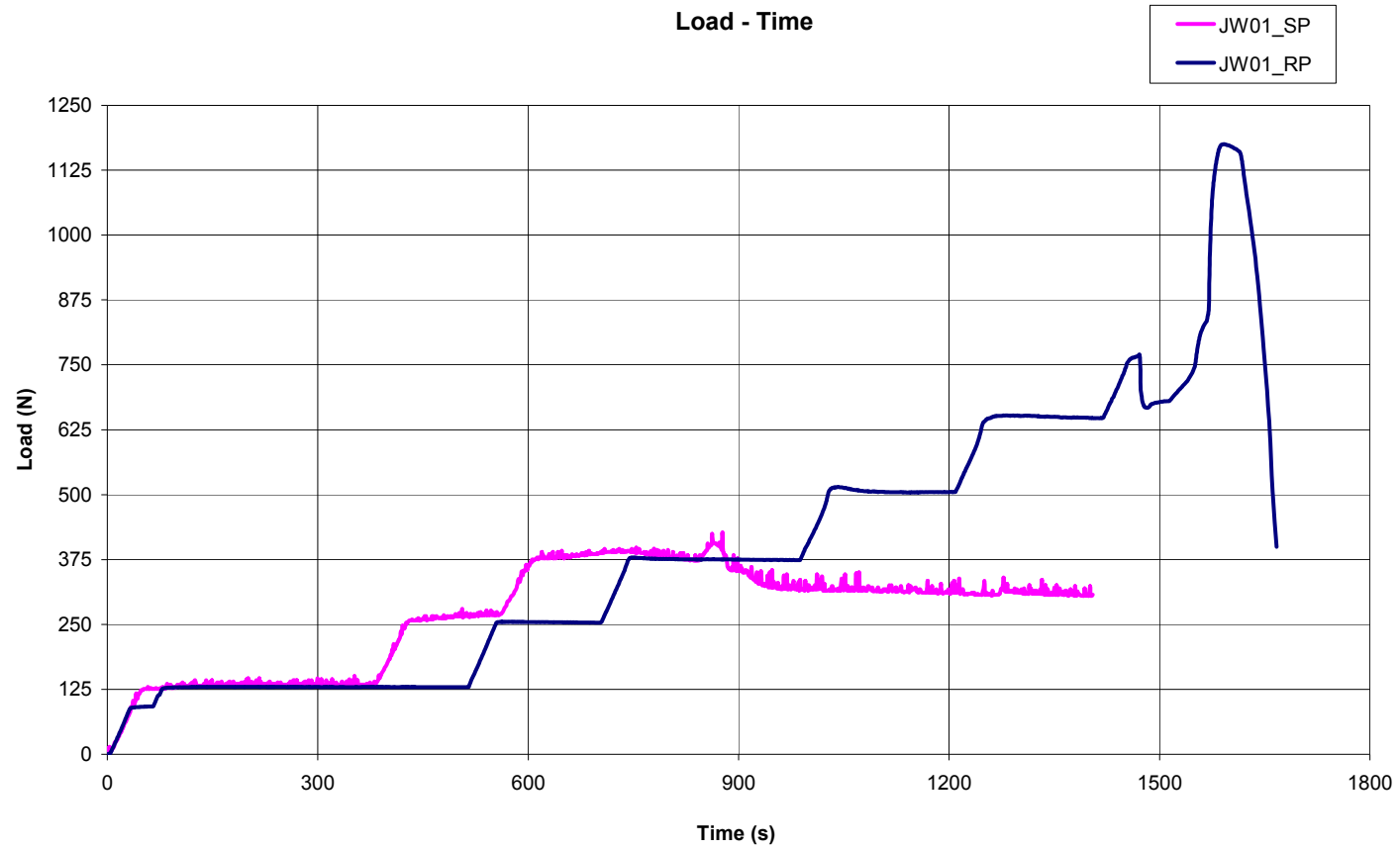


Figure 6.5 Test JW01_SP: Load-Settlement Graph



Figure 6.6 Test JW01_RP: Load-Settlement Graph

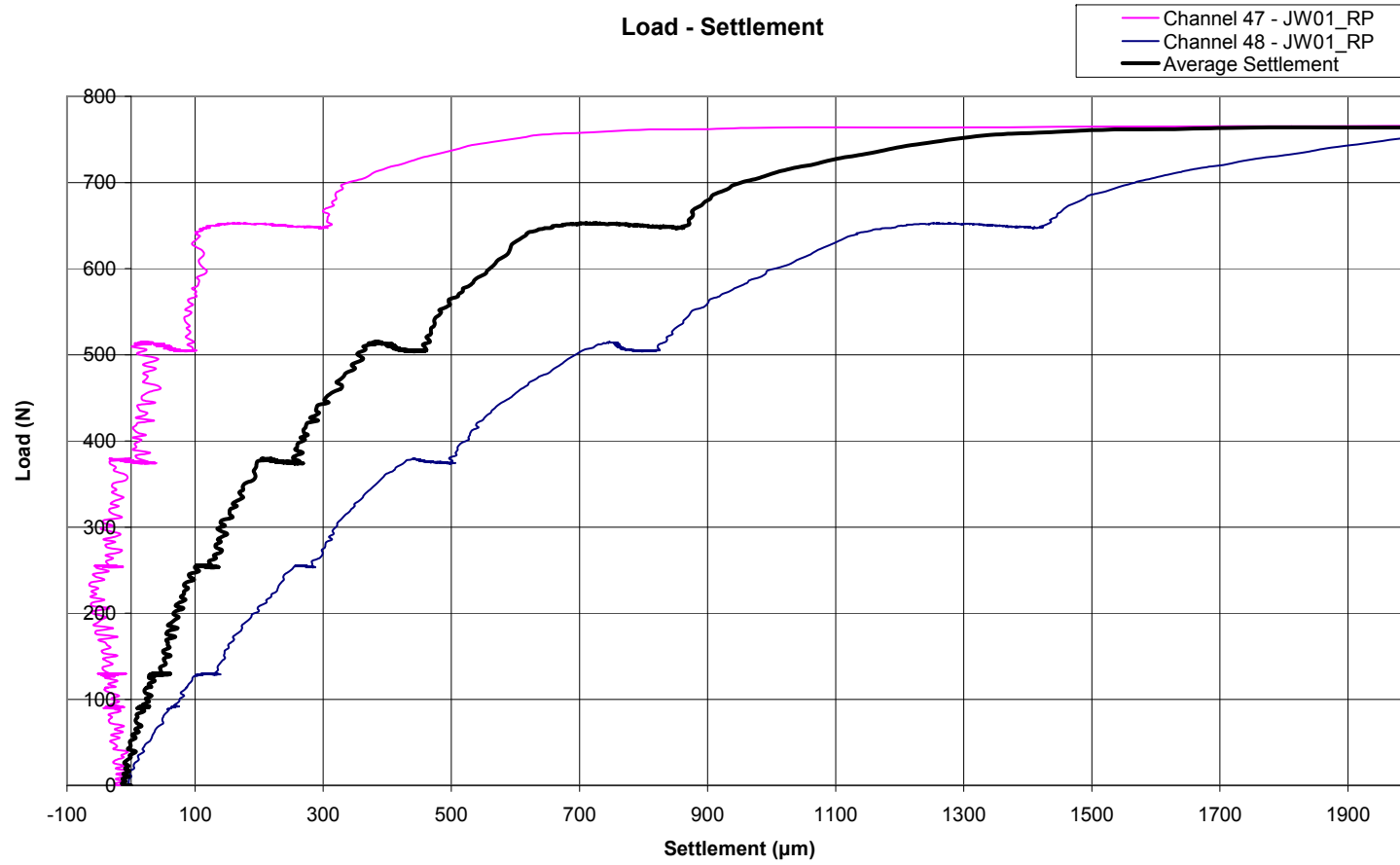


Figure 6.7 Test JW01: Load-Settlement Graph

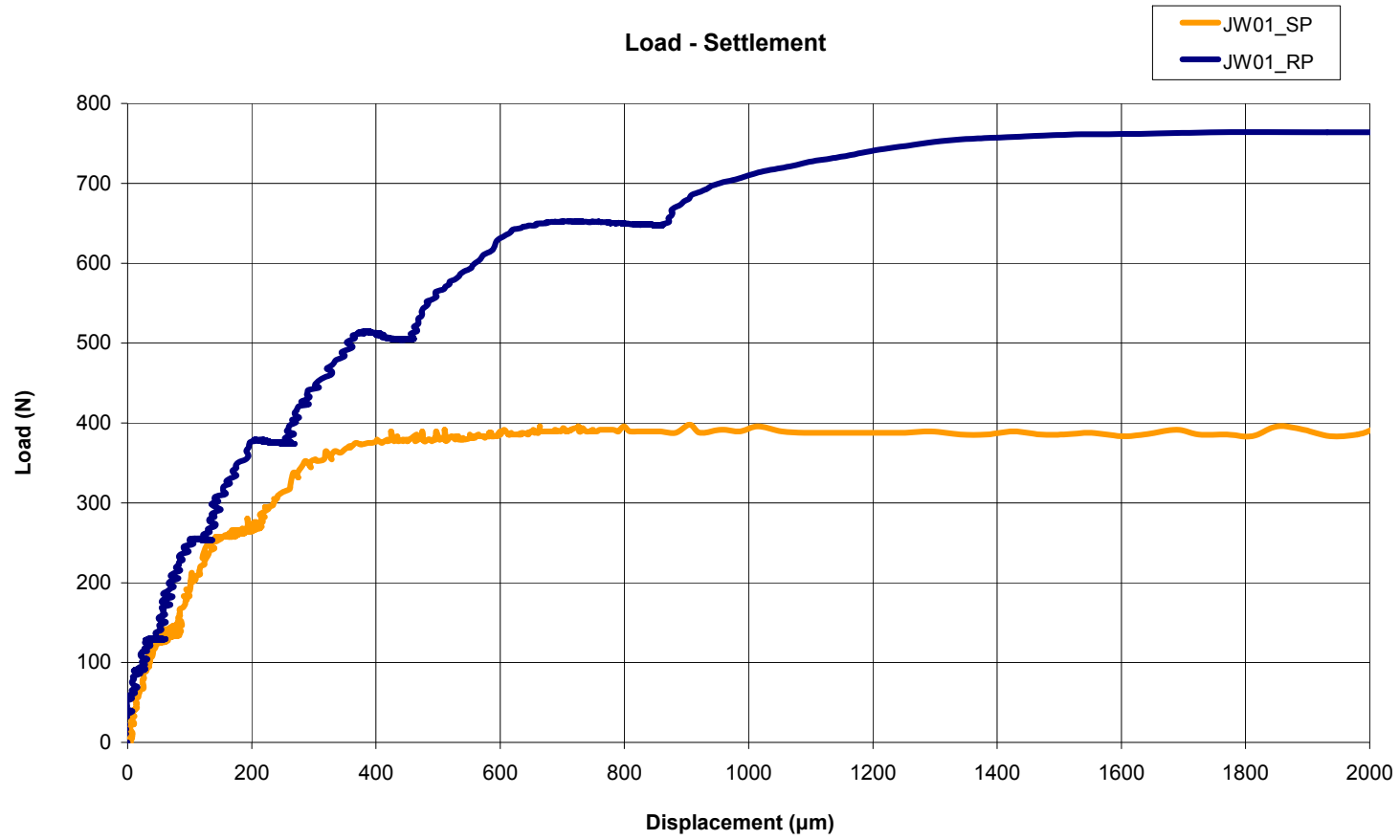
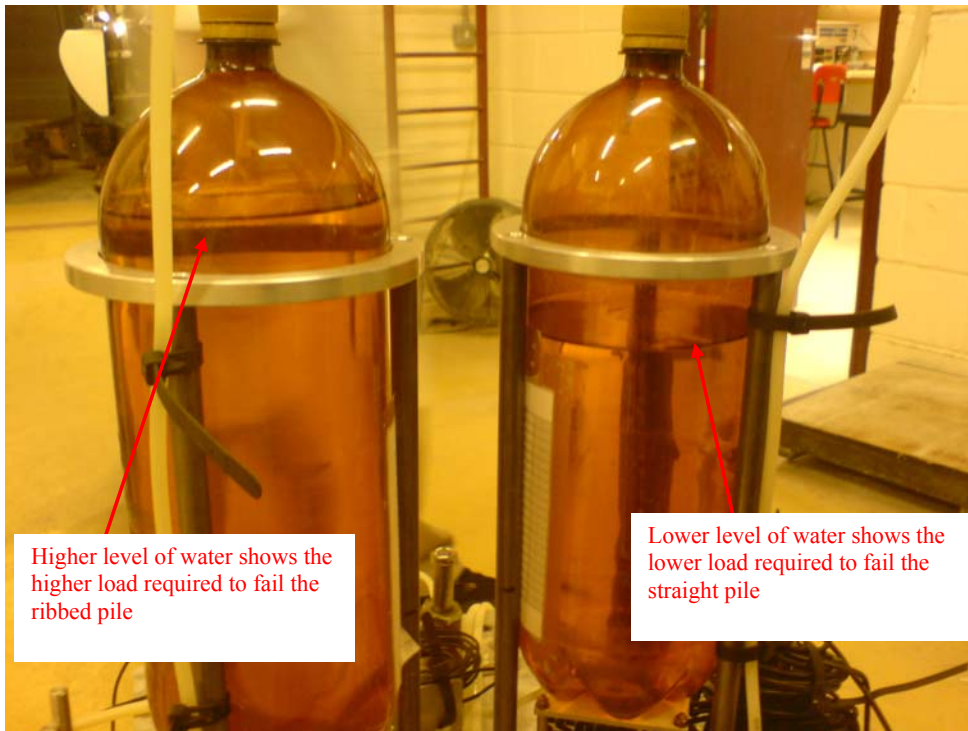


Figure 6.8 Photograph of settled pile heads on taking the sample out of the centrifuge after test JW01



Figure 6.9 Photograph showing loading apparatus on removal from centrifuge after test JW01 – water level gives indication of load applied



Higher level of water shows the higher load required to fail the ribbed pile

Lower level of water shows the lower load required to fail the straight pile

Figure 6.10 Test JW02: Pore Water Pressure-Time Graph

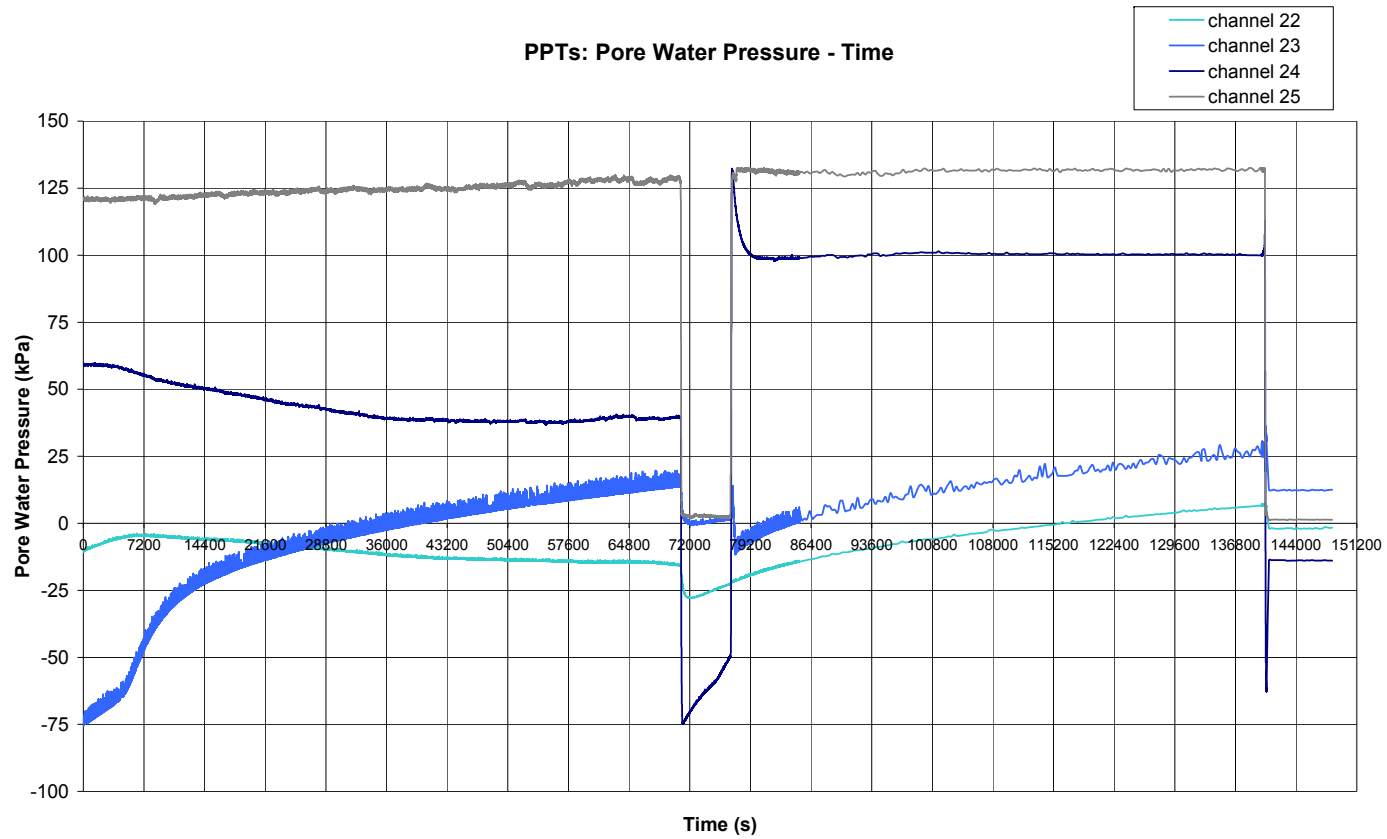


Figure 6.11 Test JW02: Displacement-Time Graph

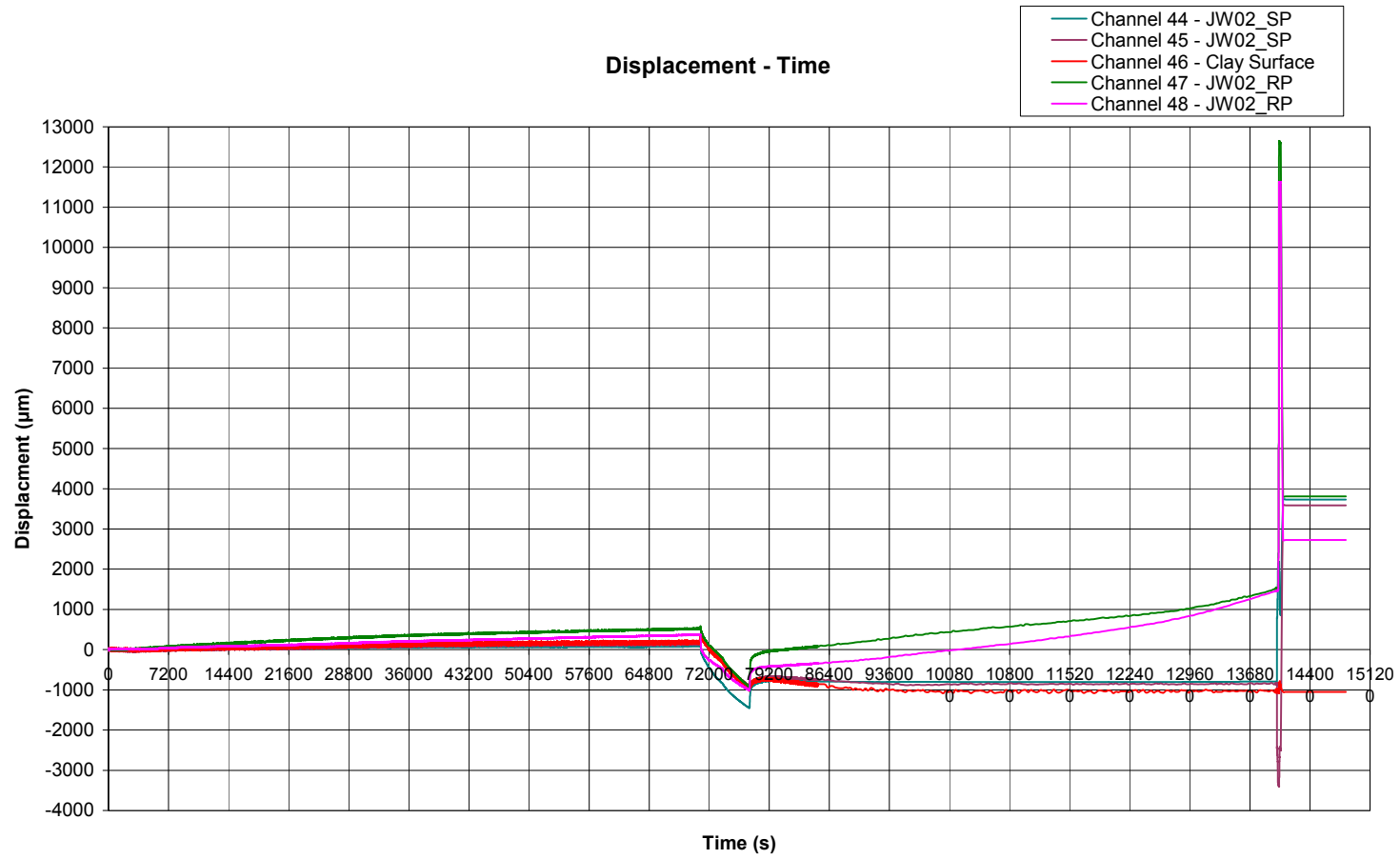


Figure 6.12 Test JW02_SP: Load-Time Graph

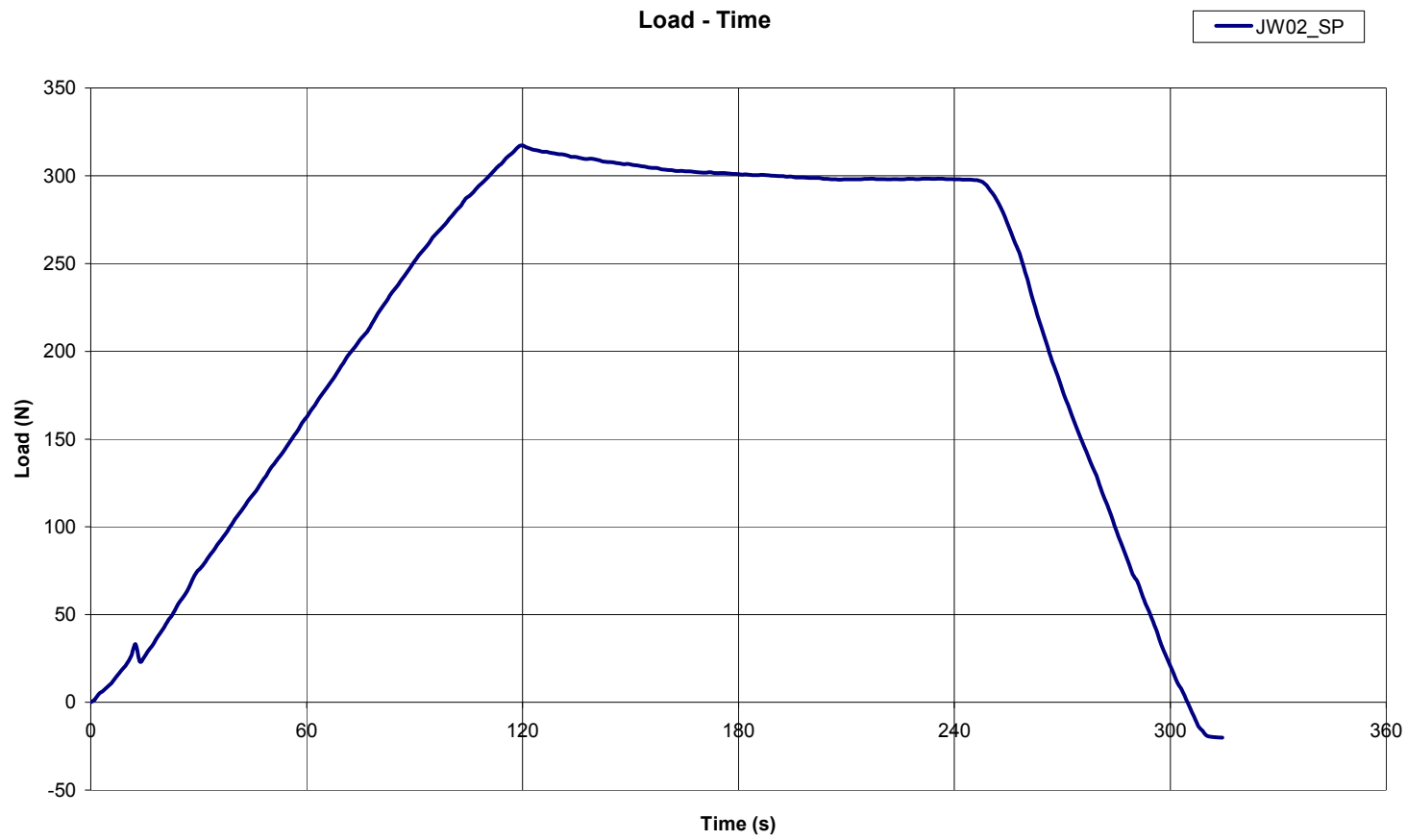


Figure 6.13 Test JW02_SP: Load-Settlement Graph

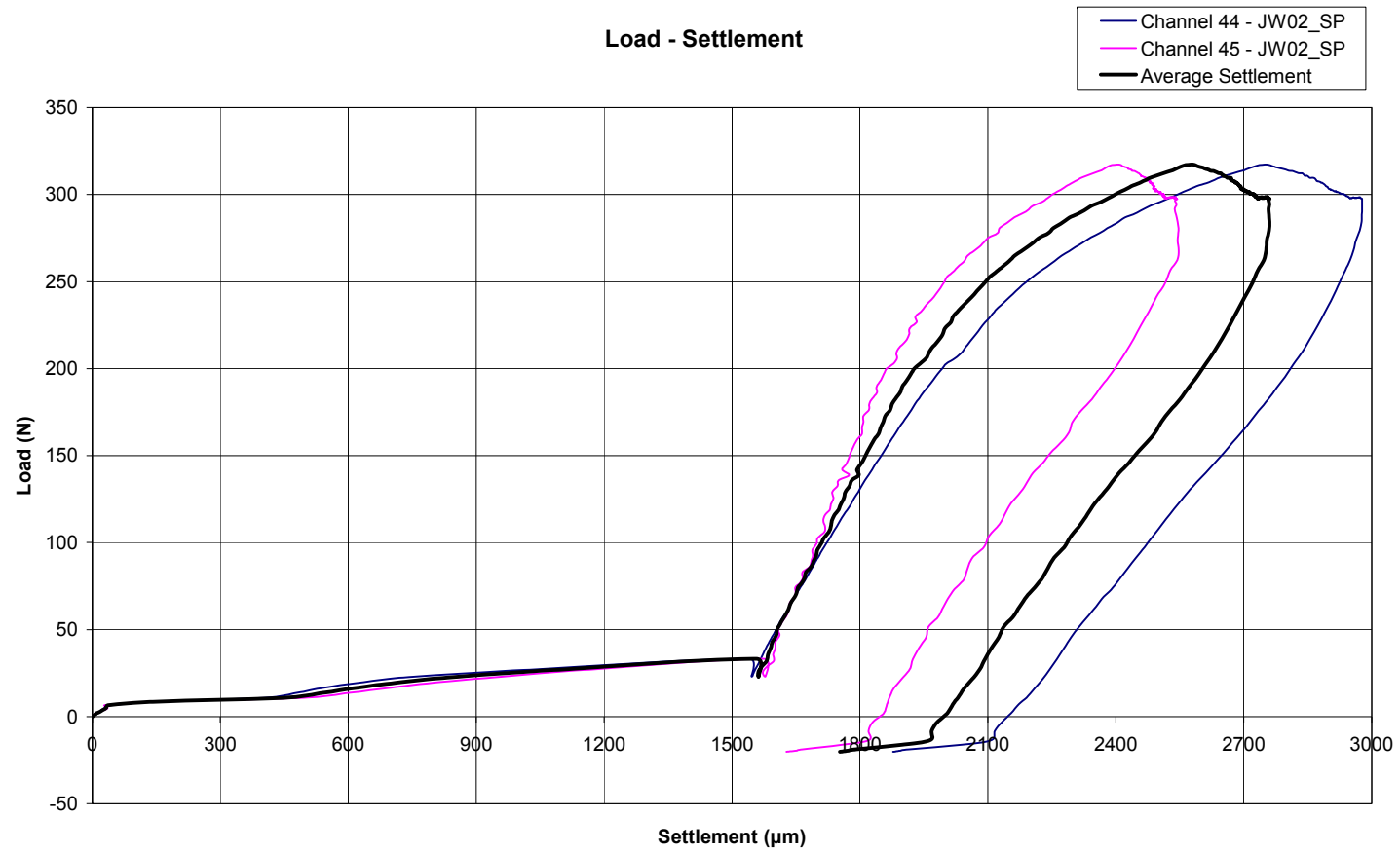


Figure 6.14 Test JW02: Load-Settlement Graph



Figure 6.15 Photograph showing pile heads after centrifuge test JW02 – resin spill on clay surface can be seen

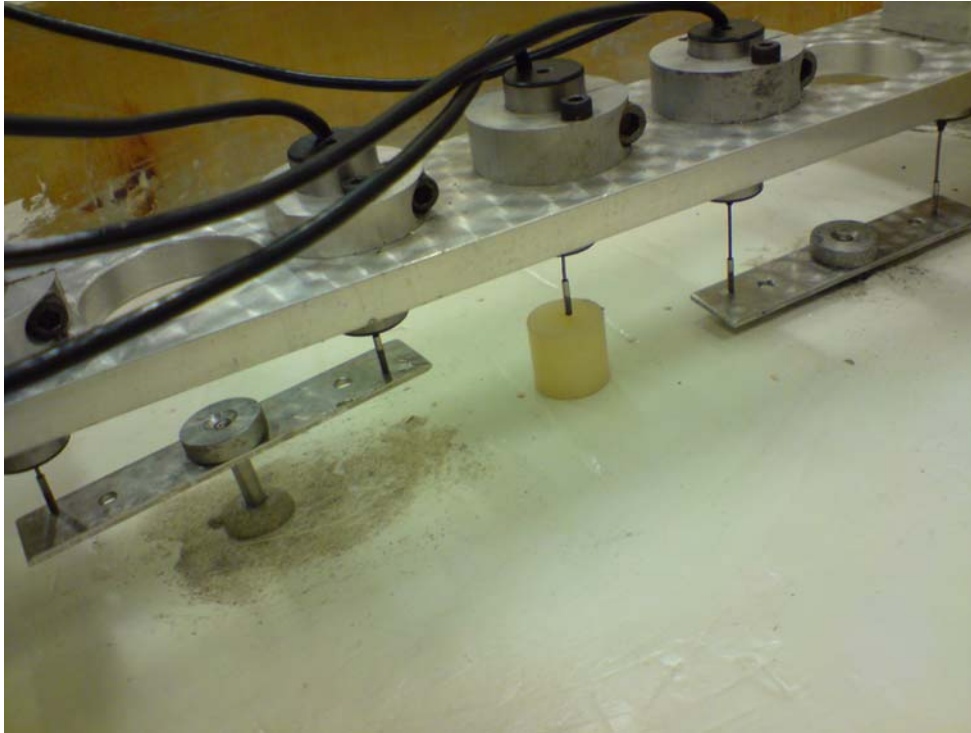


Figure 6.16 Test JW03: Pore Water Pressure-Time Graph

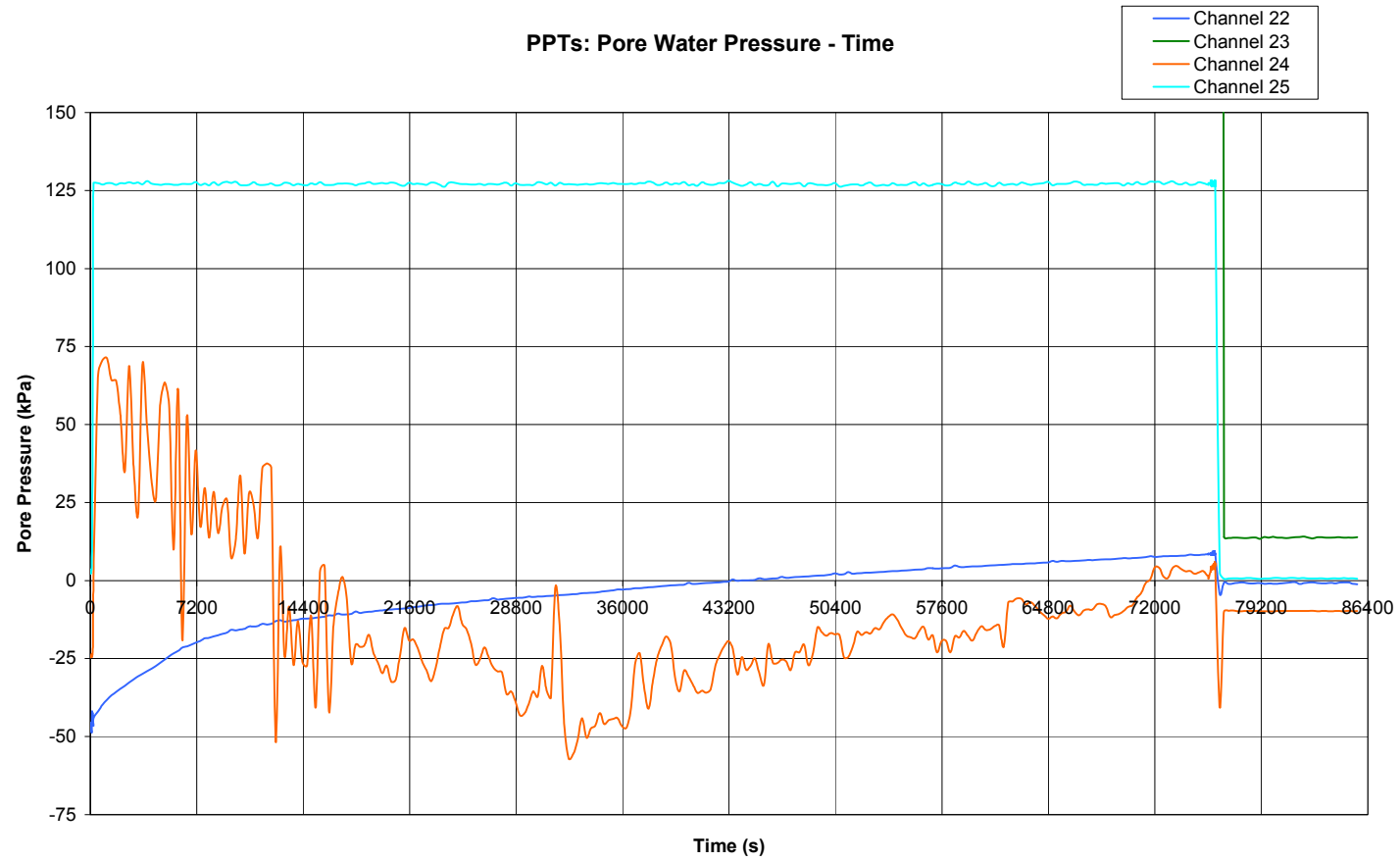


Figure 6.17 Test JW03: Displacement-Time Graph

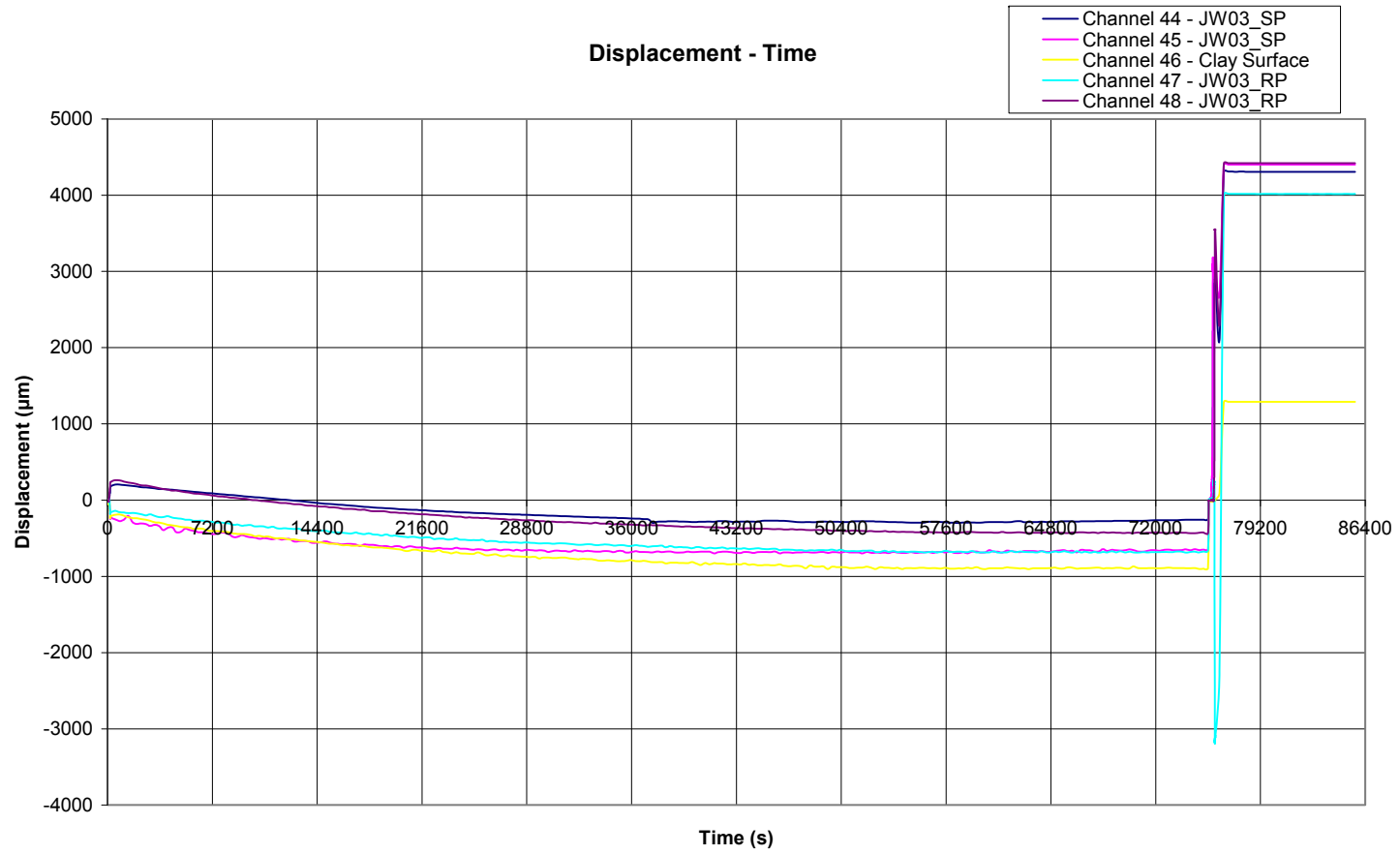


Figure 6.18 Test JW03: Load-Time Graph

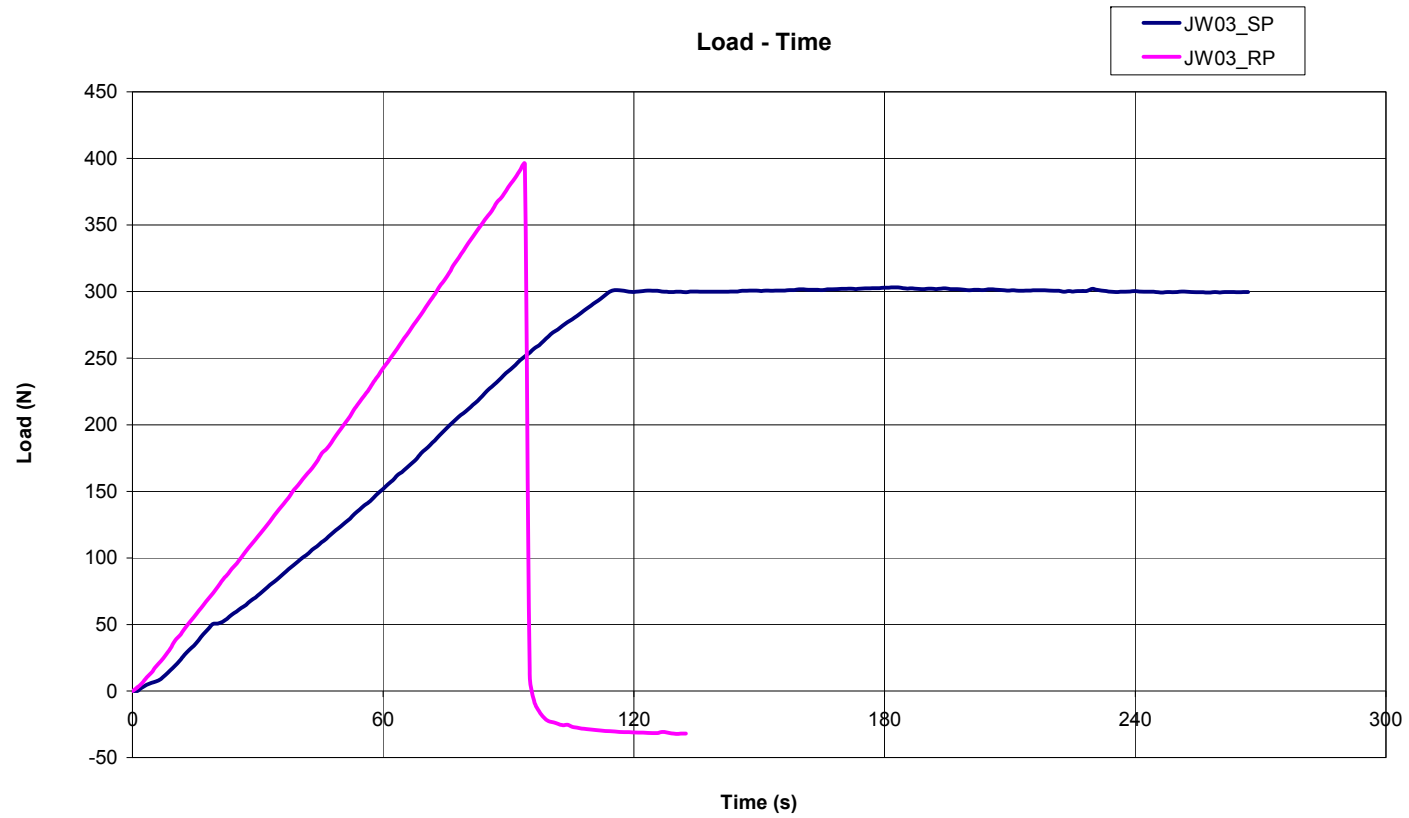


Figure 6.19 Test JW03_SP: Load-Settlement Graph

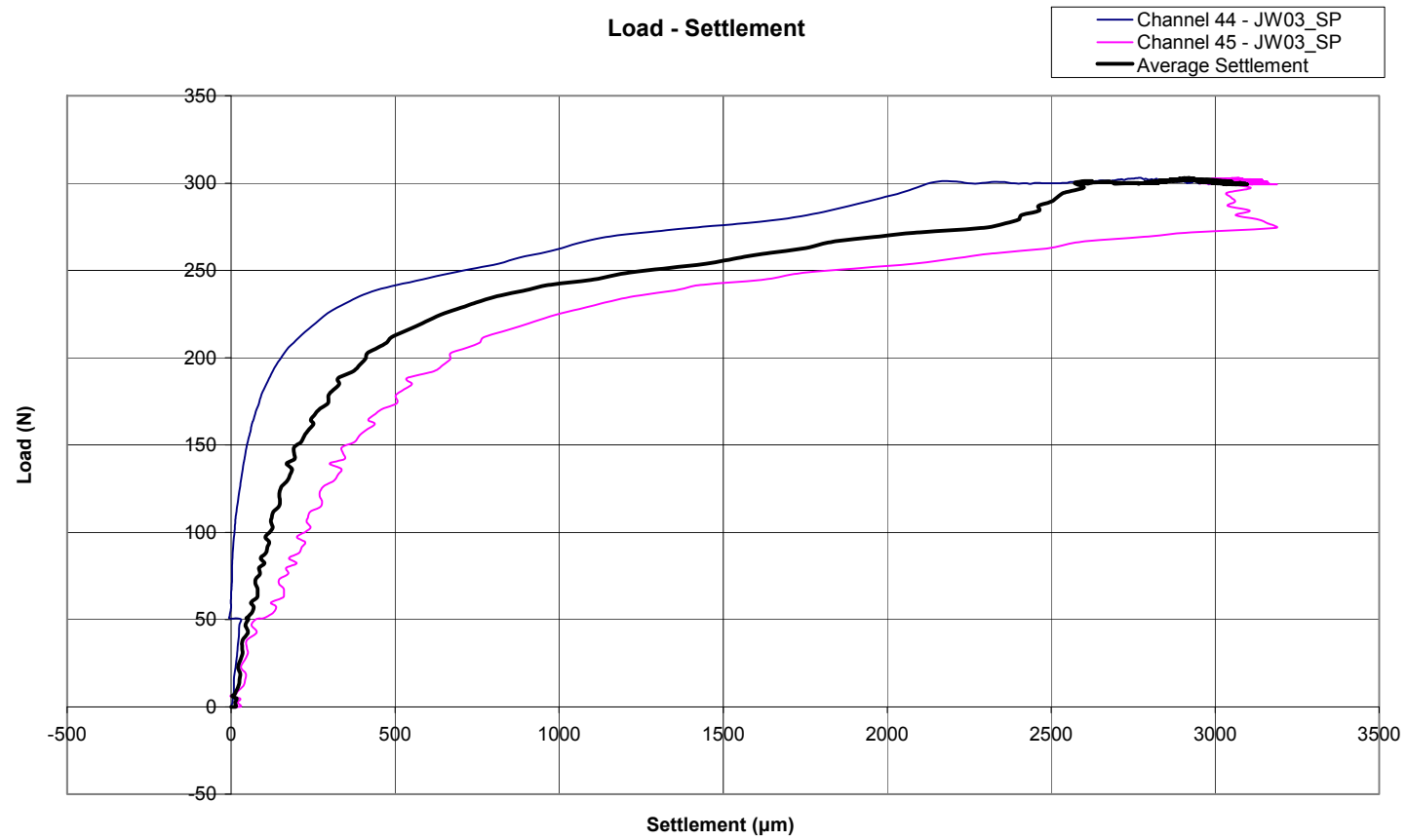


Figure 6.20 Test JW03_RP: Load-Settlement Graph

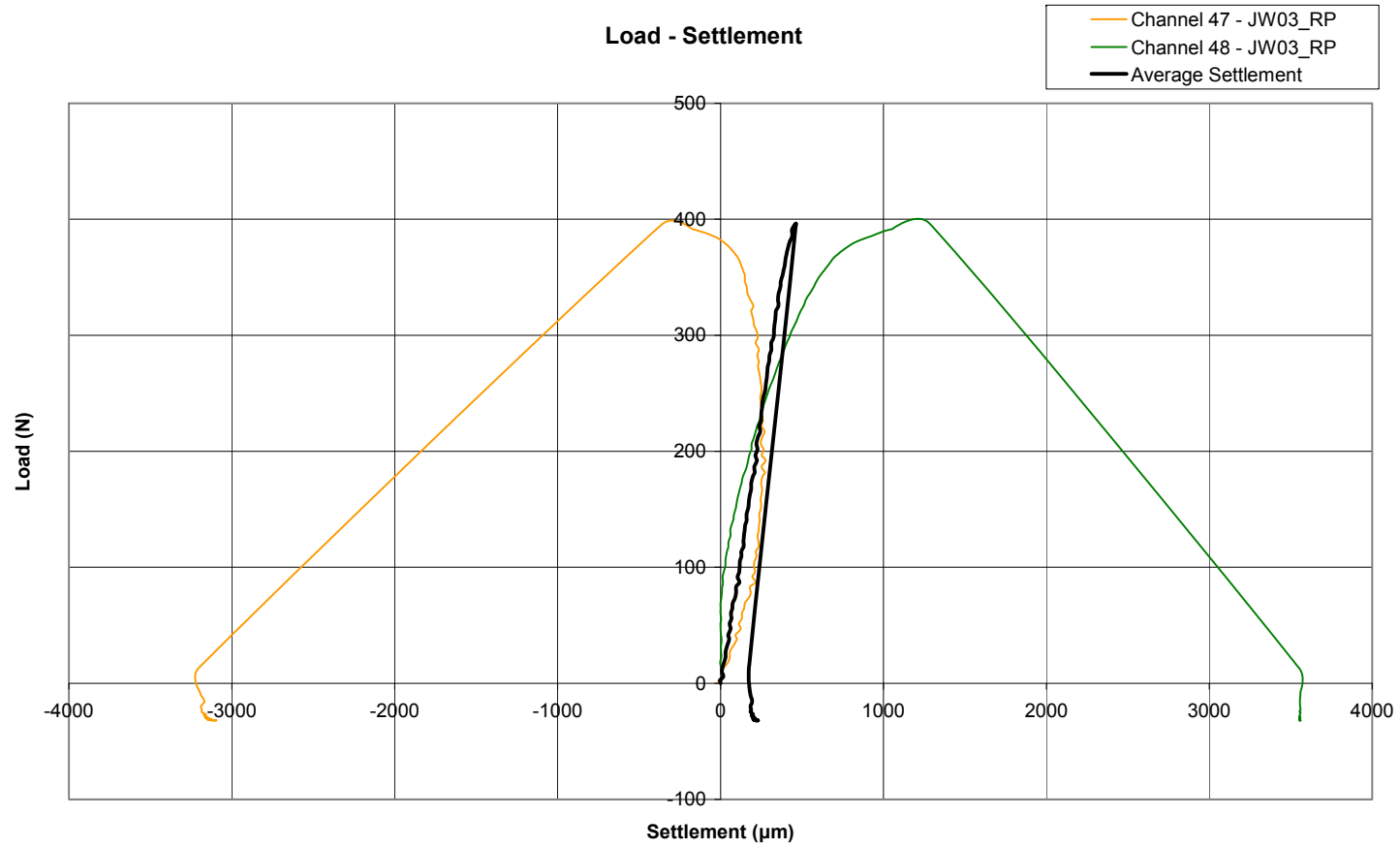


Figure 6.21 Test JW03: Load-Settlement Graph

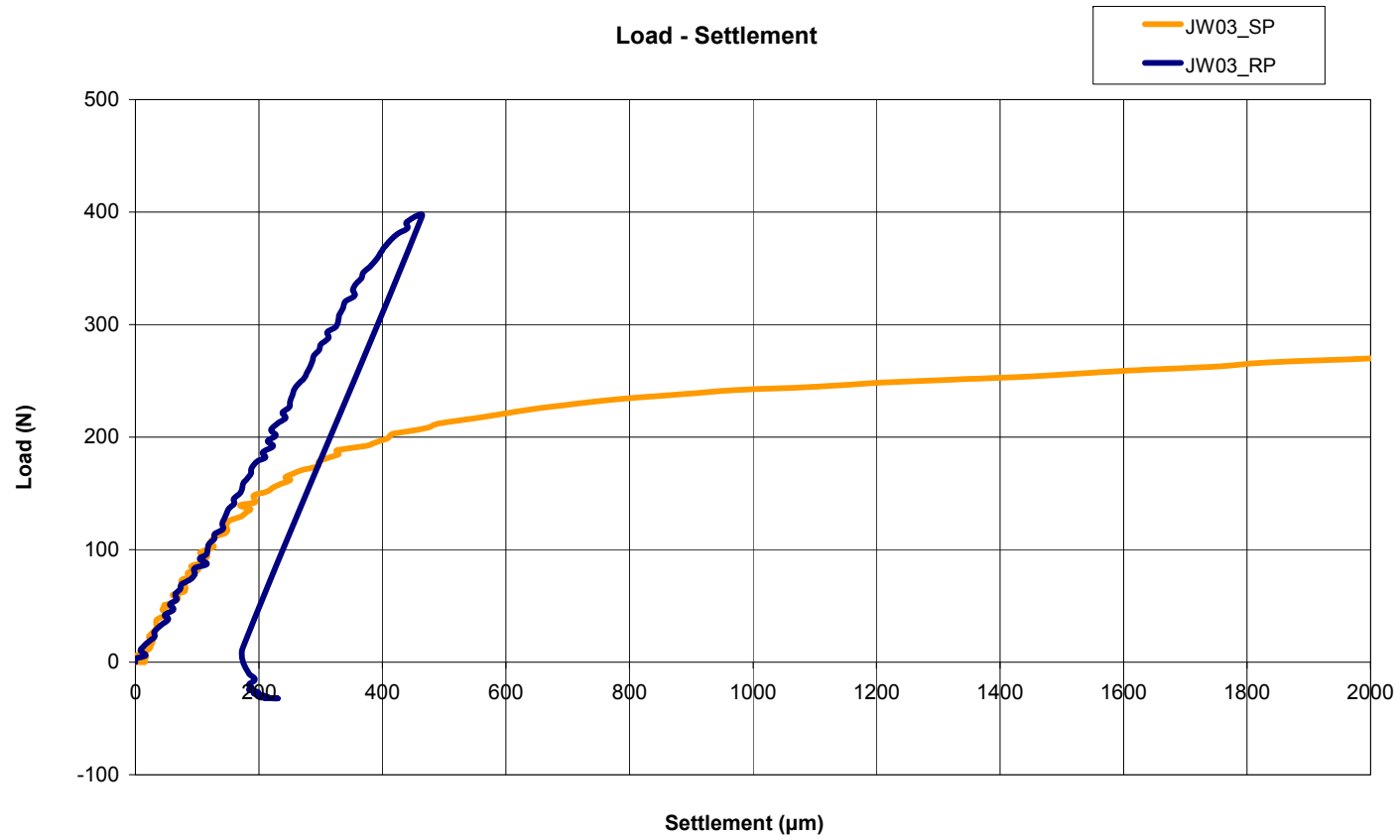


Figure 6.22 Photograph showing pile heads after test JW03

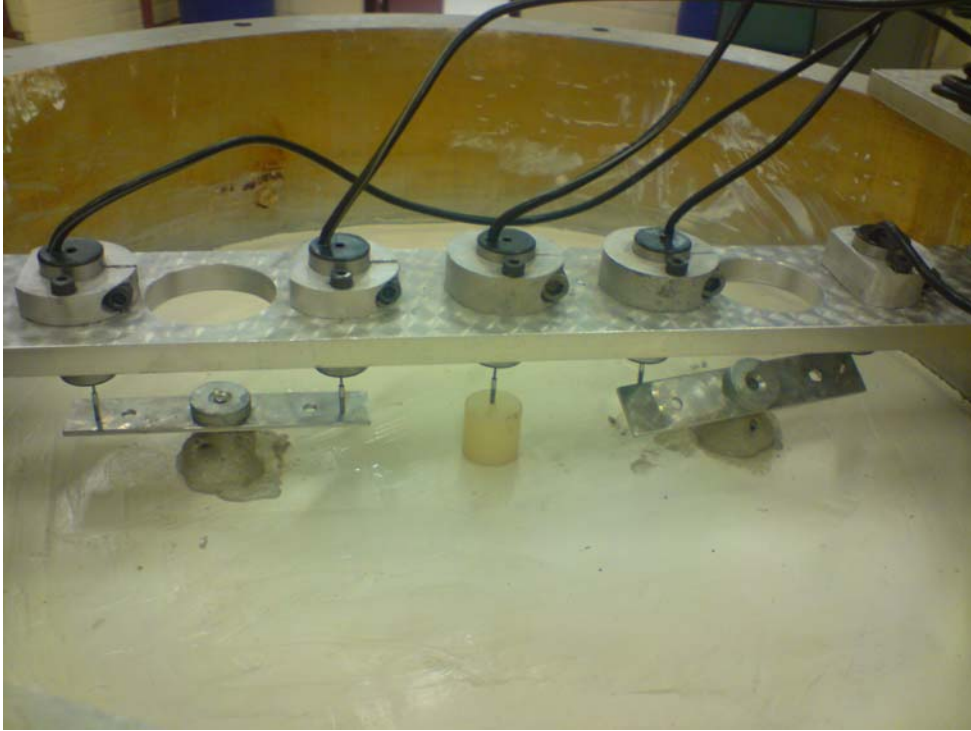


Figure 6.23 Test JW04: Pore Water Pressure-Time Graph

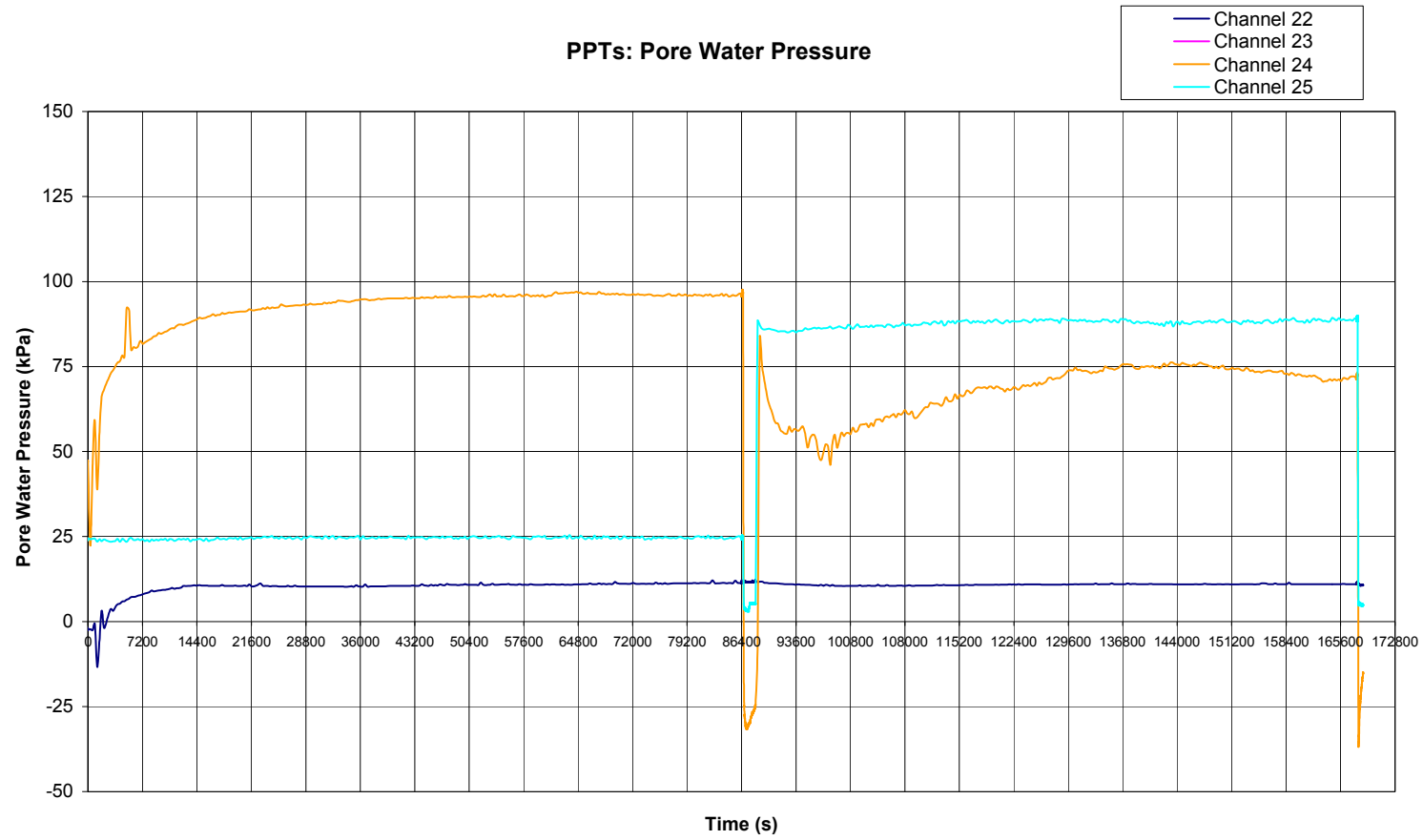


Figure 6.24 Test JW04: Displacement-Time Graph

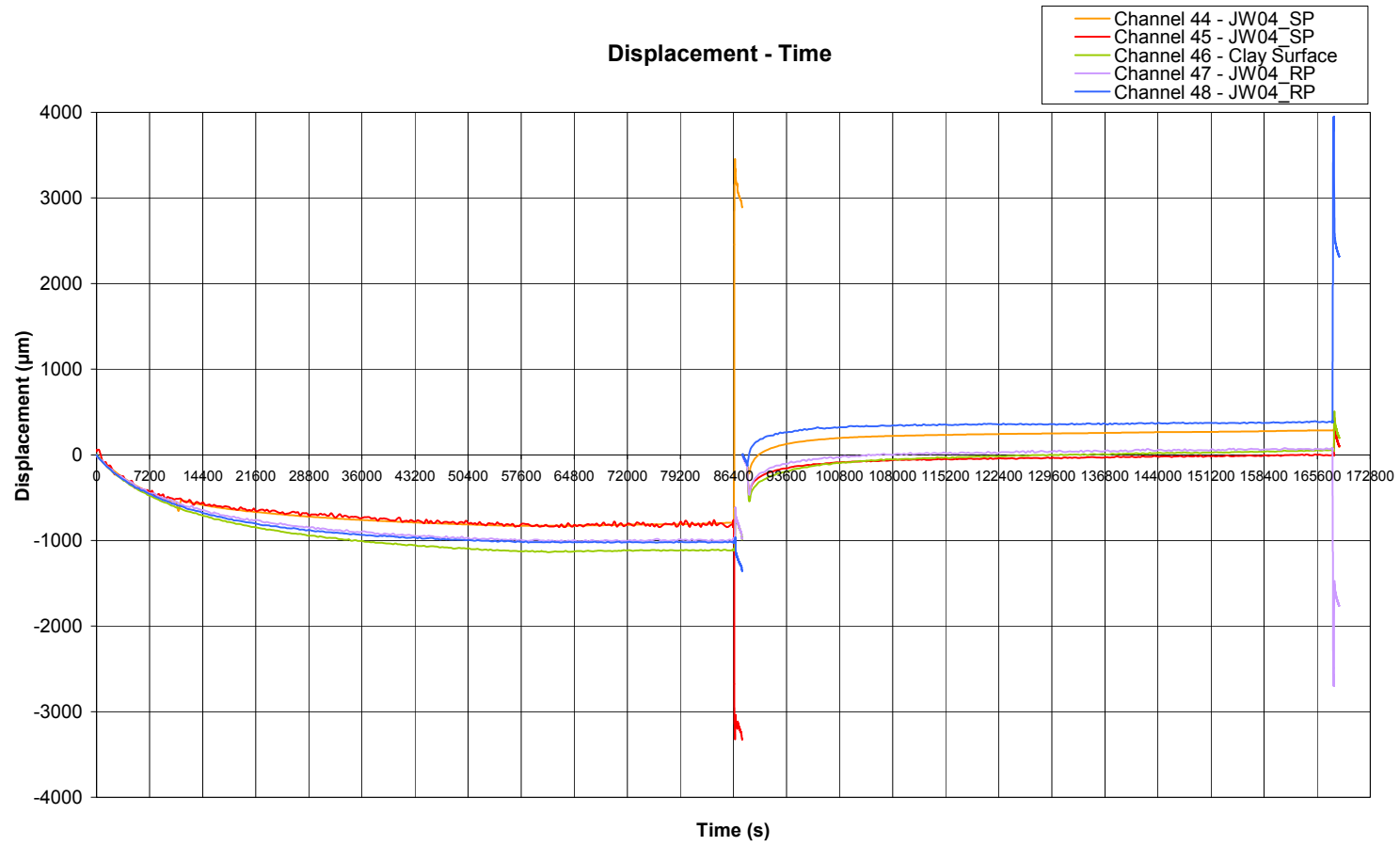


Figure 6.25 Test JW04: Load-Time Graph

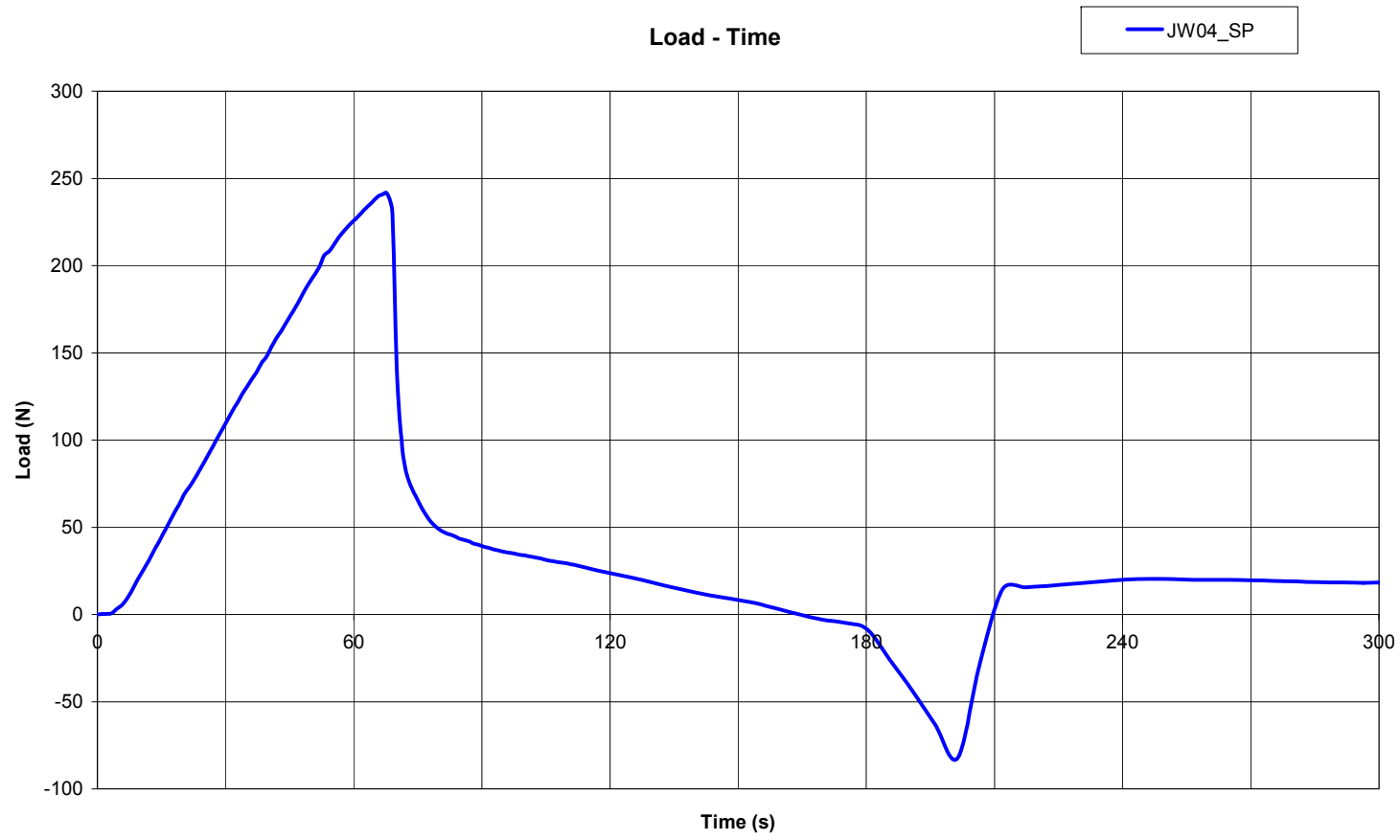


Figure 6.26 Test JW04_SP: Load-Settlement Graph

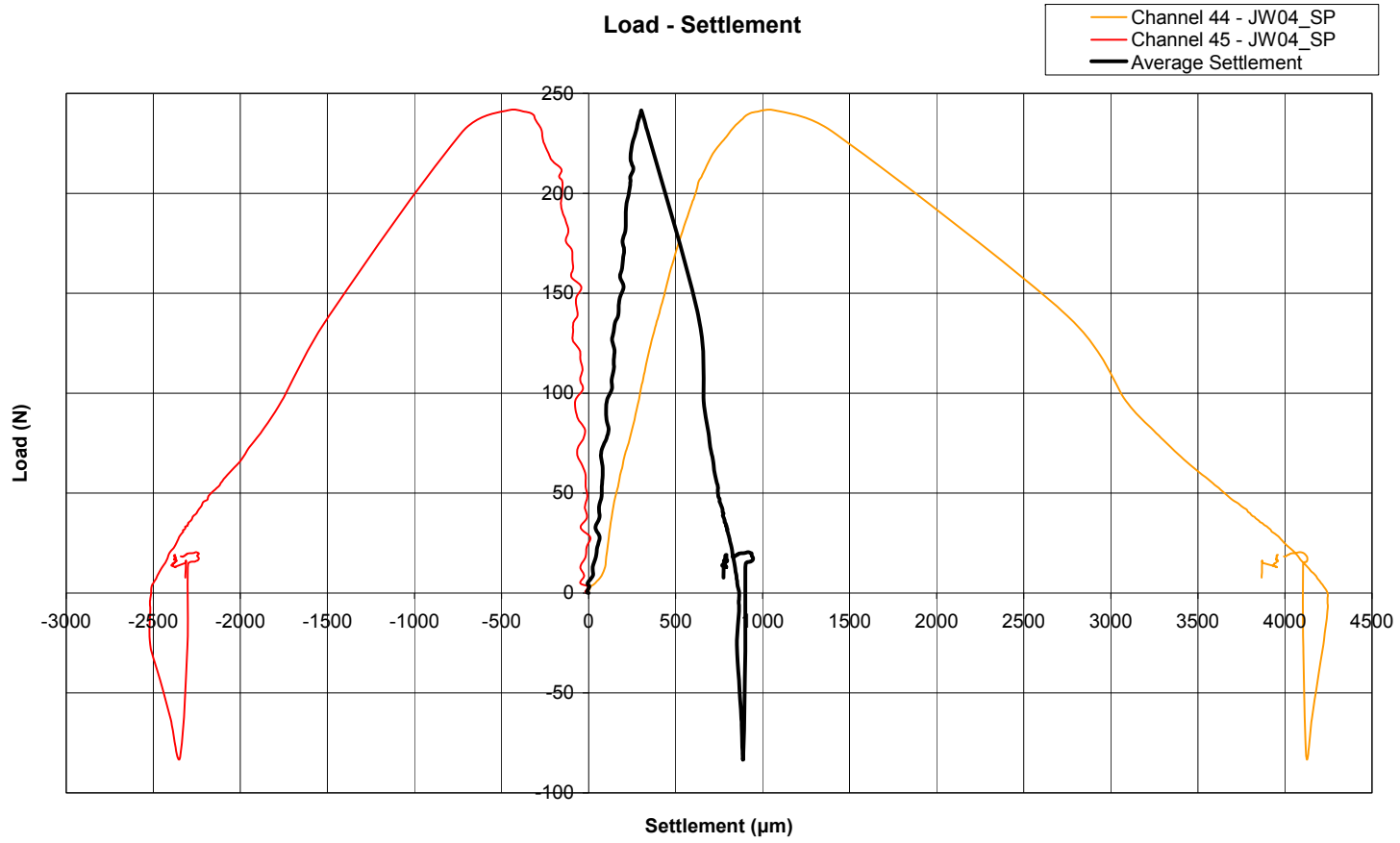


Figure 6.27 Test JW04: Load-Settlement Graph

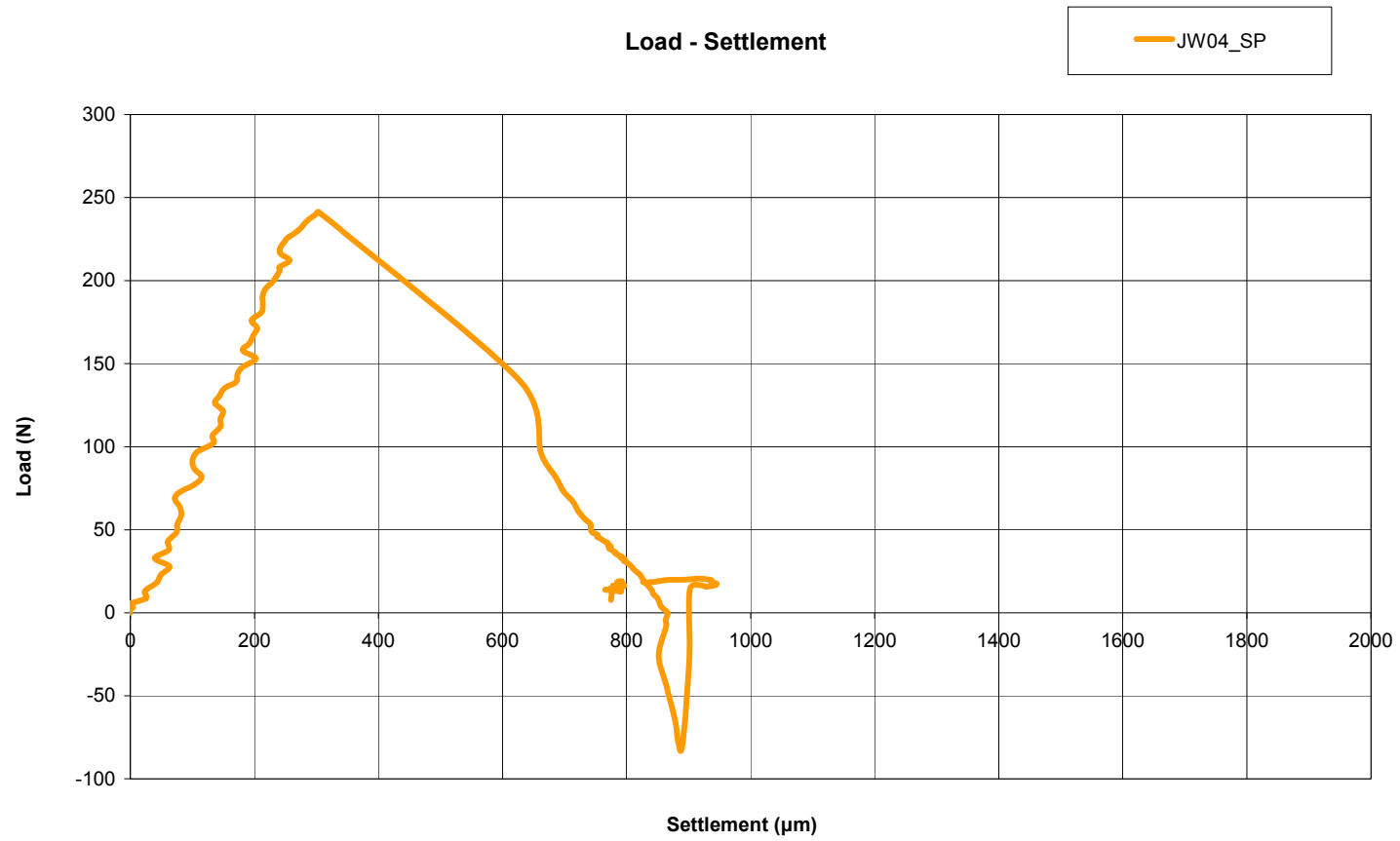


Figure 6.28 Photograph showing damaged pile head

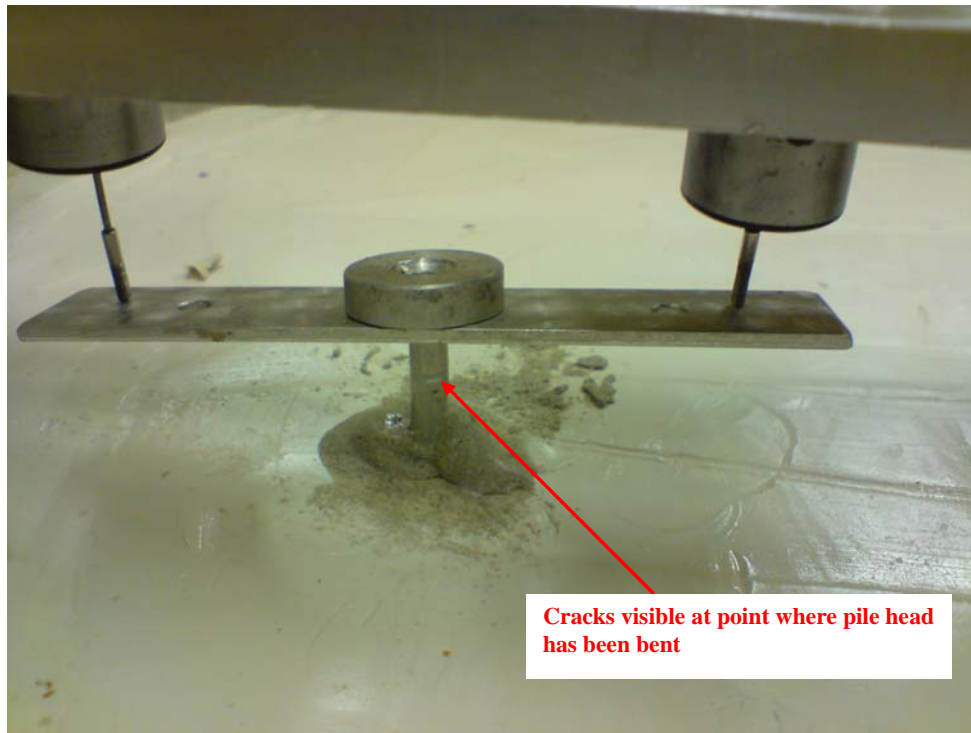


Figure 6.29 Test JW05: Pore Water Pressure-Time Graph

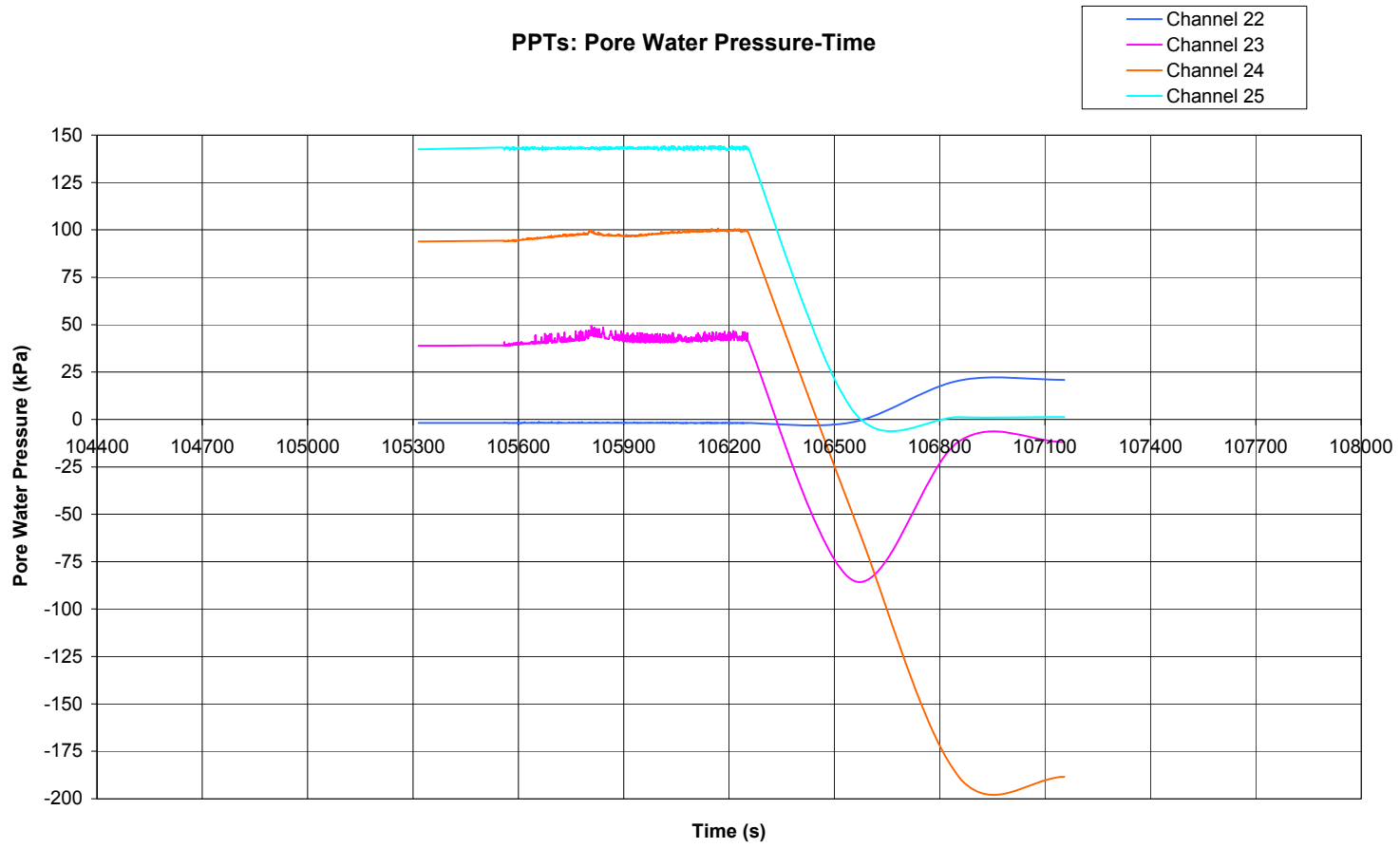


Figure 6.30 Test JW05: Displacement – Time Graph

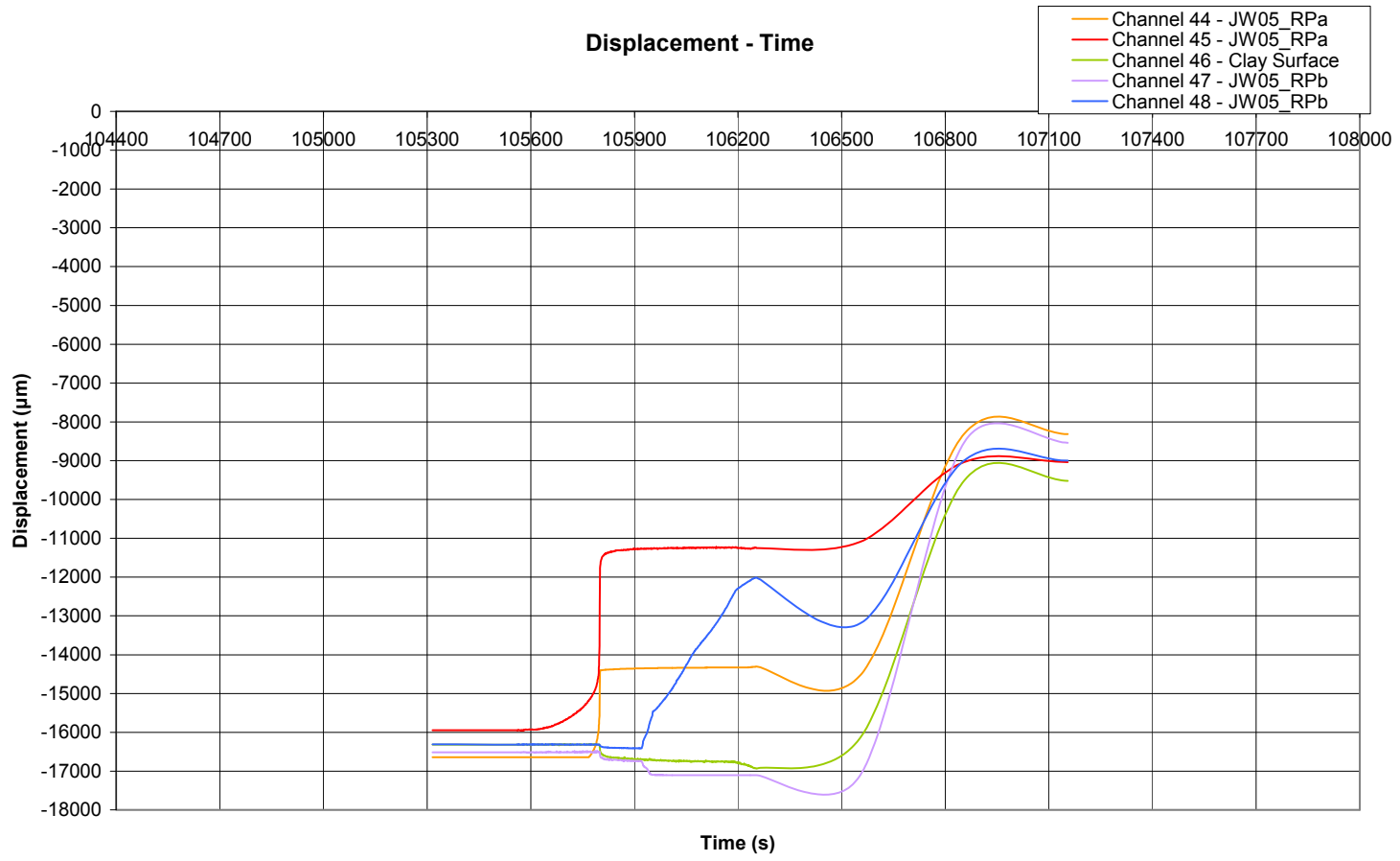


Figure 6.31 Test JW05: Load-Time Graph

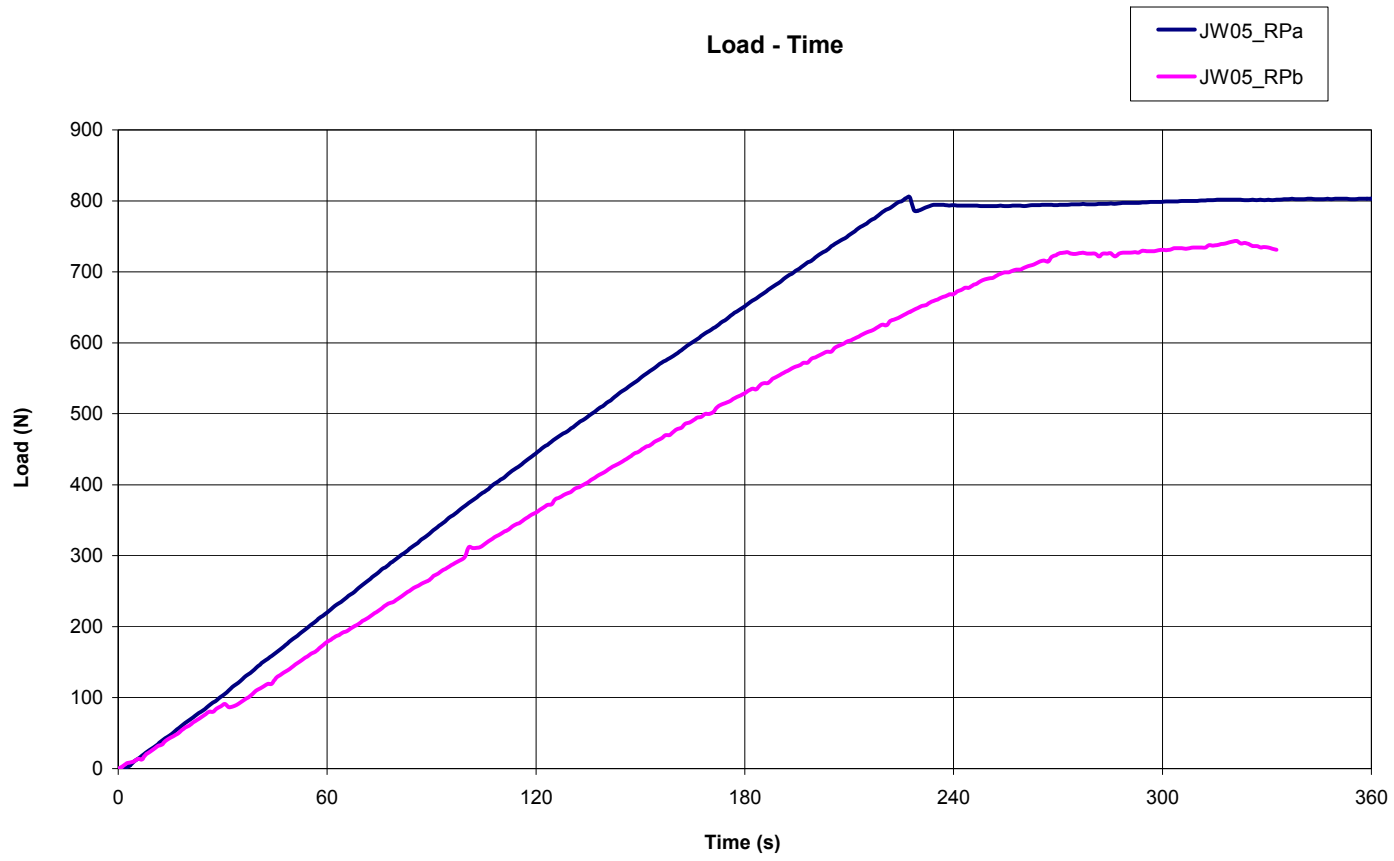


Figure 6.32 Test JW05_RPa: Load-Settlement Graph

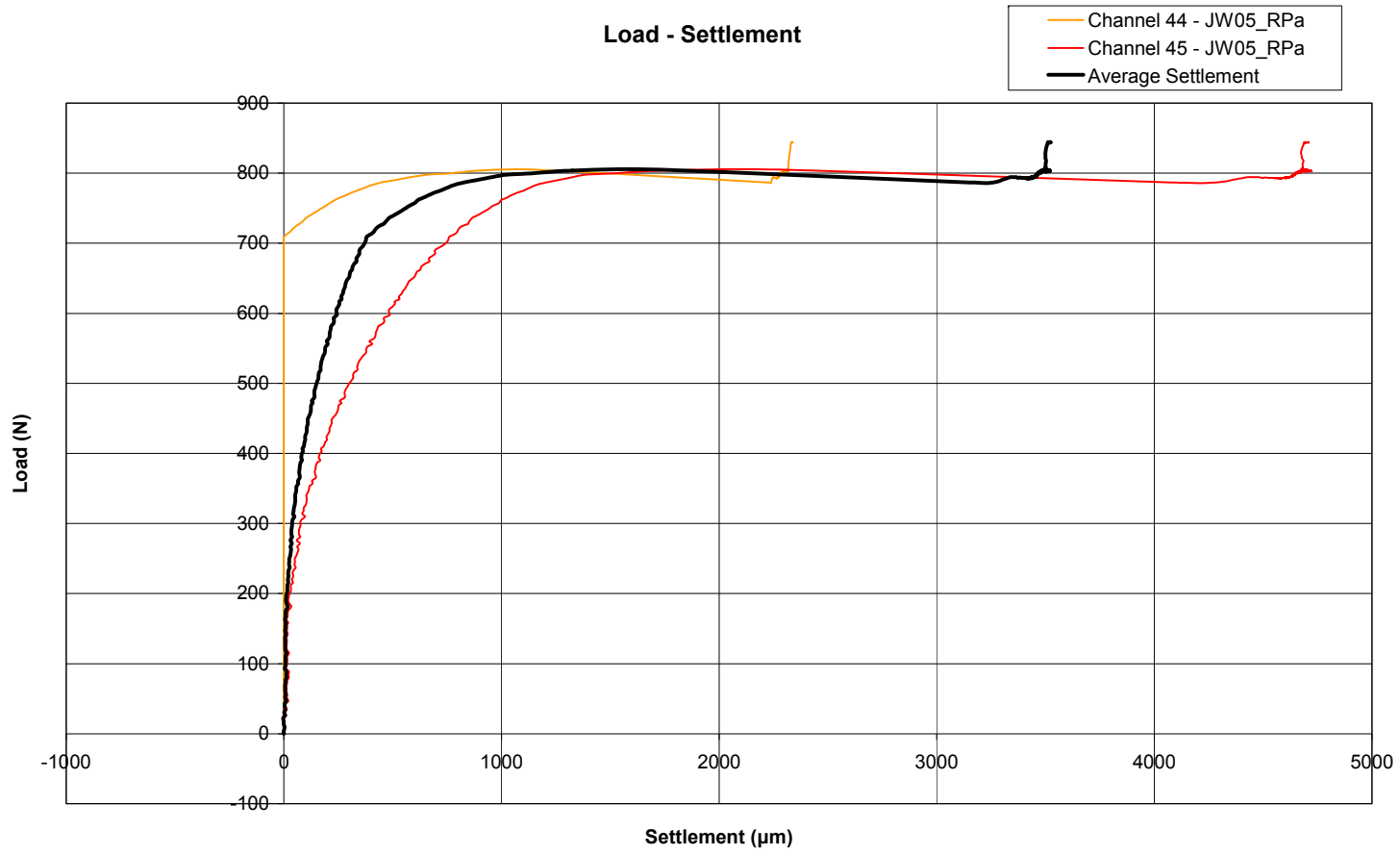


Figure 6.33 Test JW05_RPb: Load-Settlement Graph

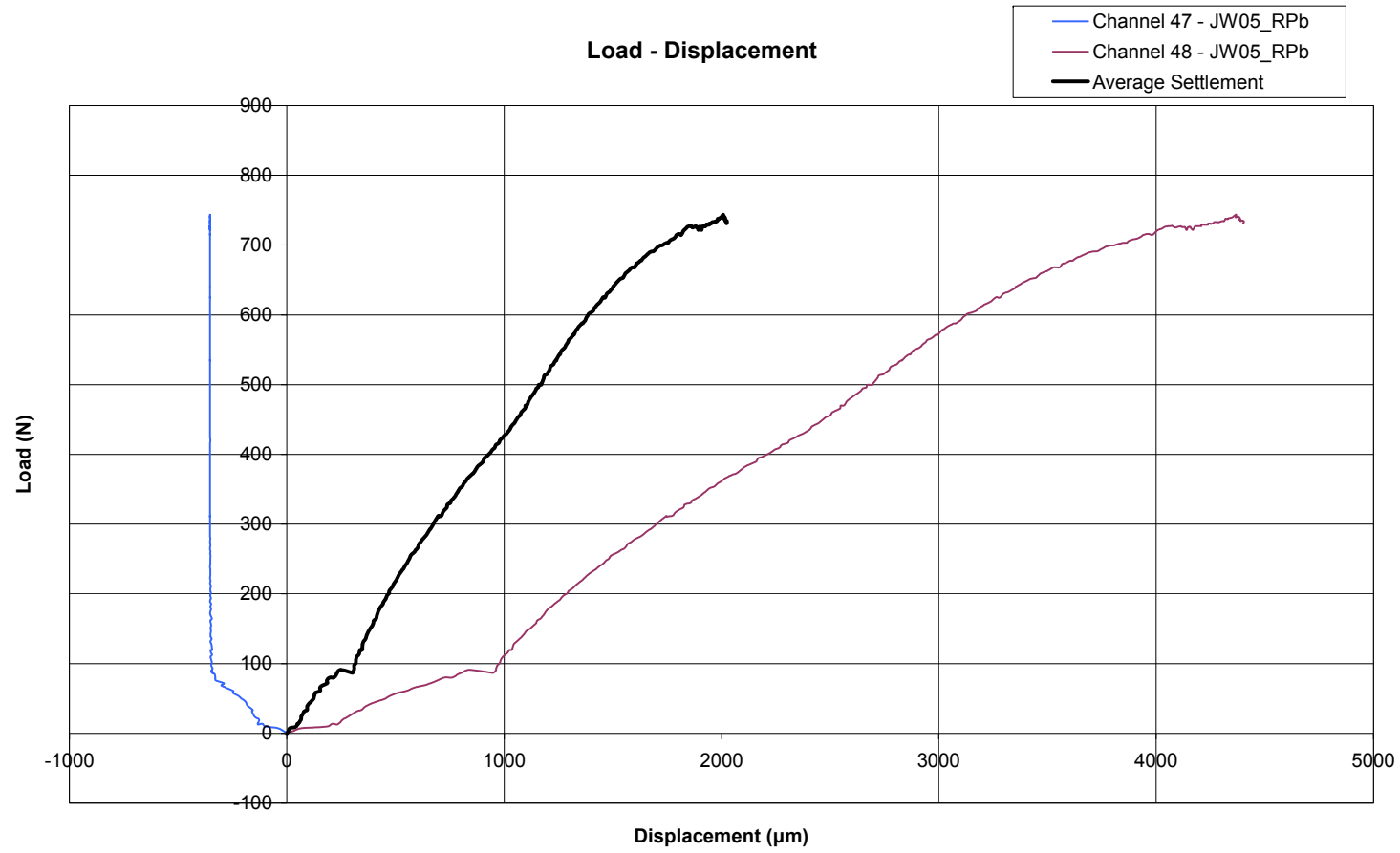


Figure 6.34 Test JW05: Load-Settlement Graph

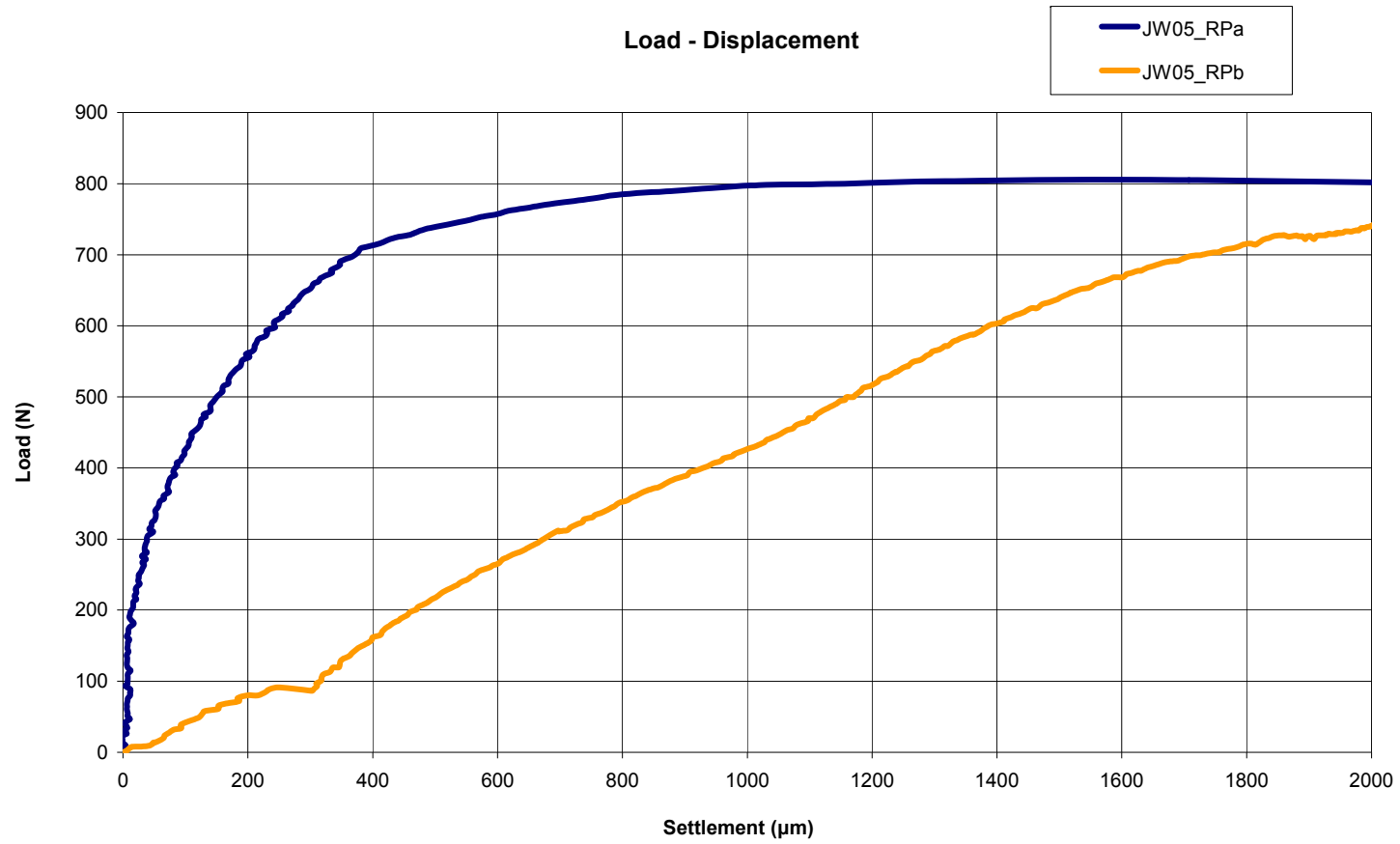


Figure 6.35 Photograph showing water levels in bottle reservoirs after test JW05

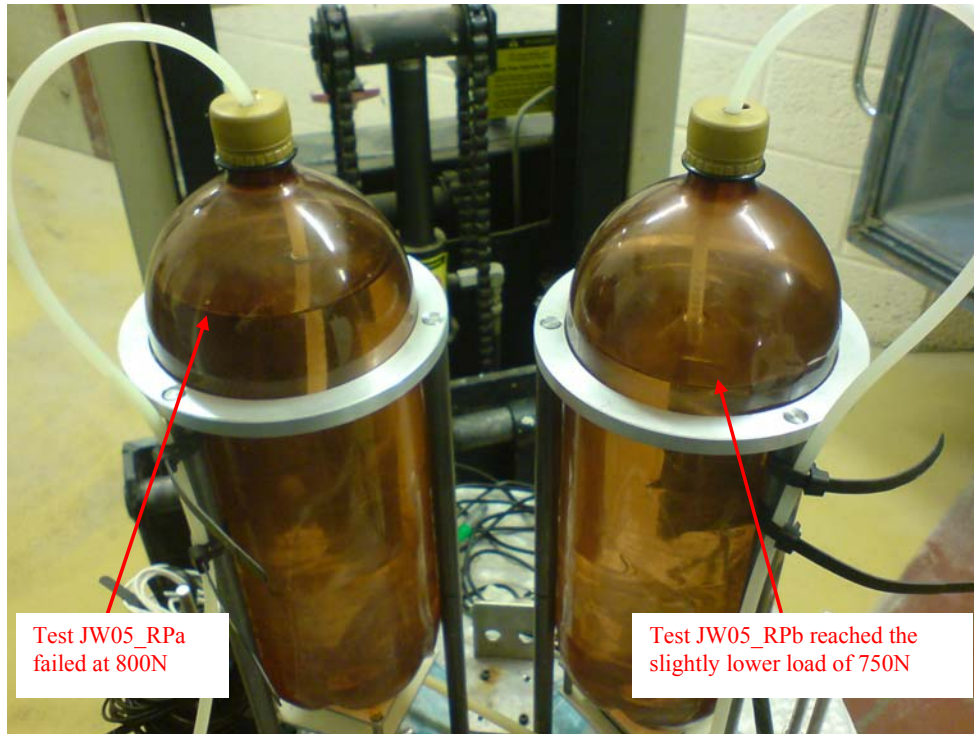


Figure 6.36 Photograph showing pile head positions after centrifuge testing

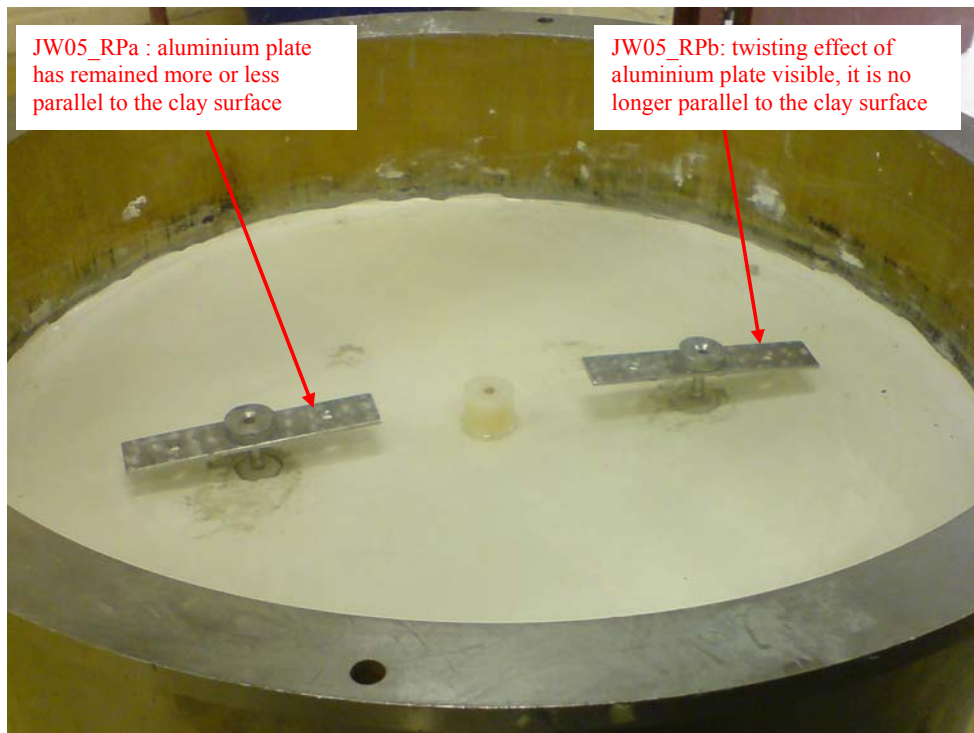


Figure 6.37 Photograph showing resin residue on clay surface around pile head



Figure 6.38 Test JW06: Pore Water Pressure-Time Graph

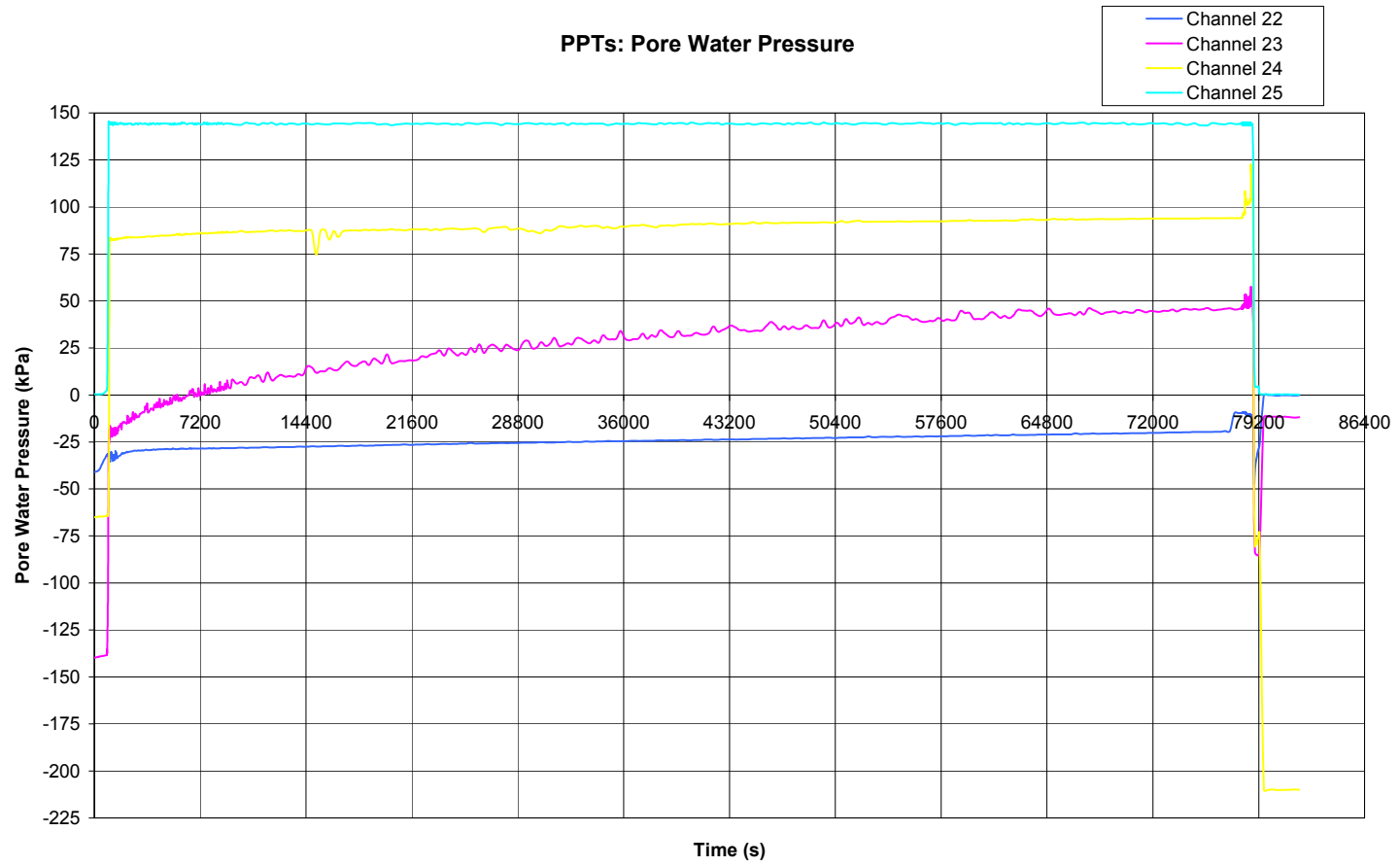


Figure 6.39 Test JW06: Displacement-Time Graph

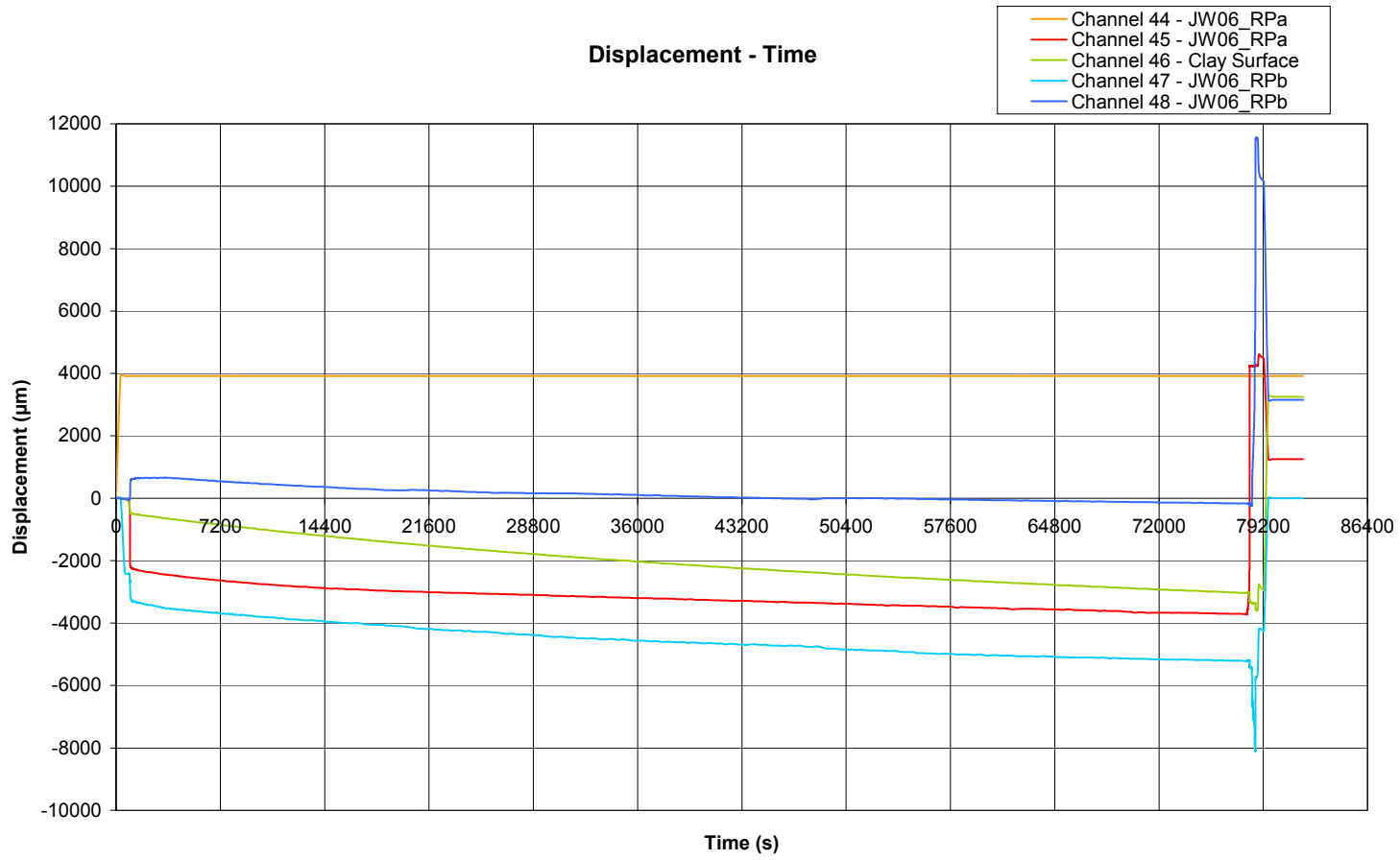


Figure 6.40 Test JW06: Load-Time Graph

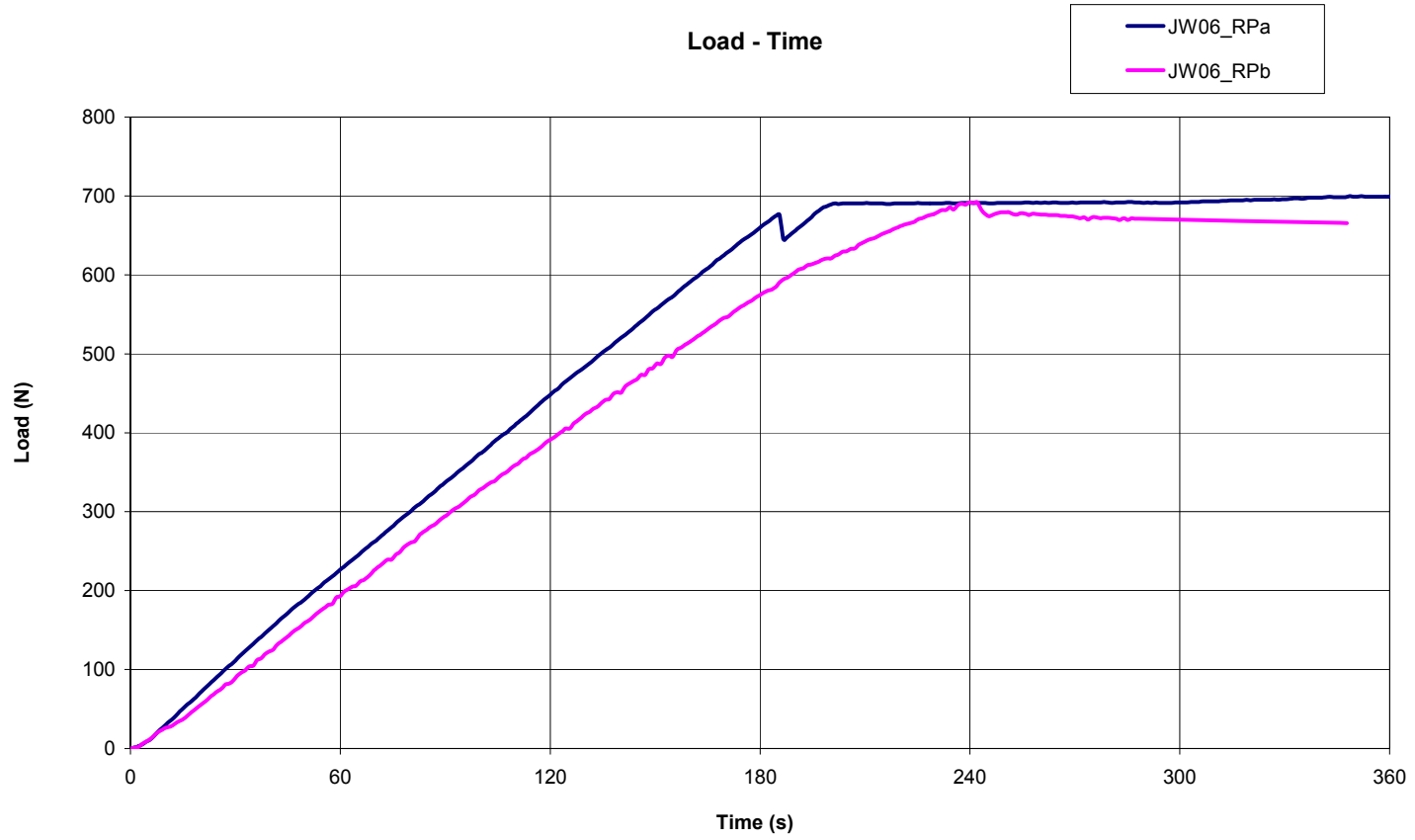


Figure 6.41 Test JW06_RPa: Load-Settlement Graph

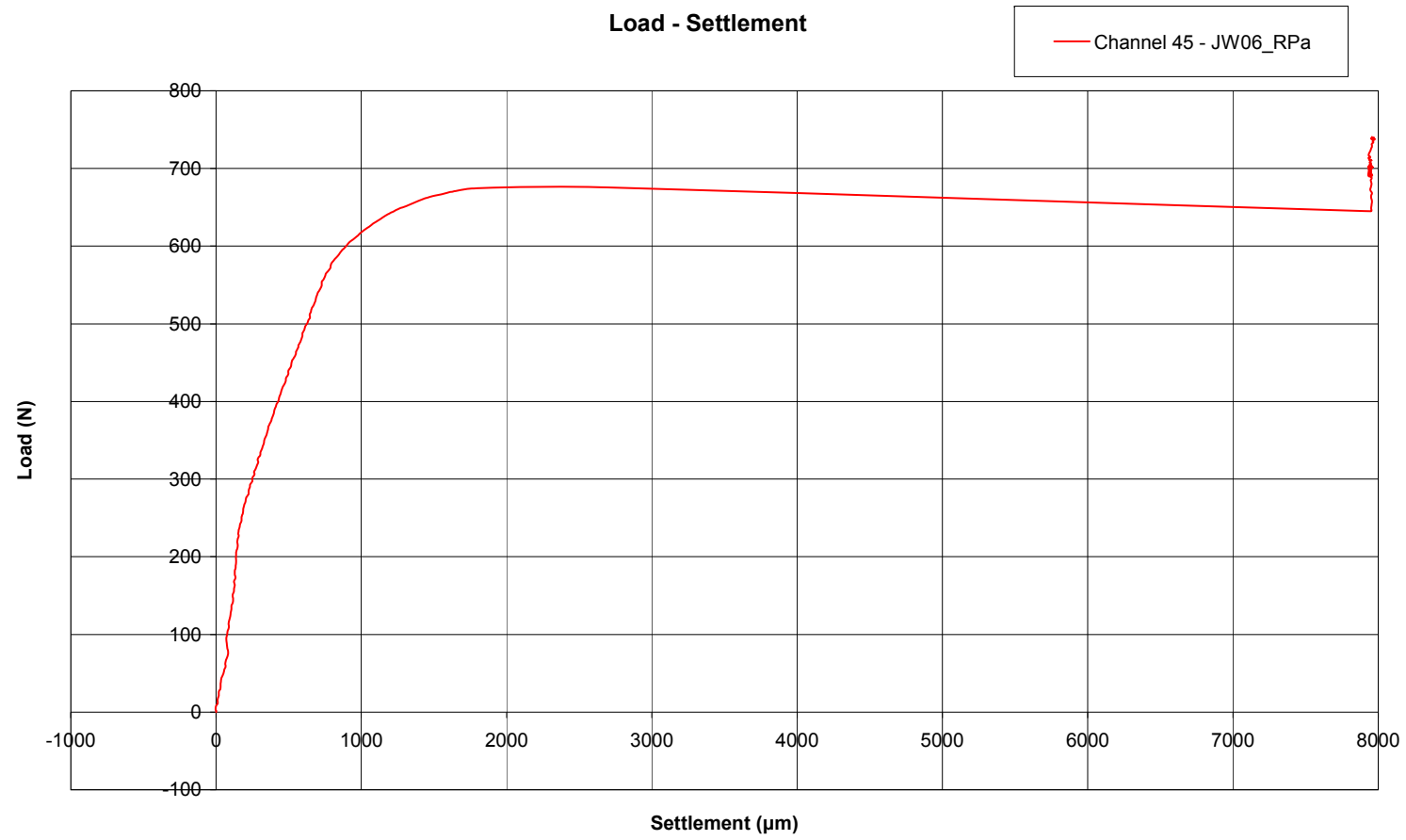


Figure 6.42 Test JW06_RPb: Load-Settlement Graph

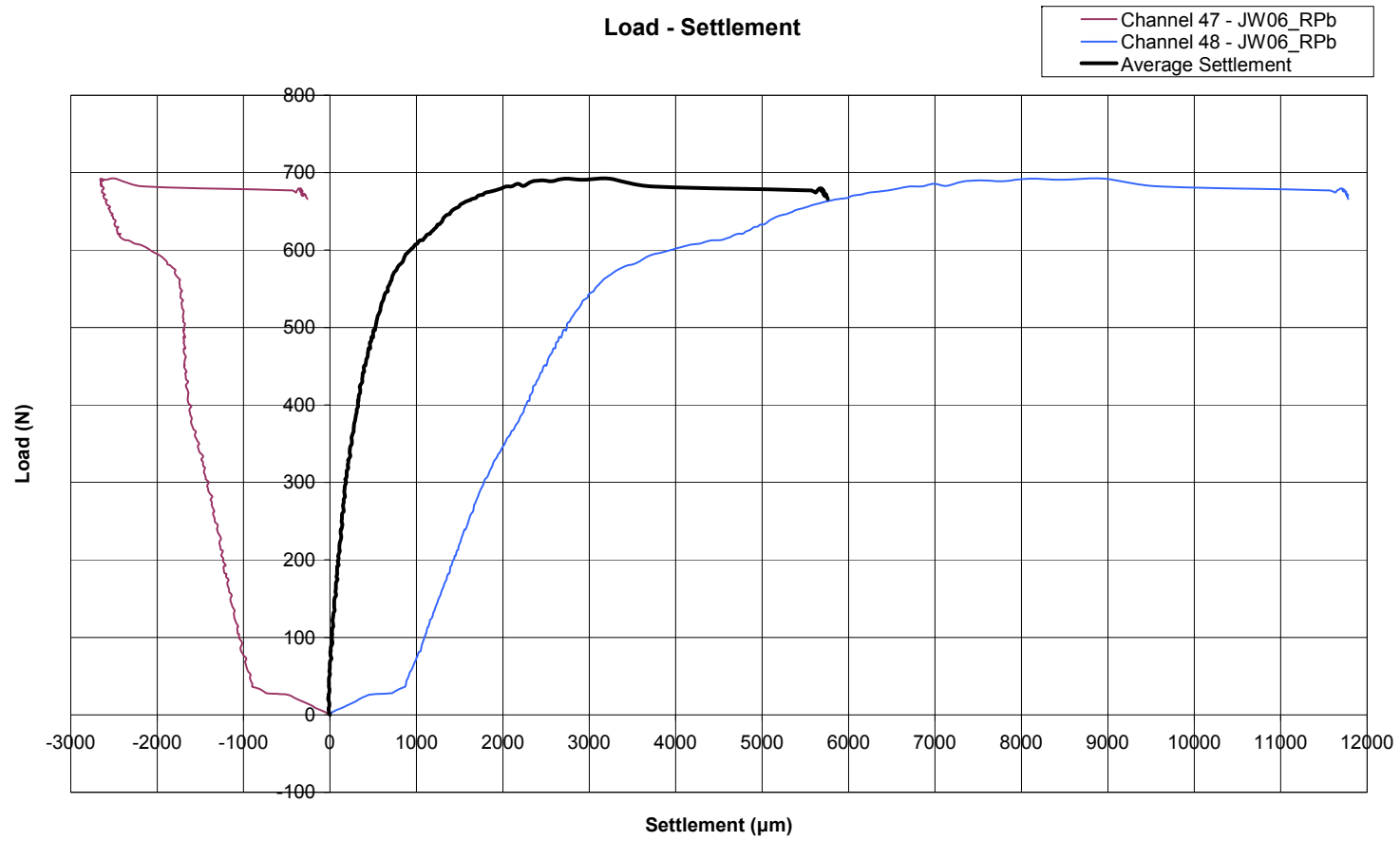


Figure 6.43 Test JW06: Load-Settlement Graph

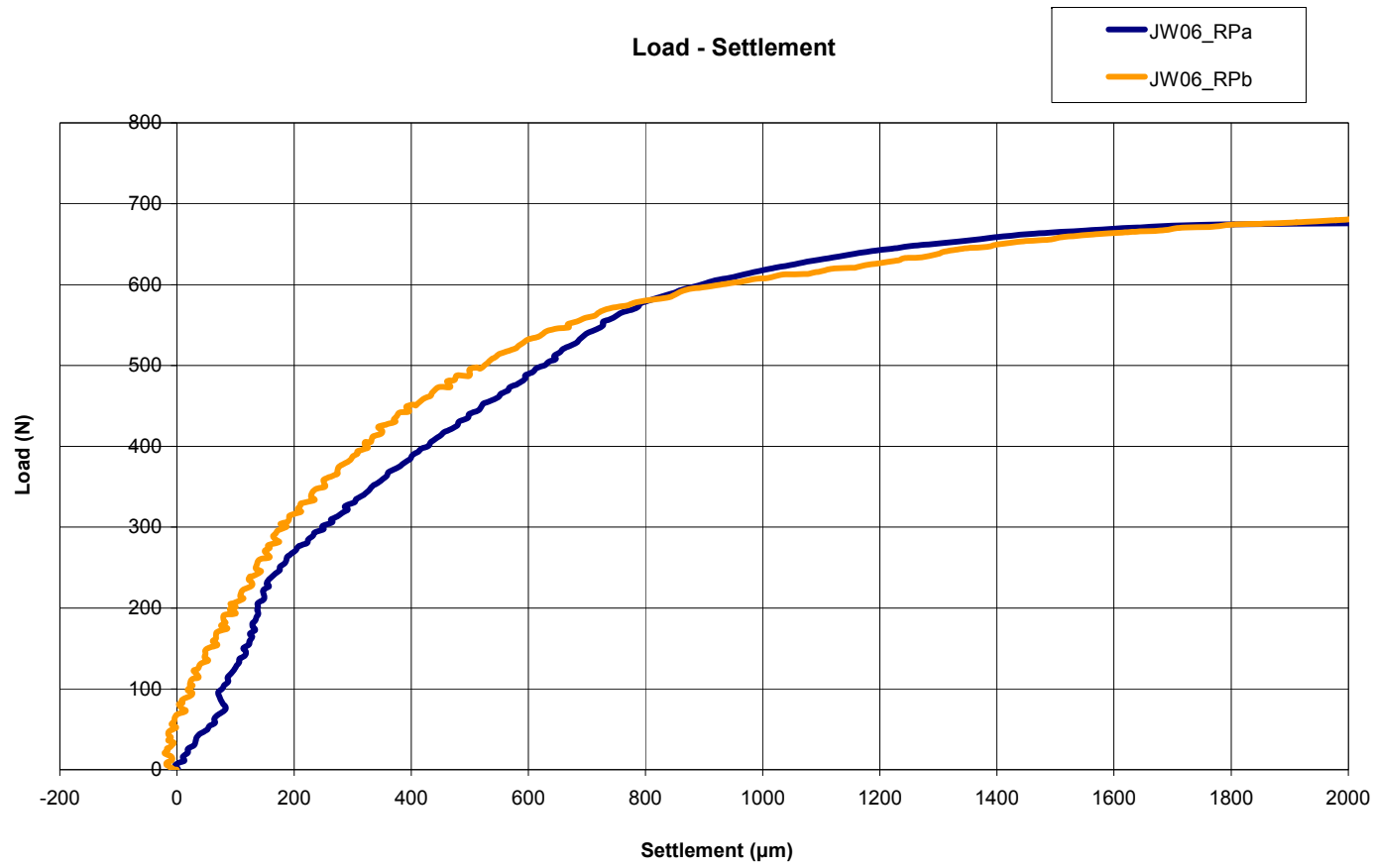


Figure 6.44 Photograph showing water levels in bottle reservoirs after test JW06



Figure 6.45 Photograph showing pile head position after test JW06_RPa

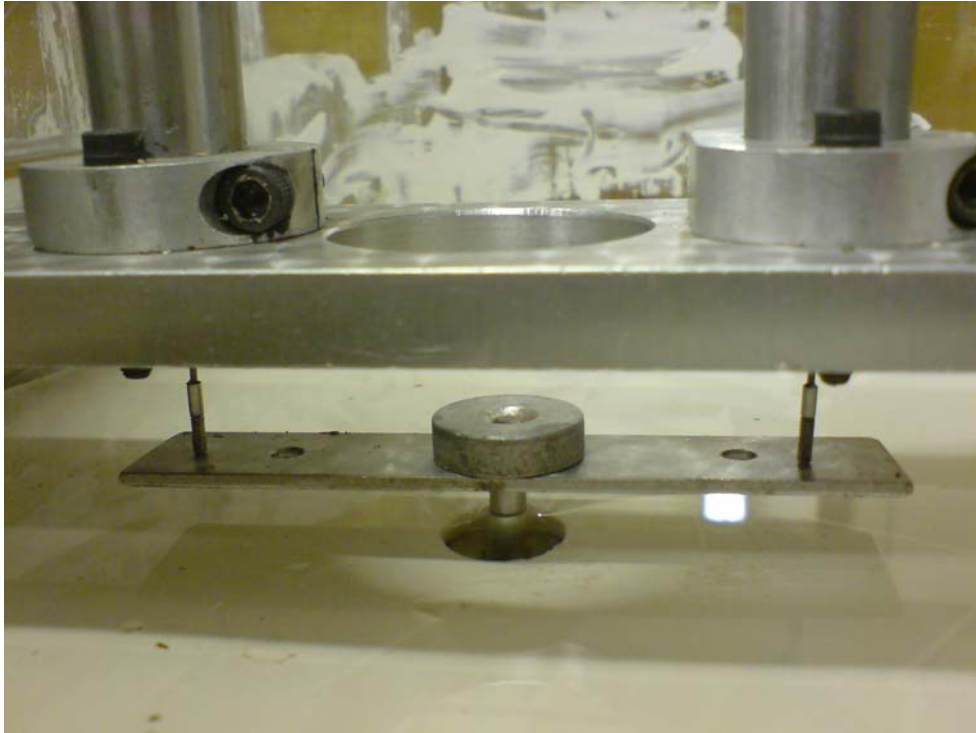


Figure 6.46 Photograph showing pile head position after test JW06_RPb

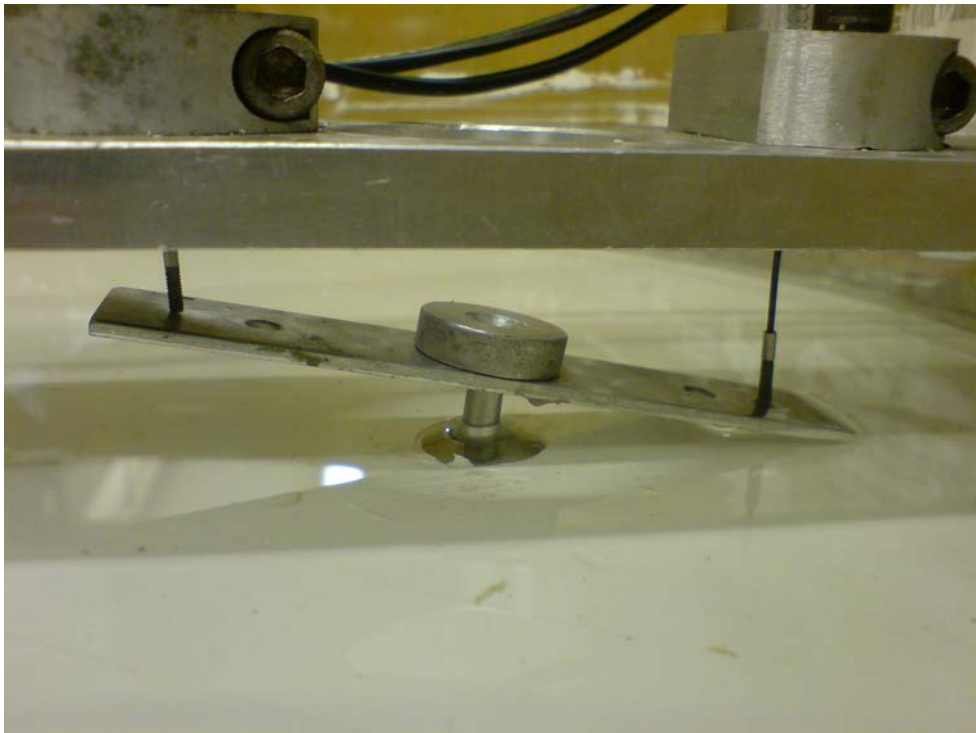


Figure 7.1 Load-settlement curves for centrifuge tests

Load-Settlement Curves for all piles

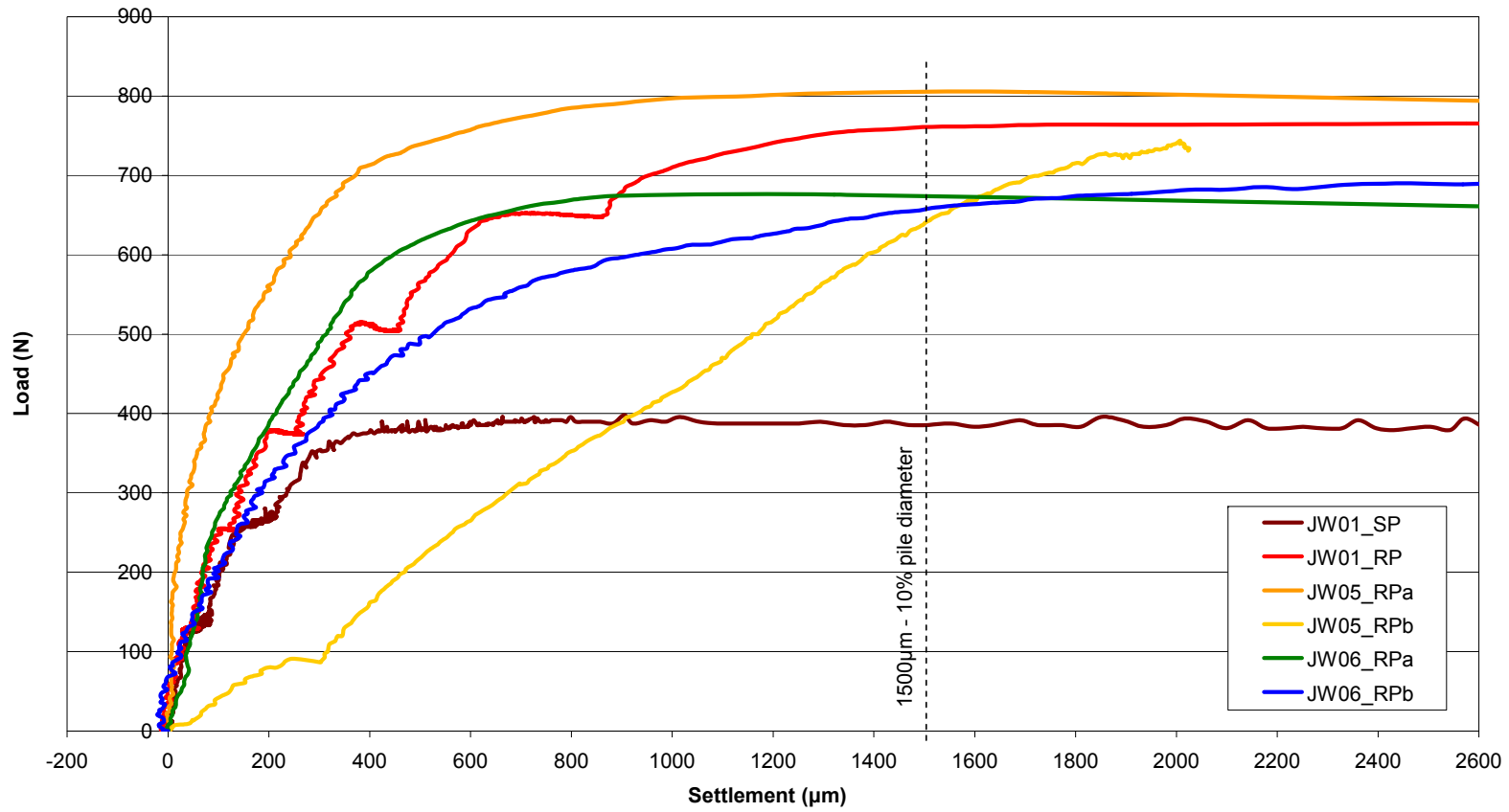


Figure 7.2 Photograph of model pile from test JW01_SP



Figure 7.3 Photographs of model pile from test JW05_RPa



Figure 7.4 Photographs of model pile from test JW05_RPb



Figure 7.5 Photograph of model pile from test JW06_RPa



Figure 7.6 Photographs of model pile from test JW06_RPb

